

SLUG CHARGE

Empowering the Homeless Community in Santa Cruz

**University of California - Santa Cruz, Baskin School of Engineering
Electrical & Computer Engineering Department
Final Report for ECE129: Senior Design Capstone Project**

Team Members: Nick Hopwood, Jeffrey Lo, Aditya Sehgal, and Jordan Tam

Client Partnership: Homeless Garden Project (December 12, 2019)

Project Sponsor: Sandbar Solar Santa Cruz (January 31, 2020)

Table of Contents

Chapter 1: Abstract	3
Chapter 2: Introduction	3
Chapter 3: Introduction to Technical Design and Implementation	6
Chapter 4: Systems Level Operation and Design	7
Chapter 5: Subsystem Design	9
Standard Operating Procedures for the Verification of the Mechanical Enclosure Durability	9
Mechanical Operation Component Selection and Design	12
Solidworks Drafting, Assembly, and Drawing	12
Locking Mechanism	15
Charging Station Mechanical Design	15
Power Requirements of All Components	18
Power System Block Diagram	21
Solar Panel Array Sizing and Selection	23
Charge Controller Selection	25
Circuit Breaker Options and Safety Ratings	25
Battery Sizing Requirements and Design Decisions	27
Power Rails Voltage Regulator Selection and Design	42
Phone Charging Circuit Design and Implementation	47
Microcontroller Usage and Choice	52
State Machine Integration of all Components	54
Selection of Hardware Components for the User Interface	55
Microcontroller Input and Output Circuits	56
Software Architecture	68
Engineering Schematics	70
PCB Integration	71
Chapter 6: Lessons Learned	72
Chapter 7: Possible Future Work	73
Chapter 8: Conclusions	74
Appendix A: System Block Diagram	76
Appendix B: MCU Choice Pugh Chart	77
Appendix C: State Machine Diagram	78
Appendix D: Component Selection Pugh Chart	81

Appendix E: Engineering Schematics and PCB Layouts	83
Microcontroller Test PCB v1	83
System Level Testbench v1	86
Motherboard PCB v2	88
Daughterboard PCB v2	92
Appendix F: Relevant Resource Links	95

Chapter 1: Abstract

For the 2,200 homeless people living in Santa Cruz, as reported by Santa Cruz County's 2019 Point-In-Time report¹, the inability to find access to a free source of power for charging smartphones has undermined attempts to contact employers, support services, case workers, and housing connections.

This project solves this problem by providing a robust, solar-powered, electronically locked charging station to the Homeless Garden Project (HGP) in Santa Cruz so that homeless people can charge their phones safely and sustainably. The charging station gives members of the homeless community a reliable resource to ensure accessible communication with emergency services, job recruiters, housing services, case workers, and all other types of support. The primary goal of this project is to lower the homelessness rate in Santa Cruz by providing a resource to increase the reliability of phones for members of the homeless community at the Homeless Garden Project. This means that the charging station gives the homeless community support in contacting employers and developing more housing opportunities. The intention is not to enable homelessness, but rather, to improve the homeless situation in the County of Santa Cruz by increasing the reliability of their most important source of communication.

The SlugCharge station uses technical engineering methods to support the homeless community. The station has six lockers that allow users to charge a single phone in each compartment. It uses a solar panel array to generate power completely independent of grid-tied electricity and incorporates a battery system that allows for the charging of phones during any weather conditions. The mechanical enclosure is made of material designed to withstand harsh weather conditions and resist vandalism and theft.

This report details the features of the charging station and the verification of the design accomplishing the high-level requirements of the client, the Homeless Garden Project.

Chapter 2: Introduction

In the past, cities have attempted to install some type of phone charging equipment to support the homeless. For example, charging stations for homeless communities have been implemented in the past in cities such as Berkeley², New York³, and Tulsa⁴ to aid the homeless community in staying connected with essential services, but support of this kind is nonexistent in the city of Santa Cruz. The results of these charging stations have been positive according to feedback from surveys of members of the homeless

¹ John Connery, Yoonyoung Kwak, Jenna Gallant, Peter Connery, and Samantha Green, "Santa Cruz County HOMELESS CENSUS & SURVEY COMPREHENSIVE REPORT 2019", Applied Survey Research, Watsonville, CA, https://static1.squarespace.com/static/5176dc7e4b0e5c0dba41ee0/t/5d48430a79c92600015c843f/1565016843951/2019+HIRD+Report_SantaCruz_Final.pdf, Accessed: April 4, 2020

² Tom Lochner, Bay Area News Group, "Berkeley homeless camps take 21st century approach with solar power", December 23, 2017, <https://www.mercurynews.com/2017/12/23/berkeley-homeless-camps-take- 21st-century-approach-with-solar-power/>, Accessed: November 17, 2019

³ CBS News NY, "LinkNYC Charging Kiosks Become Magnets For Homeless", October 10, 2018, <https://newyork.cbslocal.com/2018/10/10/linknyc-charging-wi-fi-kiosk-homeless-manhattan/>, Accessed: November 17, 2019

⁴ Engineers Without Borders USA, "Keeping Kids Connected: Engineering Students Create Solar Charging Station for Homeless Youth", February 27, 2019, <https://www.ewb-usa.org/keeping-kids-connected-engineering-students-create-solar-charging-station-for-homeless-youth/>, Accessed: November 17, 2019

community from each respective city. The charging stations have helped members of the homeless community stay connected to social networks and essential services, but these previously developed charging stations have not been entirely ideal. The charging kiosks in New York had a problem with attracting homeless people on the sidewalks of main streets which created overcrowding. The charging station in Berkeley does not have any protection against theft or weather conditions leaving the hardware vulnerable to malfunction. The charging station in Tulsa, Oklahoma has no locking mechanism and only supports the charging of a single device at any given time. Unfortunately, before this project began, there was no such support given to the homeless community in Santa Cruz.

The charging station designed in this project is secured with locks and robust mechanical materials which are improvements on previous charging station designs. This is further discussed in the *Technical Design and Implementation* chapter of this report. Additionally, the station is located at the Homeless Garden Project which preempts any concerns of increased homeless overcrowding in publicly sensitive areas. This charging station promotes the societal well-being of members of the homeless community by implementing a technologically secure phone charging station powered by cost-efficient and sustainable solar energy. The scope of this project is defined to the members of the homeless community at the Homeless Garden Project but can be scaled to a large homeless population. The table below details the differences between the charging station designed in this project and the previous attempts at solving issues of phone charging for the homeless.

Table 1: The SlugCharge Station solves the issues with previous phone charging stations

	Tulsa Student Project	NYC Kiosk Project	Encampment Charging	SlugCharge
	Tulsa, OK	New York City, NY	Berkeley, CA	Santa Cruz, CA
Theft Protection				✓
Vandalism Resist.				✓
Weather Resist.	✓	✓		✓
Backup Energy		✓		✓
User Accessibility	✓	✓	✓	✓
Charges Multiple Phones				✓
Solar Power	✓	✓	✓	✓
NIMBY Sensitive	✓		✓	✓
Lighting				✓
Fast Charging				✓

With the problem of the Santa Cruz homeless communities' unreliable communication devices and the flaws of previous solutions to this issue in mind, the following constraints for a possible charging station were developed in partnership with the Homeless Garden Project in Santa Cruz on December 12, 2019. The charging station is designed to be installed on the Homeless Garden Project's Westcliff farm location. The constraints offer the goals that must be met by the charging station designed in this project.

The functional constraints describe the requirements created by both the Homeless Garden Project and SlugCharge that outline the operation of the charging station. The performance goals describe the standards set on how well the charging station shall perform in accomplishing team-client goals. The environmental constraints examine the requirements of the charging station to minimize environmental impact.

Functional Constraints:

1. Cost – The charging station shall be developed with funds raised completely independent of the client's budget.
2. Project Timeline – The charging station will be completed and installed by a set deadline agreed upon by both the client and the team.
3. Mechanical Interface –
 - a. The charging station shall be developed using materials that can resist harsh weather conditions, vandalism, and theft while still allowing for transportation from the HGP Westcliff location to the HGP Pogonip location.
 - b. The charging station shall have an external housing for resistance to harsh weather conditions, vandalism, and theft of both the station itself and the phones that are charging.
 - c. The charging station shall provide lighting for user accessibility.
 - d. The charging station's door shall be developed with a sealant that prevents weather conditions from affecting internal components.
4. Electrical Interface –
 - a. The charging station shall provide power to components using a method of alternative energy due to the Homeless Garden Project's off-grid location.
 - b. If solar power is used, the charging station shall be developed utilizing a method of providing power to components for a minimum of 24 hours during low to zero solar energy conditions.
 - c. The charging station's power system devices shall be installed in a location that does not interfere with client activities.
5. User Interface – The charging station shall be developed to allow for easy interaction for users.
6. Features –
 - a. The charging station shall use a locking mechanism that can resist vandalism and theft.
 - b. The charging station shall give users the ability to input their own 4 digit pass-code to open and close their locker in a secure manner.
 - c. The charging station should allow for a master-code of at least 6 digits, which will be given to the HGP staff, that can open any locker at any time.
 - d. The charging station shall allow users to charge their phones for two hours.
 - e. The charging station should give users a grace period of at least 15 minutes so that users can retrieve their device before master-code input is needed.
 - f. The charging station shall give users the ability to use their own charging cables.

g. The charging station shall allow for a minimum of four phones to be charged at one time.

Performance Constraints:

1. Power Supply – The charging station shall be developed using a power system that can output sufficient power for internal components and a minimum of four phones at one time.
2. Charging Speed – The charging station shall provide “fast-charging” capabilities.
3. Lifespan Expectancy – The final charging station shall have a minimum lifespan of three years with complete functionality.
4. User Accessibility – The charging station shall utilize an interface that is easy to learn and use in both physical and software aspects.
5. Heat Dissipation – The charging station shall allow for proper heat dissipation to prevent overheating of phones and the station itself.

Environmental Constraints:

1. Resistance to Damage –
 - a. The charging station shall resist weather conditions that are common to the HGP’s Westcliff location to preserve the station’s complete functionality.
 - b. The charging station shall be developed with means of preventing theft and vandalism that preserve the station’s complete functionality.
2. Alternative Energy – The charging station shall use alternative energy methods to preserve the HGP’s off-grid nature.
3. Safe Internal Component Selection and Positioning – The charging station shall be positioned in a manner that preserves the environmental surroundings.

Chapter 3: Introduction to Technical Design and Implementation

The following chapters discuss the systems level and subsystems level design of the project. The systems level chapter will detail the high-level operation of the charging station and the necessary components for functionality. It then breaks down the systems level design into a block diagram that outlines the power system, mechanical features, and microcontroller system in that order.

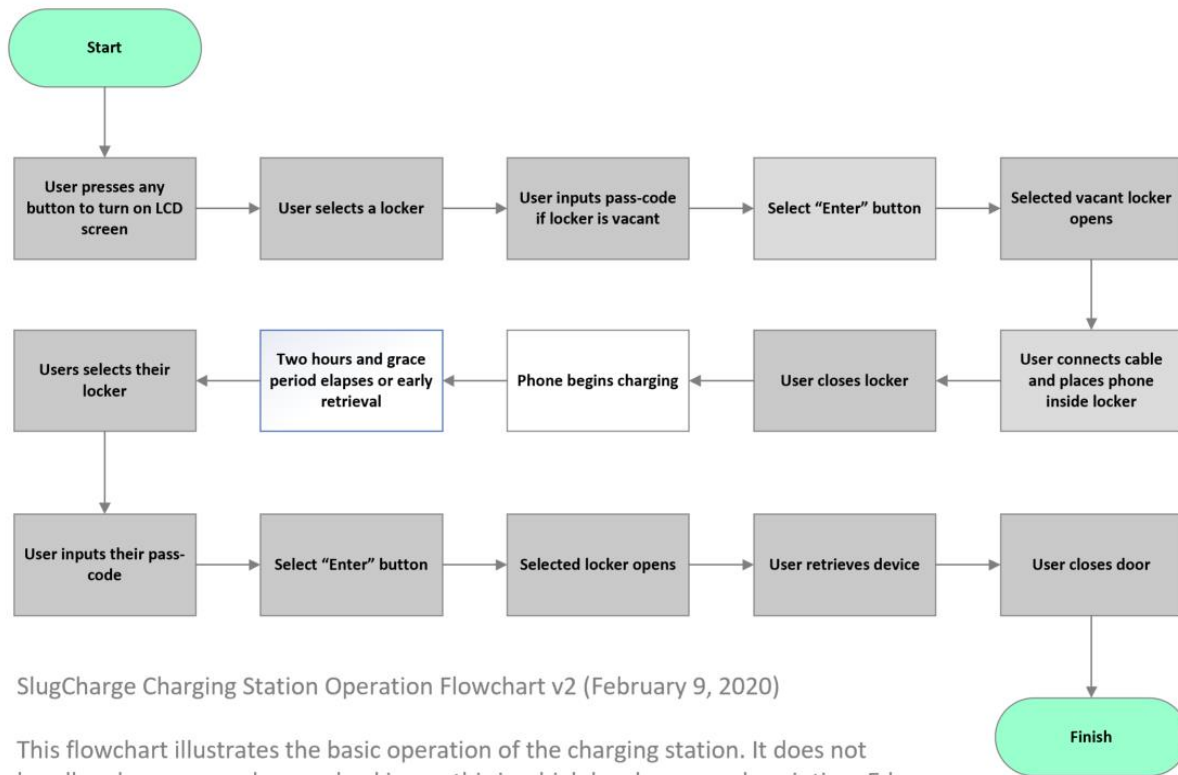
Subsequently, each subsystem chapter will be introduced by discussing the need for a specific component based on the aforementioned team-client goals in the introductory chapter. After establishing context for a component, each section will discuss design, design decisions, implementation, testing methods, and validation results. Lastly, the results will be related back to the completion of a specific team-client goal. The lessons learned from these designs are mentioned throughout each component section in the analysis of the test results. The mechanical components and designs listed after the system level section and near the beginning of the component sections are necessary for the functionality described in the operation flowchart, which is displayed in the system level section. Although many of these mechanical components require a power supply to enable successful operation. The power devices and designs listed in the component section detail the development of a power supply that is used to power all components. The mechanical interface also relies on the microcontroller and state machine for components to interact in the appropriate manner described in the operation flowchart. The software

handles the integration of mechanical and power components allowing for the charging station to operate and, also, creating a user-friendly interface for members of the homeless community at the Homeless Garden Project. The component level chapters follow the order of the systems level design chapter by explaining the necessary mechanical parts and designs that require power devices and microcontroller components to maintain operation.

Chapter 4: Systems Level Operation and Design

The charging station is operated by a user prompting an LCD screen to be turned on by pressing any button on a number keypad. The user will then select a locker compartment that is indicating vacancy and input a four-digit passcode that allows the user to reopen the locker. Subsequently, the locker door will open and the user will connect their own charging cable to the USB 2.0 port located inside the compartment. The user will then connect their phone to the charging cable, place their phone inside the locker, and close the compartment door. When the user chooses to retrieve their phone, they will prompt the screen by pressing a button on the number keypad and select their locker compartment. The user must then enter their four-digit passcode and retrieve their device. This process describes the user interface that has been verified through interviews with the client on ease of access when learning the operation of the charging station. A flowchart is shown in the figure below for visual representation of the charging station's basic operation.

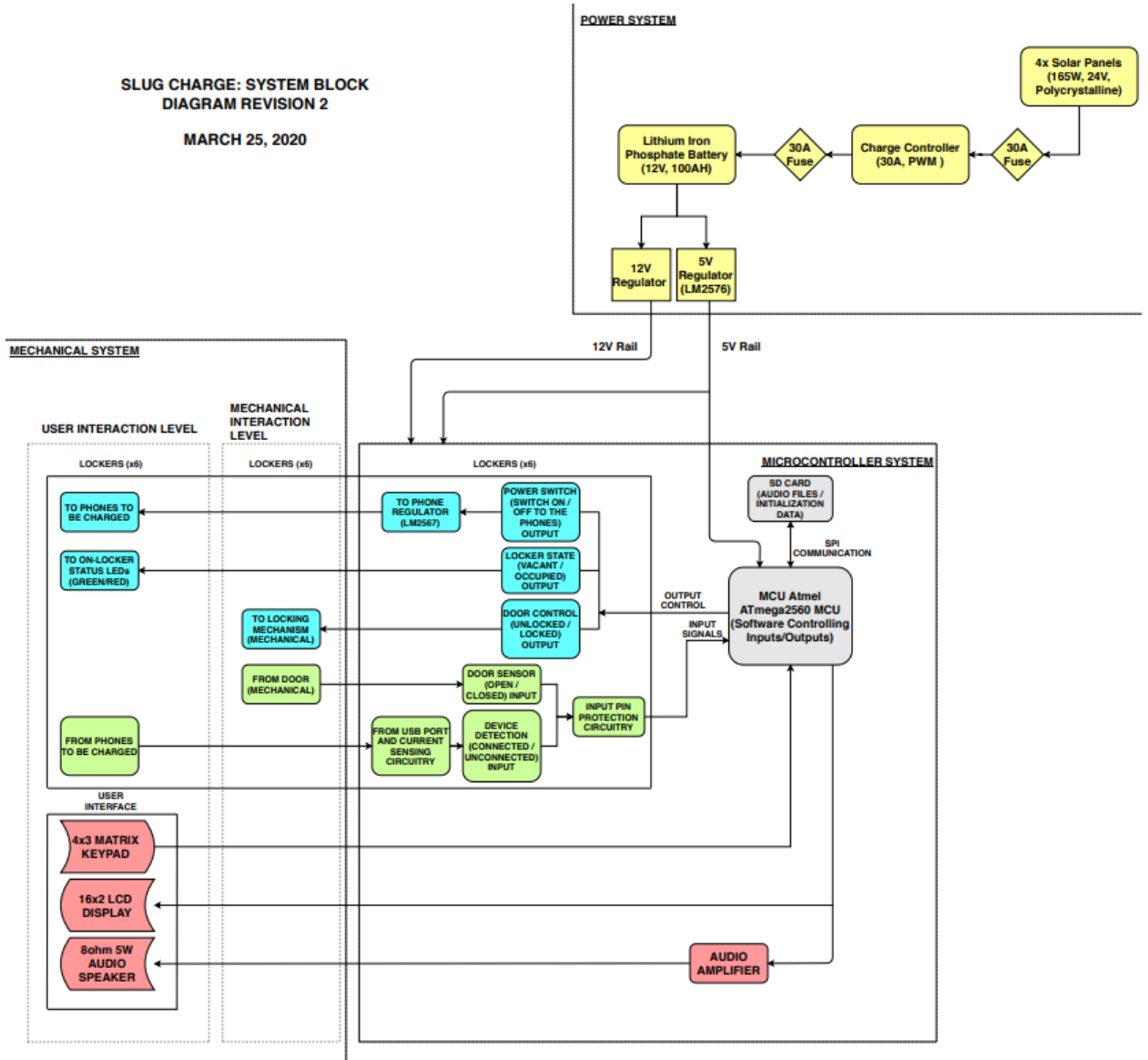
Figure 1: The operation Flowchart v2 (February 9, 2020) illustrates the procedure for operating the charging station



This flowchart illustrates the basic operation of the charging station. It does not handle edge cases and error checking as this is a high level process description. Edge cases and error checking are included in the low-level state machine.

The system level block diagram represents the overall high-level function of the charging station, connecting the power system, microcontroller system, and the mechanical components of the design. The systems level block diagram of the SlugCharge station, detailing the interconnections and dependencies between each technical subsystem is shown in the figure below.

Figure 2: The systems level block diagram shall be used to identify subsystem components



Since the Homeless Garden Project operates in an outdoor location with no electricity, the charging station relies on the use of solar energy. This power system is designed to meet the client restriction of generating power independent of grid-tied electricity. The station utilizes three 24V, 165W polycrystalline solar panels to convert solar energy into DC power during daylight hours. The solar panels are connected to a 20A circuit breaker to prevent current surging into the charge controller. The system

uses a 40A MPPT charge controller to convert voltage to an optimized current charge rate for the battery. There is a 40A fuse connected between the charge controller and the battery to prevent current surges into the battery. The battery used for this project is a 12V, 50Ah lithium iron phosphate battery which powers the entire station. The battery, when fully charged, can provide power to the station's internal components and 24 phones during a given day without any solar energy input. This fulfills the client requirement that the charging station should operate for 24 hours on energy storage alone. The 24 phones charged represents the maximum number of phones that can be charged if the station cycles through four cycles of 6 phones charging for two hours over an 8-hour work day. The battery is connected to a 5V and a 12V regulator circuit which create 5V and 12V power rails. The 5V rail is used to power phones and internal components while the 12V rail is used solely for powering internal components. Design decisions for all power devices are explained in the subsequent sections. The power system is then connected to the microcontroller system.

The microcontroller (ATmega2560 MCU) and every hardware component except the locking mechanism, which is powered by 12V, are powered with the 5V supply rail. The MCU is programmed to interface with each I/O hardware component to develop the interface at the user interaction level with the station. The user interface, or the primary components the user will be interacting with, includes a 4x3 matrix number keypad, a 1602a LCD display, and an 8ohm audio speaker playing PCM audio with a respective audio amplifier. The mechanical interactions with the microcontroller includes a locking mechanism (pull lock-style solenoid) and its control (output signal), door sensors (snap-action switch, reed switch, input signal), phone current-sensing (input signal), power control to the phone (LM2567 ON/OFF pin, output signal), and status LEDs (output signal). Each input signal passes through an input protection circuit which includes a resistor for current surge reduction, a decoupling capacitor for noise removal and hardware debouncing, and clamping diodes for voltage spiking and hardware debouncing. The microcontroller communicates with an SD card for purposes of containing audio and to contain information on the locker states (number of lockers charging, which lockers are occupied, each occupied locker's passwords) for the purpose of initialization (see *State Machine Diagram*).

The mechanical system facilitates the accessibility of the station by mechanically positioning the mechanical user interface components and implementing the lockers with each electrical component for the microcontroller to read inputs and control outputs.

Chapter 5: Subsystem Design

The following subchapters explain the different subsystems of the charging station that accomplish the goals of the client outlined in the introduction. The subsystem design chapters are organized by explaining the mechanical operation of the charging station which illustrates the need for a power system and a microcontroller system that allows the mechanical and electrical components to interact with each other.

Standard Operating Procedures for the Verification of the Mechanical Enclosure Durability

The client requirement for the durability of the mechanical enclosure of the charging station was simply defined by the goals of the enclosure withstanding the common, harsh weather conditions of Santa

Cruz and resisting theft and vandalism. This charging station accomplishes both of those objectives by using materials mentioned in the next chapters and is tested against a formal SOP outlining instructions on verifying the durability of the charging station. The SOP⁵ is referenced in the footnote below and in Appendix F.

This SOP is the required documentation of the durability standards that the enclosure of the charging station shall meet after testing. The tests described in the document shall illustrate the necessary procedures to develop durability standards for the external enclosure. These standards shall be explained to the client, the Homeless Garden Project staff and employees, so that both parties involved understand the maximum durability ratings for the charging station's external enclosure.

IP (or "Ingress Protection") ratings are defined in international standard EN 60529 (British BS EN 60529:1992, European IEC 60509:1989). They are used to define levels of sealing effectiveness of electrical enclosures against intrusion from foreign bodies (tools, dirt etc) and moisture. Ingress Protection 34 or IP34 stands for specific intrusion and moisture protection standards. The first digit '3' defines intrusion protection as "Protection from entry by tools, wires etc, with a diameter of 2.5 mm or more" and the second digit '4' defines moisture protection to "Protected against water splashes from all directions. Tested for a minimum of 10 minutes with an oscillating spray (limited ingress permitted with no harmful effects)".

The following are the testing procedures required for the charging station's mechanical enclosure to meet the durability standard of IP34

The testing of the intrusion follows the guidelines set by the first digit '3' of IP34. This first digit '3' represents the "Protection from entry by tools, wires etc, with a diameter of 2.5 mm or more". The instructions for testing below detail the method of ensuring that the charging station enclosure can withstand intrusion by force using tools that fall under the IP rating criteria.

Testing of Intrusion Protection – "Protection from entry by tools, wires etc, with a diameter of 2.5 mm or more"

Step 1) The tester shall use common, non-specialized tools available to the general population such as screwdrivers, wiring, pipes, crowbars, hammers, etc. with a diameter of 2.5mm or more and attempt intrusion of each locker compartment door. Attempts at intrusion shall be made at every point of opening between the door and the enclosure surrounding the door. An example area of testing is illustrated in the red rectangle in the figure of the draft of the charging station enclosure below.

⁵ Jordan Tam. *SlugCharge SOP for External Enclosure Durability rev1.1*. May 4, 2020. SlugCharge.
<https://drive.google.com/open?id=1h4FE-AmjUl84HppMgnB3OVhnc4bnuUHo>

Figure 3: Example area of testing for intrusion protection

Step 2) The tester shall use common tools described in ‘Step 1’ to test for protection against intrusion through openings in the LCD screen.

Step 3) The tester shall use common tools described in ‘Step 1’ to test for protection against intrusion through openings in the number keypad.

Step 4) The tester shall use common tools described in ‘Step 1’ to test for protection against intrusion through openings for ventilation.

Step 5) The tester shall define any other points of entry using common tools described in ‘Step 1’ and proceed to attempting intrusion in those locations.

Step 6) The tester shall use common tools described in ‘Step 1’ to test for protection against intrusion by penetration at any point on the charging station’s enclosure.

The testing of the moisture entry follows the guidelines set by the second digit ‘4’ of IP34. This second digit ‘4’ represents the protection “against water splashes from all directions. Tested for a minimum of 10 minutes with an oscillating spray (limited ingress permitted with no harmful effects)”. The instructions for testing below detail the method of ensuring that the charging station enclosure can prevent moisture from entering and damaging components when applying moisture according to the IP rating.

Testing of protection against moisture - Protected against water splashes from all directions. Tested for a minimum of 10 minutes with an oscillating spray (limited ingress permitted with no harmful effects).

Step 1) The tester shall use a common garden hose to spray the enclosure from all directions at a spray velocity of 25 m/s. This velocity is chosen as it is approximately the calculated terminal velocity for a rain drop with a radius of 2.5mm. A reference is included in the reference section of this document. [2]

Step 2) The tester shall record any limited ingress of moisture in sensitive areas of the charging station such as the door sealant area between the door itself and the enclosure surrounding the door. The tester will then determine if the potential limited ingress of moisture has harmful effects to electrical components or the enclosure itself.

In conclusion, the document defines the SOP for the durability of the charging station's external enclosure. The goal is to define testing procedures that simulate natural weather conditions and environments and to meet the Ingress Protection standard of IP34. The tests are defined by the procedures for protection against intrusion and moisture outlined in the previous section.

Mechanical Operation Component Selection and Design

The operation flowchart shown in *Figure 1* in Chapter 4 exhibits a sample of the required components required to meet the mechanical interface constraints established in the team-client goals.

Medium Density Fiberboard (MDF) was used for the single locker compartment prototype. This prototype can be used indoors as it provides ample security in collaboration with monitoring staff workers. For the final design, the charging station uses polycarbonate plastic for the outer enclosure with an aluminum frame and 316 stainless steel for the inner enclosure. Pugh charts for the inner and outer housing of the charging station are located in Appendix D.

Solidworks Drafting, Assembly, and Drawing

The footprint of the locker is a 13" by 9" rectangle, which allows for common large phones to be placed into the compartment. The phone slot is placed in the center and is wide enough for almost all phones to fit. There is a small structure on each side of the locker. This allows space for electronics and wiring on both the left and right concealed sides of the locker. It also serves to allow space for only a phone (though it is impossible to eliminate all extra space). The figures below display the SolidWorks drafts of a single locker prototype.

Figure 4a: NorthEast Isometric view of a single locker prototype

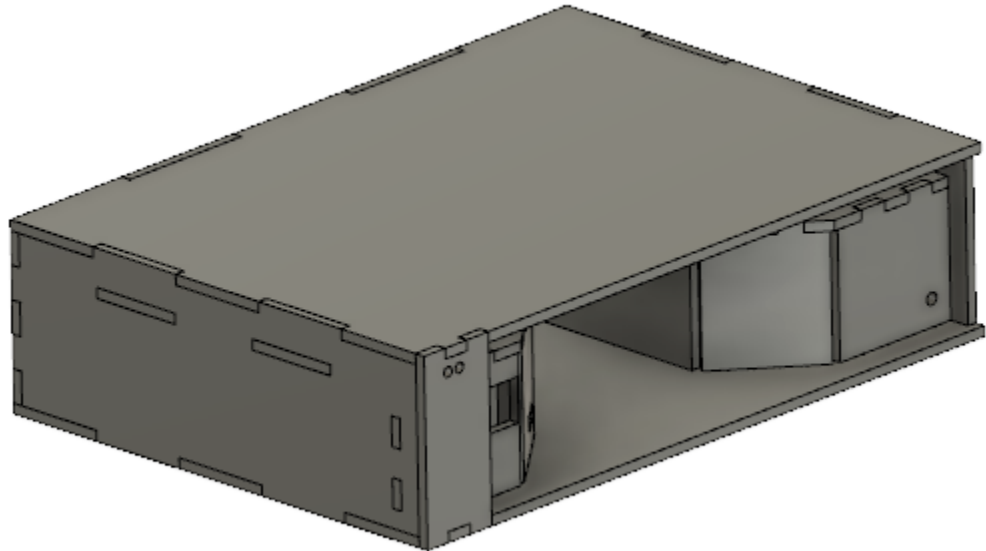
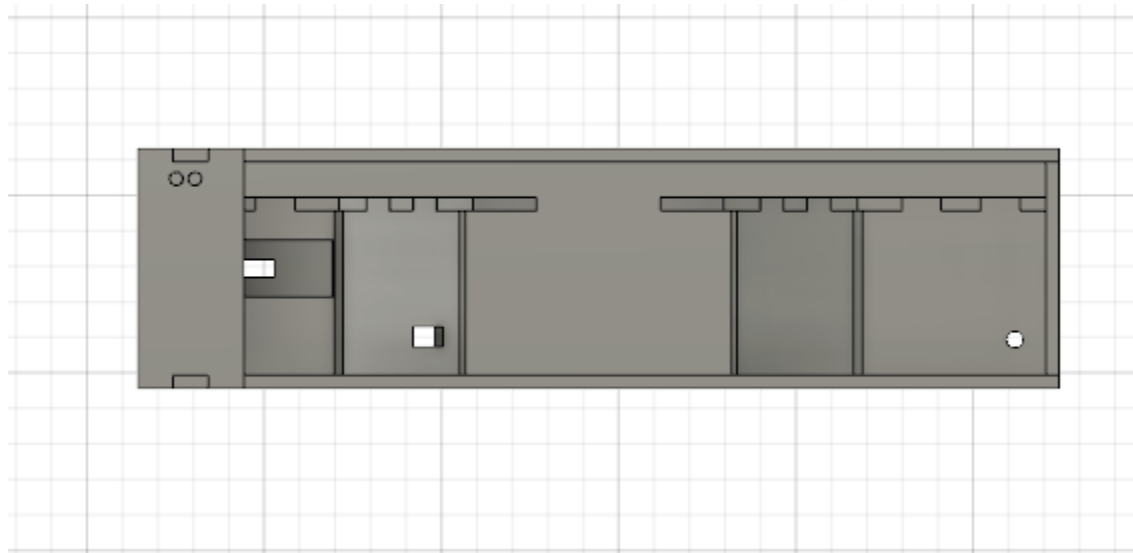


Figure 4b: Front view of a single locker prototype

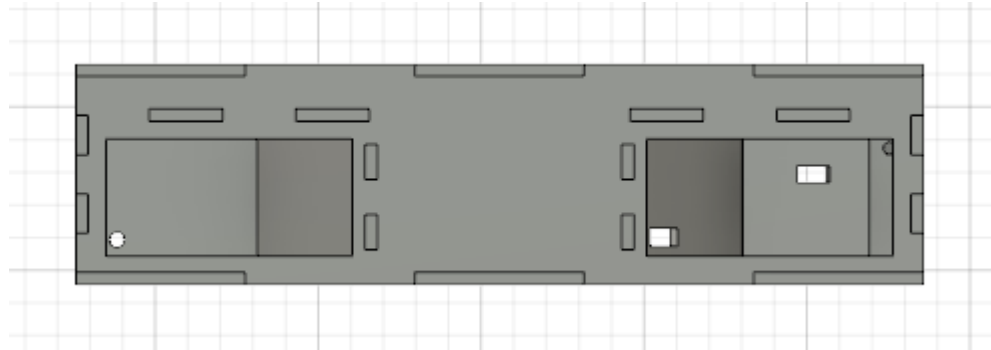


The phone slot is designed with 45 degree angles that allow for easy access to the charging port, which is positioned on the angled wall on the left.

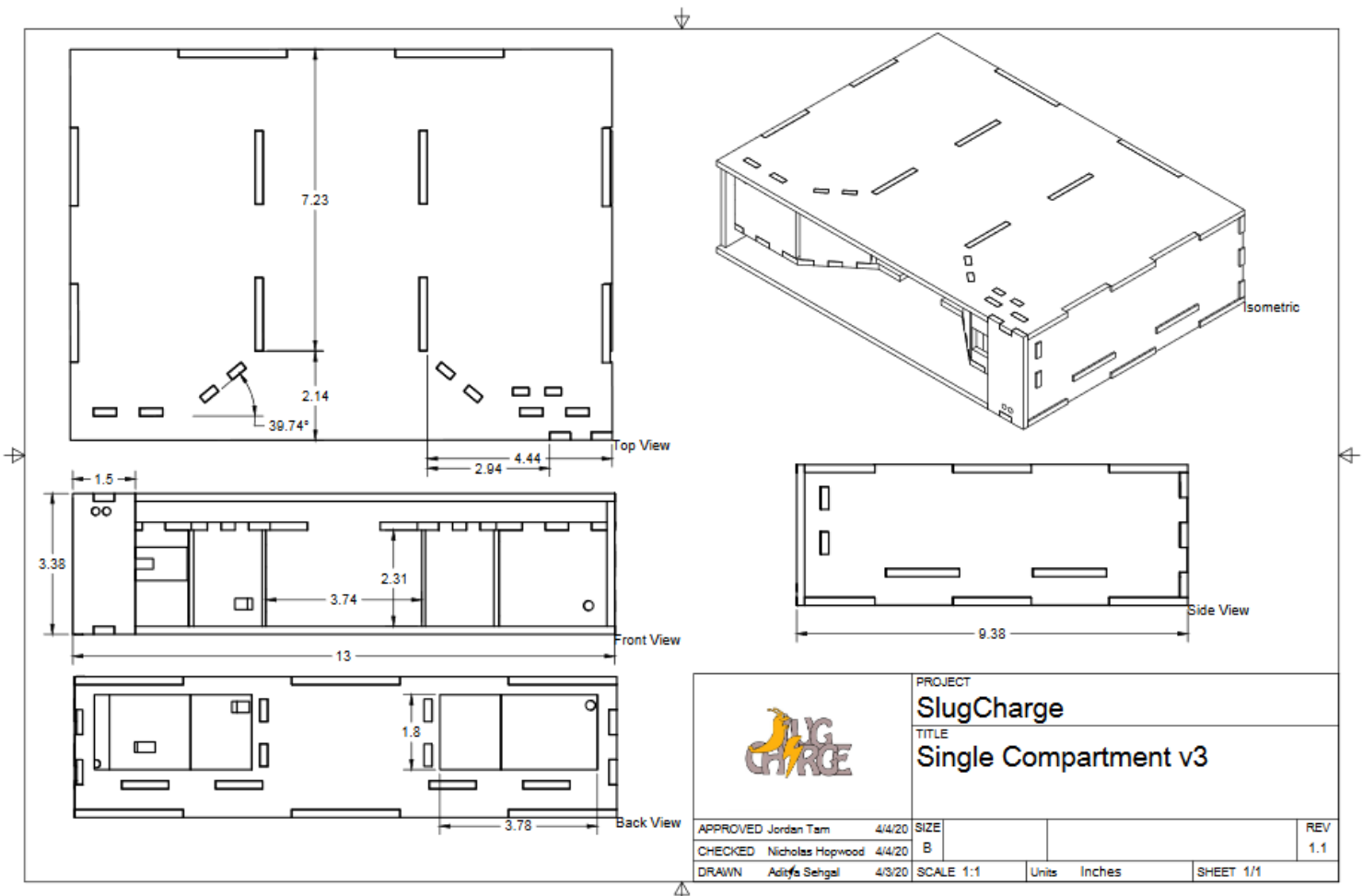
The locker has a slot for tablet charging as well. To accommodate for this, there is a half-inch thin layer slot for tablets to be placed. There is a platform on both sides with a space in the middle, above where the phone goes. The platforms on both sides hang over the space in the center to prevent phones from falling through in the case that the user desires to place their phone in the tablet slot. The platform has cutouts for all of the pieces under it to fit into.

There is a cutout on the inside of the left wall for where the locking solenoid fits when the door is closed. This solenoid locks on the small leftmost wall as displayed in the front view. The figure below displays the view of the back of the locker prototype.

Figure 4c: Back view of a single locker prototype



In order to allow for access in the case of necessary maintenance, cutouts were fabricated in the back of the locker prototype. The figure below displays the isometric drawing of the locker prototype.

Figure 4d: Component drawing displaying dimensions of the locker prototype

These dimensions outline the minor details of the locker prototype. Note that all dimensions are in units of inches as displayed in the bottom right-hand corner of the drawing file.

Locking Mechanism

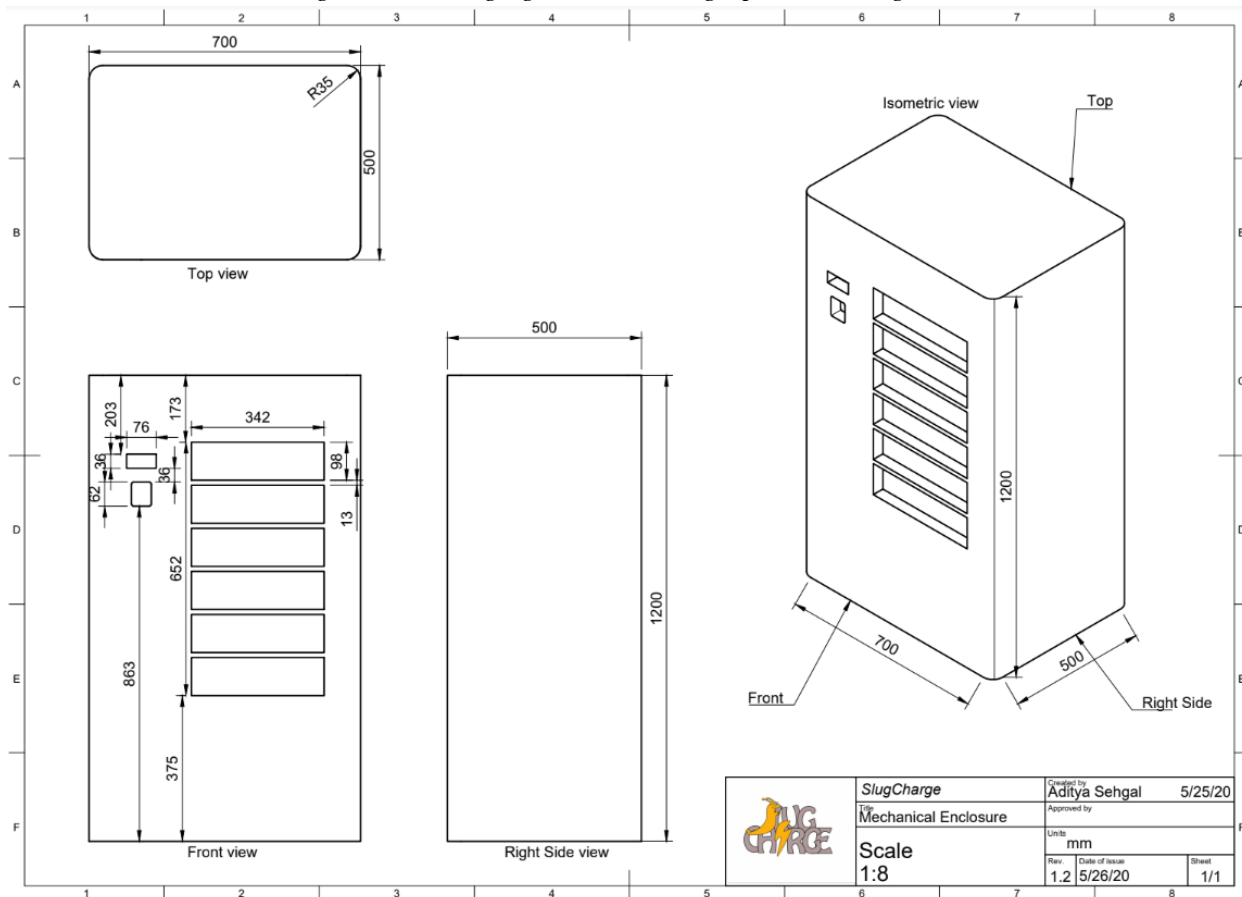
As defined in the product requirements, the locker is required to have protection against theft of devices and vandalism. The clearances between each wall and the door were minimized as to mitigate any possibility of tampering. This narrow clearance also provides resistance against leaks especially with the support of an inner silicone layer that would further block out any liquids that could damage internal components. Additionally, each locker utilizes a locking-style solenoid that grants the authorized user access to their respective locker after entering their 4-digit passcode. The locking solenoid requires a 12V rail and the ability to be triggered by user inputs. Therefore, the subsequent component sections in this report outline the necessary power and microcontroller devices required to maintain the operation of mechanical components.

Charging Station Mechanical Design

To produce the station as a final product, any fabrication house would require an orthographic drawing portraying required dimensions and necessary details. Key details of the mechanical drawing are placement of each locker as shown on the right side of the station having 6 linear cutouts to mount each

individual locker as designed above. The UI is placed to the left of the station with the 16x2 LCD placed closer to the top and the numpad placed right under. The LCD is used as a visual annunciator and to guide users through the process of selecting and accessing a locker. The numpad will aid the users in selecting the appropriate lockers and entering a chosen passcode. The drawing is shown in the following orthographic drawing:

Figure 5a: Charging Station Orthographic Drawing V1.2



Following the above orthographic drawing, 3D models of the station were designed to further provide clarity on the final product. This model was then further used to develop tutorials for the station to educate users how to use it.

Figure 5b: Isometric view of the charging station V1.1

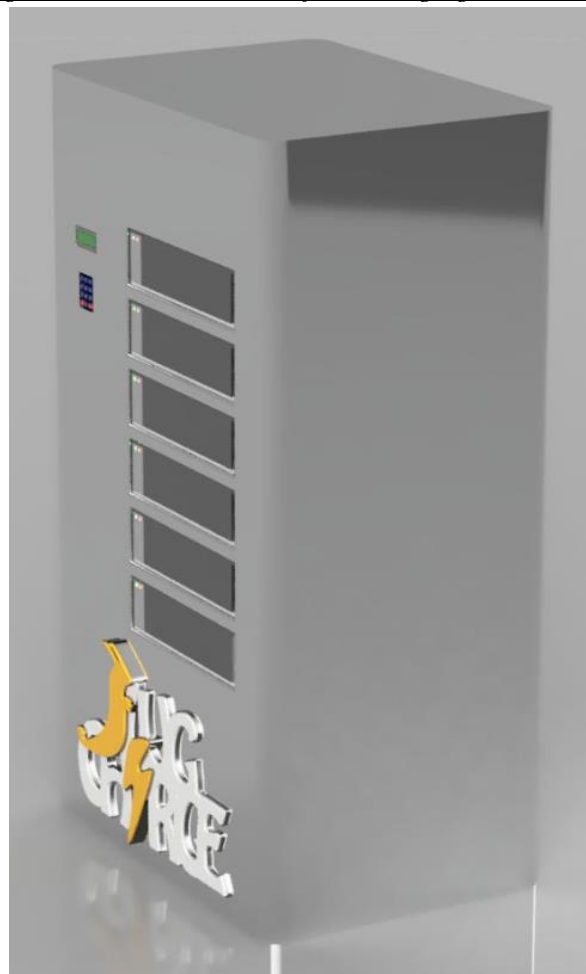


Figure 5c: Render of charging station showcasing a locker in use V1.1



Figure 4d: Render showing inside of the charging station V1.1



Considering the charging station may have a learning curve, tutorials are provided using the same 3D model as above to teach users how to use the station. These tutorials are a two-part video, the first one guiding how to select an available locker and using it to charge a device and the second part teaching how to access a previously selected locker and retrieve a device. The tutorials can be referred to in *Appendix F*.

Power Requirements of All Components

The charging station requires many electrical components to maintain operation and to charge phones. These electrical components necessitate a power system that can provide sufficient power to all

parts. All electrical specifications for components are listed in the power budget. This power budget outlines the nominal voltages, tolerances, max and average expected current draw, average activation time per day, days activated per week, average expected charge usage per day, and max and average expected energy usage per day for each component. The charging station has six locker compartments, a limitation of two hours of charging per phone, and the Homeless Garden Project operates for eight hours each day. Thus, there can be a maximum of 24 phones charged each day if six phones are rotated through four 2-hour periods.

The power budget is used to estimate the power required for all internal components and 24 phones that charge at a 5V, 2A rate. The power budget is then used to size power generation components such as the solar panel array and the battery. This charge rate was chosen because this equates to the common maximum fast charging capabilities of standard phone battery smart chargers. The complete Power Budget v17 (April 20, 2020)⁶ is referenced in the links in *Appendix F* and in the footnotes below. This power budget is relevant to the sizing of the solar panel array and the battery. Furthermore, specifications in the power budget help in making decisions on other components such as the circuit breaker, fuse, and the charge controller. The subsequent section discusses the power block diagram which outlines each component selected for the power system based on the power budget specifications.

In addition to the general power budget, a demand factor power budget has been developed for this project to aid in the scalability of the charging station. The demand factor power budget estimates the power usage for a single operation of the charging station. This includes any interaction that a user might have to place their phone inside the locker, the process of charging the phone itself, and the interaction between the user and the station when retrieving the phone.

The demand factor power budget is important because a future project may require the charging station to charge more or less phones during a period of one day. Thus, having the power usage estimate for a single operation would allow the charging station's power systems components to be easily scaled for the new requirements. Furthermore, this demand factor power budget is used in this project for better estimation of power usage as surveys can be conducted to define a more exact number of phones that may be charged by the station during a given day instead of using the maximum number of phones that can be charged. Ultimately, the conclusion that can be made from this document is that a single operation of the charging station shall take approximately 22.2Wh. This data can be used to help size the capacity of the 12V battery as 22.2Wh would mean a capacity of 1.85Ah for a 12V battery. The demand factor power budget⁷ is referenced in the footnotes below and in *Appendix F*.

The demand factor power budget was then broken down into the individual steps in order to operate the charging station completely for one phone charge cycle. This data was compiled into a document called *Power Usage per State* and it illustrates the amount of power used during each step when operating the charging station. This document shall be used to scale the activation times for each step when operating the charging station. For instance, currently the *Power Usage per State* document

⁶ Jordan Tam. *SlugCharge Power Budget v17*. SlugCharge. April 20, 2020.
https://drive.google.com/file/d/1jPmQjeSzCVY3QaD_JMbgSGqo6sQEci6D/view?usp=sharing

⁷ Jordan Tam. *SlugCharge Demand Factor Power Budget v2*. SlugCharge. April 21, 2020.
https://drive.google.com/file/d/1jPmQjeSzCVY3QaD_JMbgSGqo6sQEci6D/view?usp=sharing

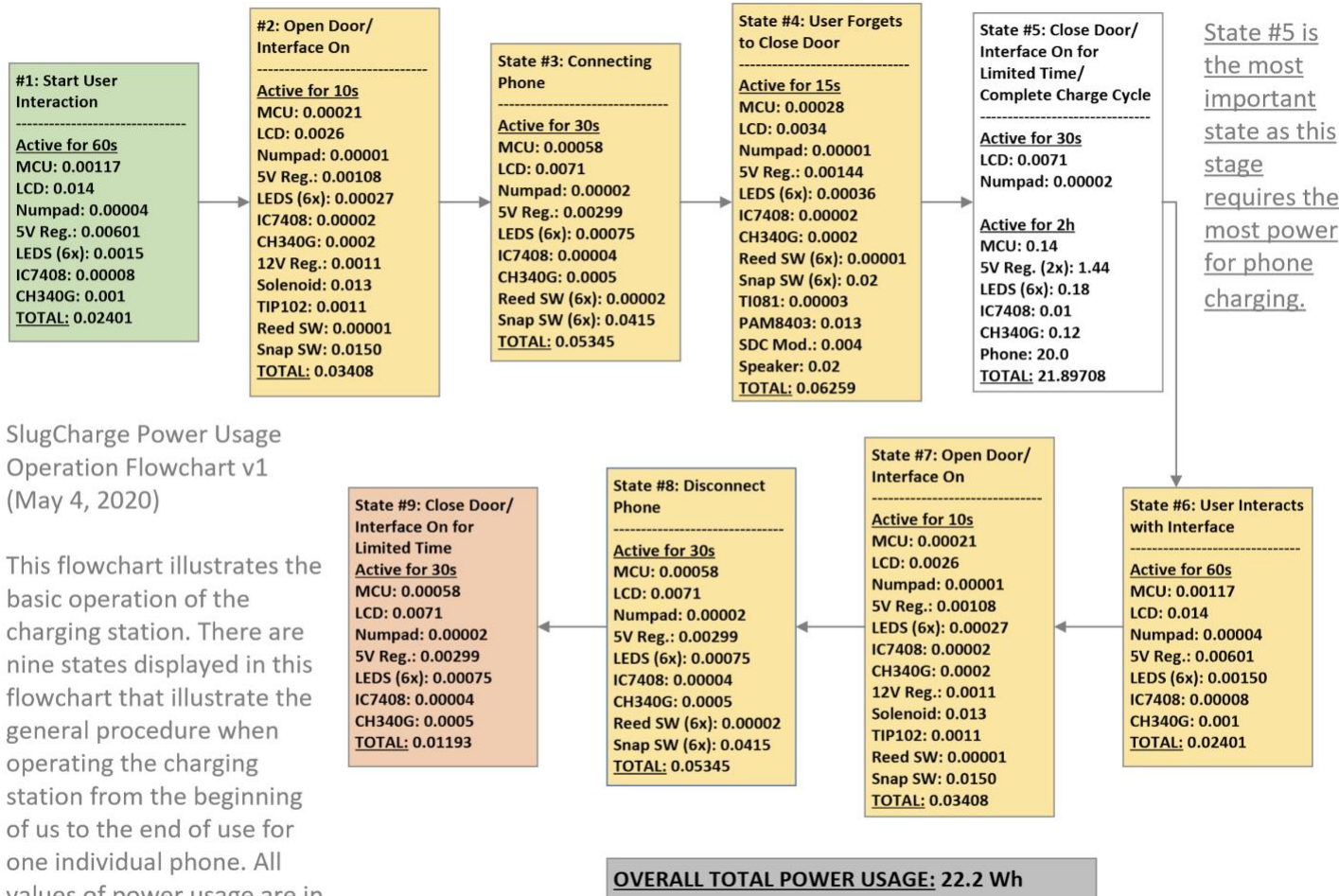
outlines that it shall take one minute for a user to interact with the charging station before the station eventually opens a locker compartment door. After testing with the client and recording data on the average time spent for this step, the charging station's power usage for that specific stage shall be scaled according to the new average activation time obtained through testing.

Additionally, this document is used to include the power usage of certain edge cases. For instance, if a user forgets to close the door after connecting their phone to the charging station, there will be an audible notification that signals to the user to close the door. This edge case requires additional power and, therefore, the *Power Usage per State* document makes it easy for the power estimation to be scaled for specific edge cases. This document⁸ is referenced in the footnotes below and in *Appendix F*.

Lastly, the *Power Usage per State* estimations were compiled into an operation flow chart that visually displays the amount of power used per step during a single operation of the flowchart. The flowchart takes into account the edge case described in the previous paragraph. The *Power Usage Operation Flowchart* is shown in the figure below.

⁸ Jordan Tam. *SlugCharge Power Usage per State v1*. SlugCharge. April 21, 2020.
<https://drive.google.com/file/d/1v6U0OVjHBuJJWFmCbxqTeMYFdtsyuvnLO/view?usp=sharing>

Figure 5: The Power Usage Operation Flowchart is used to visually display the estimated power usage during a single operation of the charging station



SlugCharge Power Usage

Operation Flowchart v1

(May 4, 2020)

This flowchart illustrates the basic operation of the charging station. There are nine states displayed in this flowchart that illustrate the general procedure when operating the charging station from the beginning of use to the end of use for one individual phone. All values of power usage are in units of [Wh].

This flowchart serves the same purpose as the *Power Usage per State* spreadsheet. The flowchart is used to visually display the amount of power that is used during a single operation of the charging station. This document is useful for scaling the project for the charging of more phones on battery storage alone. For instance, if the project required 36 phones to be charged without solar energy input, this diagram and the *Power Usage per State* spreadsheet would make it easy in scaling the battery storage to meet the new requirement.

Power System Block Diagram

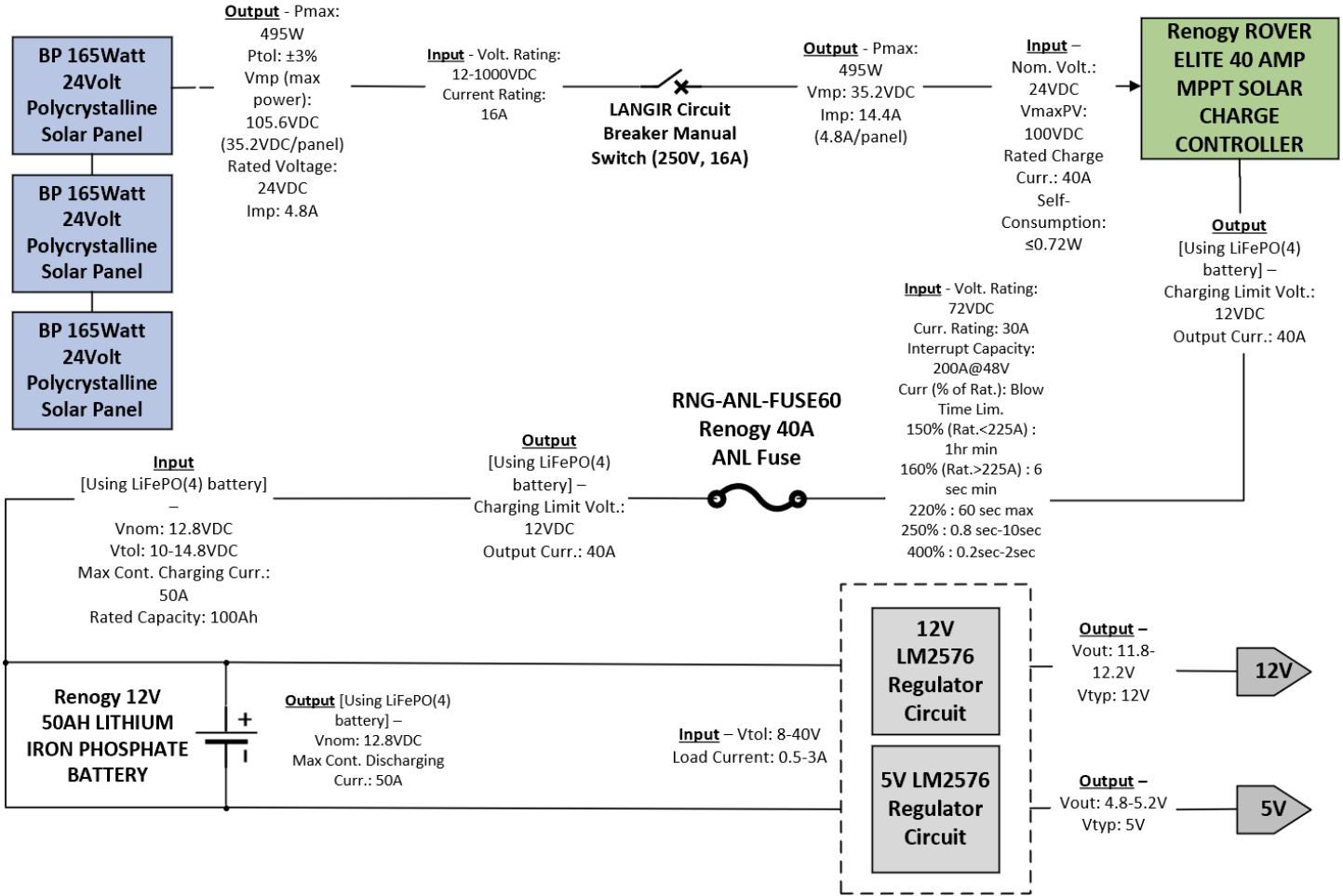
The power system block diagram displayed below is a visual representation of the input and output connections from the solar panel power supply to relevant power supply rails. The block diagram includes all input and output specifications, relevant tolerances, nominal voltages, and component-

specific information. The diagram shows the connections between the solar panel array⁹, the circuit breaker¹⁰, the MPPT charge controller¹¹, the fuse¹², the battery¹³, and the voltage regulator circuits.

Figure 6: Power System Block Diagram v13 (June 6, 2020) displays interconnection specifications between power components

Power System Block Diagram v13 – June 6, 2020

Jordan Tam



⁹ BP Solar, BP Solar Pty Ltd 2005, https://www.solarpanelsaustralia.com.au/downloads/bpsolar_bp_3165.pdf, accessed: June 6, 2020

¹⁰ LANGIR 250V Single Pole Voltage Protection Miniature Circuit Breakers Switch For DC And Solar Generation C Curve (40A). https://www.amazon.com/LANGIR-Protection-Miniature-Breakers-Generation/dp/B06XF1YG12/ref=sr_1_20?dchild=1&keywords=Solar%2BBreaker%2B40A%2B200VDC&qid=1591479674&sr=8-20&th=1, accessed: June 7, 2020

¹¹ Renogy. LITHIUM IRON PHOSPHATE BATTERY 12 VOLT 50 AH. SKU: RNG-BATT-LFP-12-50. <https://www.renogy.com/lithium-iron-phosphate-battery-12-volt-50-ah/>, accessed: June 6, 2020

¹² Renogy. 20A/30A/40A/60A/100A ANL FUSE SET W/ FUSE RNG-SET-ANL40. <https://www.renogy.com/20a-30a-40a-60a-100a-anl-fuse-set-w-fuse/>, accessed: June 7, 2020

¹³ Renogy. ROVER ELITE 40A MPPT SOLAR CHARGE CONTROLLER SKU: RCC40RVRE-G1. <https://www.renogy.com/rover-elite-40a-mppt-solar-charge-controller/>, accessed: June 7, 2020

Components displayed in the power block diagram were chosen by using specifications listed in the power budget. With the power block diagram as a high-level visual reference, design decisions, tests, and results will be discussed starting from the solar panels and ending with voltage regulator circuits. The components that utilize the voltage regulator circuits are discussed in subsequent sections.

Solar Panel Array Sizing and Selection

Solar power was chosen to fulfill the team-client constraint of providing power to electrical components despite the Homeless Garden Project's off-grid location. The charging station utilizes solar panels because the Homeless Garden Project is located in an area that receives large amounts of solar energy. The Homeless Garden Project location has no large building obstructions or shaded areas which makes solar power a convenient source of energy. Furthermore, solar panels have been installed at the location and have proven successful in powering lights and heating water for the staff workers. This provides a warrant for the usage of solar panels as a power supply for the charging station. Selection of solar panels also applies to the team-client constraint of positioning power devices in an area that does not affect the client's day-to-day operations.

The power output requirement of the solar panels was determined by estimating the average expected daily load of the charging station and accounting for different issues that affect solar energy conversion. The average expected daily load was calculated to be 415.5Wh and the average expected daily load with increase was calculated to be 407.5Wh. The client did not set a constraint on the minimum allowable number of days to charge the backup battery. This project allows for two days to completely charge the battery while also providing power to components since an MPPT charge controller will maximize the charge rate of the battery. Since this project uses a lithium iron phosphate battery, the battery efficiency was set to 95%. This represents the common efficiency for a LiFePO₄ battery. The derating factor due to temperature was set to 90% as this is common for LiFePO₄ batteries. The required energy input per day was then calculated as follows:

$$\frac{[(\text{total average daily load with increase} + (\text{required usable energy storage} / \text{allowable days to recharge}))]}{\text{battery efficiency}}$$

The required energy input per day equated to 714.9Wh when the required usable energy was set at 407.5Wh. Solar insolation is the amount of electromagnetic energy incident on the surface of the earth. The average GHI solar insolation for Santa Cruz is 4.8 kWh/m²/day according to the United Nations Environment Programme's Solar and Wind Energy Resource Assessment. The variation of solar energy for Santa Cruz is 35%. The derate factor for module temperature and for module age was set to the estimated 90%. This accounts for the loss in power output due to real-world conditions in comparison to the conditions under which a PV panel was rated. Dirt losses, manufacturing losses, and cable losses account for 5%, 3%, and 3% respectively. The optimal solar array size was then calculated by taking the required energy input and dividing it by the solar insolation, then dividing that by the derate factor for module temperature, then dividing that by the derate factor for module age, and then, lastly, dividing it again by the cable, dirt, and manufacturing losses. The final optimal solar array size was calculated to be 200.7DC-Watts at STC.

The solar panel array must also fit the constraints of the physical location of the Homeless Garden Project. The solar panel array is allowed to be as large as needed as long as they are installed on a foundation near the ground. Although if the solar panel array is to be installed on a roof of a structure at the location, the solar panels must fit the dimensions of that roof. Furthermore, the team is required to test the load bearing capacity of the structure that the solar panels are installed on. Both the electrical and mechanical requirements listed in this section are the main constraints for the system to utilize solar energy. The table below describes two solar panel options and their respective specifications. Specifications for the JA350W¹⁴ solar panel and the BP165W¹⁵ solar panel come from their respective datasheets.

Table 2: Datasheet Specifications Illustrate that Three BP 165W Series-Connected Panels can Provide High Battery Charge Rate

	JA 350W Solar Panels	BP 165W Solar Panels
Available Quantity	3	5
Max Rated Power	350W	165W
Nominal Voltage	36V	24V
Voltage at Max Power	38.72V	34.3V
Current at Max Power	9.04A	4.8A
Open Circuit Voltage	47.28V	44.2V
Short Circuit Current	9.52A	5.1A
Power Tolerance	+2%	±3%
Composition	Monocrystalline	Polycrystalline
Dimensions (LxWxD)	77.5in x 39.1in x 1in	62.7in x 31.1in x 2in
Weight	61.7 lbs.	33.95 lbs.
Operating Temp. Range [Celsius]	-40 to +85	-40 to +85

*All quantities tested at 20 degrees Celcius as the Nominal Cell Operating Temp (NCOT).

Assuming the use of an MPPT charge controller, which will be discussed in a later section, we can convert voltage from the solar panel to maximize current output. Using one JA 350W solar panel, which has a maximum power voltage of ~39.0V and an output current of ~9.0A, we can charge the 12V battery referenced in the *Power Block Diagram* (that is rated for a 50A charging rate) at an optimized current of 29.25A. By connecting three BP 165W solar panels in series, which each have a maximum power voltage of ~35.0V and an output current of ~5.0A, the station can charge a 12V battery (that is rated for a 50A charging rate) at an optimized current of 43.7A.

This project uses the three BP165W solar panels connected in series due to the higher maximum output current capability and physical dimension and weight constraints. The three solar panel array is warranted because the higher charge rate allows for the battery to be charged quickly and most effectively

¹⁴ JA Solar, Shanghai JA Solar Technology Co., Ltd., <https://www.jasolar.com/uploadfile/2018/0927/20180927022927653.pdf>, accessed: June 6, 2020

¹⁵ BP Solar, BP Solar Pty Ltd 2005, https://www.solarpanelsaustralia.com.au/downloads/bpsolar_bp_3165.pdf, accessed: June 6, 2020

even during low sunlight hours. This system charges the battery in about two hours if the maximum output from the solar panel array is reached for two hours. Even though the system is rated to allow the battery to charge over a span of two days, according to the power budget sizing worksheet, the disadvantages of having the larger array are insignificant. This is because the main disadvantage is space in which the solar panels would occupy as three BP165W solar panels would have a total surface area of ~45ft². There is no team-client determined restraint on the amount of area occupied by the solar panel array and the three solar panels would be donated, so therefore, the power system would only be benefitted from having a higher charge rate. The high charge rate is also prioritized over other requirements due to days with low solar power input. For instance, using three solar panels connected in series would provide three times the energy during a given day with little solar irradiation. Therefore, during certain days with low solar irradiation, a single BP165W or JA350W solar panel would be unable to charge the battery over two days. This, of course, depends on how little of solar energy input is available. Although note that there are no disadvantages to having a three solar panel array that outweigh the benefit of a higher charge rate for the battery. In terms of scaling this system for other projects, if there is an area restriction or cost of solar panels restriction, the charging station would be more effectively served by using a single BP165W solar panel or a single JA350W solar panel as the power requirements would be met while using less expensive and smaller resources.

Charge Controller Selection

The charge controller relates to the team-client goal of powering all components for 24 hours during low to zero solar energy conditions. This is because the charge controller provides a safety measure while charging by preventing over-charge while also optimizing the rate at which the battery is charged. The charging station uses a Maximum Power-Point Tracking (MPPT) charge controller because of the higher maximum output current created by the current multiplier. By connecting three BP 165W solar panels in series, with each having a maximum power voltage of ~35.0V and an output current of ~5.0A, the station can charge a 12V battery (that is rated for a 50A charging rate) at an optimized current of 43.8A as noted in the previous section on solar panel array sizing. This value is derived¹⁶ by taking the maximum voltage of the solar panel array (35V * 3 panels in series = 105V) and dividing it by the voltage rating of the battery (105V * 12V = 8.75). This new value represents the current multiplier which increases the current output (8.75 * 5A = 43.8A). Using the Renogy Rover Elite 40A MPPT Solar Charge Controller, the station limits the charging down to a maximum rate of 40A, but this is still 80% of the charge rating of the Renogy 12V, 50Ah Lithium Iron Phosphate battery we chose to utilize. Therefore, the charging station utilizes a Renogy Rover Elite 40A MPPT Solar Charge Controller to control the charge rate for the battery. This supports the fulfillment of the team-client goal to power devices in low to zero solar energy conditions for 24 hours.

Circuit Breaker Options and Safety Ratings

Circuit breakers help to maintain the lifespan of the charging station while also providing safety to the power systems. According to a reference¹⁷ from a solar panel distributor, there are two locations in

¹⁶ Adam Dischino. *MPPT Charge Controllers Upgrades Help Compensate for Less Winter Sun*. altE Store. February 13, 2015. https://www.altestore.com/blog/2015/02/upgrade-to-a-mppt-charge-controller-to-get-more-power-now/#:~:text=MPPT%20charge%20controllers%20have%20the,higher%20voltage%20into%20additional%20current.&text=18%20%C3%B7%2014V%20%3D%201.28%20Current.3.57%20Amps%20%3D%2050.03W_, accessed: June 6, 2020

¹⁷ Stephen Clifton. "How to Fuse your Solar System", Renogy Solar. October 5, 2016, <https://www.renogy.com/blog/how-to-fuse-your-solar-system/>, accessed: June 6, 2020

the charging station's power system that require circuit breakers when the system is not tied to the grid. The circuit breaker and fuse are necessary to maintain functionality while preventing current surges that will damage the system components.

The first location that requires a circuit breaker, as outlined in the power systems block diagram, is between the solar panels and the charge controller. This is to prevent current from surging into the charge controller from the solar panels. To find the current rating of the breaker in this location, we consider the three 24V, 165W panels that are connected in series to power the system. The current rating is calculated by taking the power and dividing it by the maximum output voltage ($165\text{W} / 35\text{V} = 4.71\text{A}$) and then multiplying it again by a 25% safety factor, which was defined to be a common safety factor used in industry. The current of 4.71A was verified to be the current at maximum output voltage with 20 degrees Celsius being the Nominal Cell Operating Temperature (NOCT). The maximum output voltage is used in these calculations to verify safety during maximum power output conditions. Thus, the final calculation is as follows, ($4.71\text{A} * 1.25 = 5.88\text{A}$). We round this result to 10A which tells us that the circuit breaker in this location is required to be 10A. Furthermore, we consider the maximum output voltage of the solar panel array to be the maximum output voltage of one solar panel multiplied by three which gives us an output voltage of 105V. Multiplying this result by the safety factor gives us the voltage rating for our circuit breaker which is ($105\text{V} * 1.25 = 131.25\text{V}$). We will round this to 130V for the voltage rating of the circuit breaker.

The second location requires a fuse between the charge controller and the battery. The current rating for this fuse was calculated by simply matching the current rating on the charge controller. Therefore, the minimum required current rating for this circuit breaker is 40A when using the Renogy Rover Elite 40A MPPT Solar Charge Controller.

It is also important to note that these values are based on NOCT of 20 centigrades. The month with the hottest average temperature in Santa Cruz is September at 26 centigrades and the month with the coldest average temperature is December at 16 centigrades¹⁸. The solar panel array will operate more efficiently during the colder months but not above the nominal ratings, which means that the current and voltage ratings for the breaker and fuse are still appropriate. Meanwhile, during the warmer months, the efficiency of the system will decrease due to heat loss despite the increase in the number of days with high solar irradiance. This is shown in the I-V curve of the BP165W solar panel datasheet¹⁹. Ultimately, since the calculations for the breaker and the fuse were taken at nominal power conditions, the selected components operate as designed.

The circuit breaker and the fuse help to fulfill the lifespan, electrical interface, and safety team-client goals mentioned in the introductory chapter.

¹⁸ US Climate Data. Climate Santa Cruz - California. US Climate Data 2020. <https://www.usclimatedata.com/climate/santa-cruz/california/united-states/usca1020>, accessed: June 6, 2020

¹⁹ BP Solar, BP Solar Pty Ltd 2005, https://www.solarpanelsaustralia.com.au/downloads/bpsolar_bp_3165.pdf, accessed: June 6, 2020

Battery Sizing Requirements and Design Decisions

The battery is the main component that allows for the powering of devices in low to zero solar energy conditions for 24 hours. Using the information that is listed in the power budget based on component data sheets, an appropriate battery was sized to supply power to the system during the evening or for 24 hours of low to zero solar energy conditions. Note that the battery selected is a lithium iron phosphate battery that is constrained to two days of recharging and one day of complete powering to devices according to load estimates. The battery sizing worksheet is displayed in the figure below.

Figure 7: Battery Sizing Worksheet v16 (April 3, 2020) using information from the power budget

SlugCharge Sizing Design Calculations			
Enter Average Daily Loads & Inverter Efficiency		How to Calculate:	Common Values
Average DC Daily Load (Wh):	407.2	refer to load estimator worksheet	
Average AC Daily Load (Wh):	0		
Inverter efficiency (%):	100%	relevant for AC loads	85% Depends on MPPT vs PWM; peak efficiency is not the same as general operating efficiency 80% - 99%
Charge Controller Efficiency (%):	98%	relevant for DC loads	97% 80% - 99%
Total Average Daily Load (Wh):	415.5	DC load + (AC load / inverter efficiency)	
Find Total Daily Load from Load Calculations:			
Expected Load Increase (%)	0%	oversize factor	0% 30-50%
Total Average Daily Load With Increase (Wh):	407.2	Total Average Daily Load) * (1 + Expected Load Increase)	for net zero when using PG&E bill when accounting for suppressed demand
Continue if your system design includes battery storage:			
Find Required Amount of Usable Energy Storage			
Desired Days of Autonomy:	1.0	1 day = total load consumed in 24 hr period.	1-3
Required Usable Storage (Wh):	407.2	Total Average Daily Load with Increase * Desired Days of Autonomy	
Find Required Energy Storage Capacity:			
Allowable Depth of Discharge (%):	80%	Recommended LiFePO4 20-50%	Pb-Acid 80% 50%
Required Energy Storage (Wh):	509.0	Required Usable Storage / Allowable Depth of Discharge	
Battery Bank Voltage (V)	12	input system voltage	12, 24, 48 V
Battery Capacity Required (Ah)	42.4		

From the battery sizing worksheet, note that the charging station has an estimated average daily load of 415.8Wh. The battery should be able to fully charge over a maximum of two days and power the entire system's expected usage for a given day without solar energy. Furthermore, the battery bank voltage is required to be 12V and the resulting battery capacity is calculated to be 42.4Ah. This is rounded to 40Ah.

This means that the main requirements for the battery is that it is a 12V, 40Ah battery. The charging station fulfills this requirement by utilizing a Renogy 12V, 50Ah Lithium Iron Phosphate battery²⁰ with a maximum charge and discharge rate of 50A. This battery accomplishes the team-client goals for powering all internal components and 24 phones during a given day with low to zero solar energy. It can also discharge at a 50A rate which means that 6 phones can receive 2A of charge while all

²⁰ LITHIUM IRON PHOSPHATE BATTERY 12 VOLT 50 AH. SKU: RNG-BATT-LFP-12-50. <https://www.renogy.com/lithium-iron-phosphate-battery-12-volt-50-ah/>, accessed: June 6, 2020

the internal components are still powered. The power budget outlines the current draw for all the devices and is used to verify that the power system satisfies the current draw constraint of the charging station.

The station uses a battery with Lithium Iron Phosphate composition because this battery composition is rated for a high efficiency rate usually near 95%. Furthermore, LiFePO₄ batteries have a long lifespan. In this case the battery that is listed has a lifespan of 2000 cycles at 80% DoD. DoD represents the Depth of Discharge and it defines the amount of energy that can be discharged from the battery in comparison to the capacity of the battery. The Renogy 12V, 50Ah LiFePO₄ battery can discharge 80% of its 50Ah capacity for 2000 cycles before it deteriorates below 80% DoD.

Verification of the Power Systems Design

The power systems design has been verified by simulating the system through real and varying weather conditions. The most important output requirements that must be fulfilled are the output current of approximately 40A and the output voltage of approximately 12.8V. These two values are chosen as the verification values because 40A represents a high, yet safe, charge rate for the battery and 12.8V represents the nominal voltage. The following chapter shows that the output of the power systems design fulfills those output voltage and current requirements which verifies the design. The two most important inputs for a solar panel array to generate power is solar irradiance and temperature. Solar irradiation is the amount of electromagnetic radiation received from the sun per unit area (usually square meters)²¹. In general, a higher amount of solar irradiance helps in providing more solar energy input into the PV array. Temperature also affects the performance of the solar panel array as it changes the efficiency of the solar panel's ability to convert PV energy into power for the charging station²².

The entire power system was simulated using MATLAB Simulink by inputting real weather conditions in Santa Cruz over a 24-hour period to find the output of the solar panel array after energy is converted through the MPPT charge controller and inputted into the battery. The simulation takes into account all the specifications from the BP165W solar panels²³ and the specifications from the Renogy 12V, 50Ah Lithium Iron Phosphate battery²⁴. Furthermore, using the MPPT charge controller which bucks the voltage to boost the current, the system output shows the high output current during simulation.

The power system model has been constructed using systems and subsystems. The highest level of the system is the high-level diagram of the entire system with blocks for PV array, battery, and charge controller. This diagram is shown in the figure below.

²¹ Kevin Addison. *Solar Irradiance*. June 6, 2008. NASA. https://www.nasa.gov/mission_pages/sdo/science/Solar%20Irradiance.html, accessed: June 6, 2020

²² Boston Solar, *How do temperature and shade affect solar panel efficiency?*. [https://www.bostonsolar.us/solar-blog-resource-center/blog/how-do-temperature-and-shade-affect-solar-panel-efficiency/#:~:text=The%20temperature%20coefficient%20tells%20you,C%20\(77%C2%B0F\).&text=Conversely%2C%20for%20every%20one%20degree,panel%20will%20increase%20by%200.38%25](https://www.bostonsolar.us/solar-blog-resource-center/blog/how-do-temperature-and-shade-affect-solar-panel-efficiency/#:~:text=The%20temperature%20coefficient%20tells%20you,C%20(77%C2%B0F).&text=Conversely%2C%20for%20every%20one%20degree,panel%20will%20increase%20by%200.38%25).

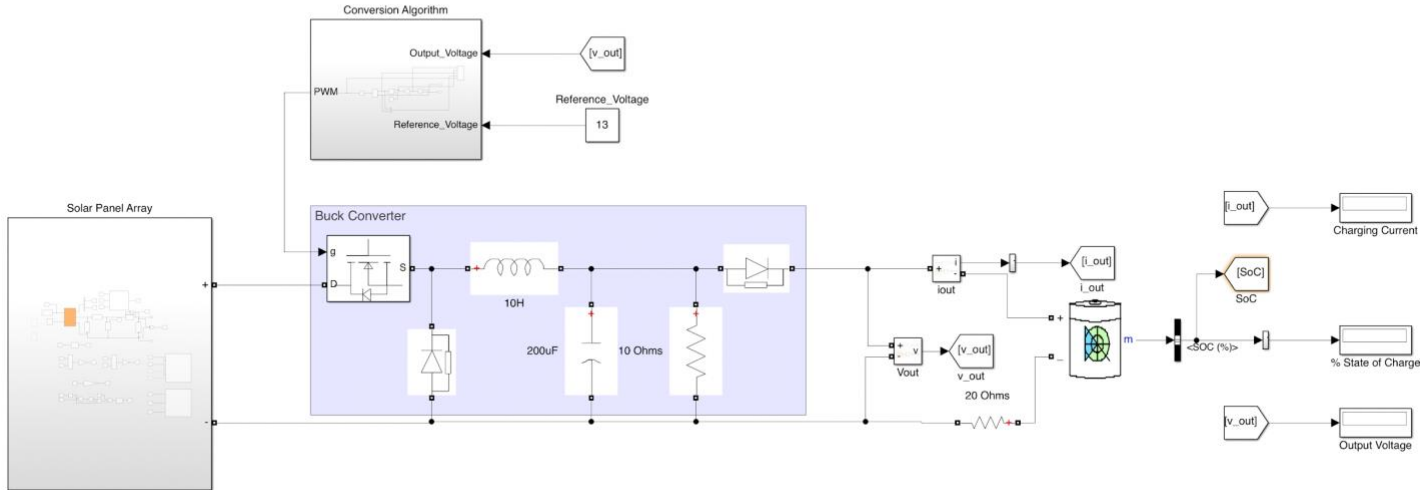
²³ BP Solar, BP Solar Pty Ltd 2005, https://www.solarpanelsaustralia.com.au/downloads/bpsolar_bp_3165.pdf, accessed: June 6, 2020

²⁴ LITHIUM IRON PHOSPHATE BATTERY 12 VOLT 50 AH. SKU: RNG-BATT-LFP-12-50. <https://www.renogy.com/lithium-iron-phosphate-battery-12-volt-50-ah/>, accessed: June 6, 2020

Figure 8: Verification of the power system through simulation in MATLAB Simulink

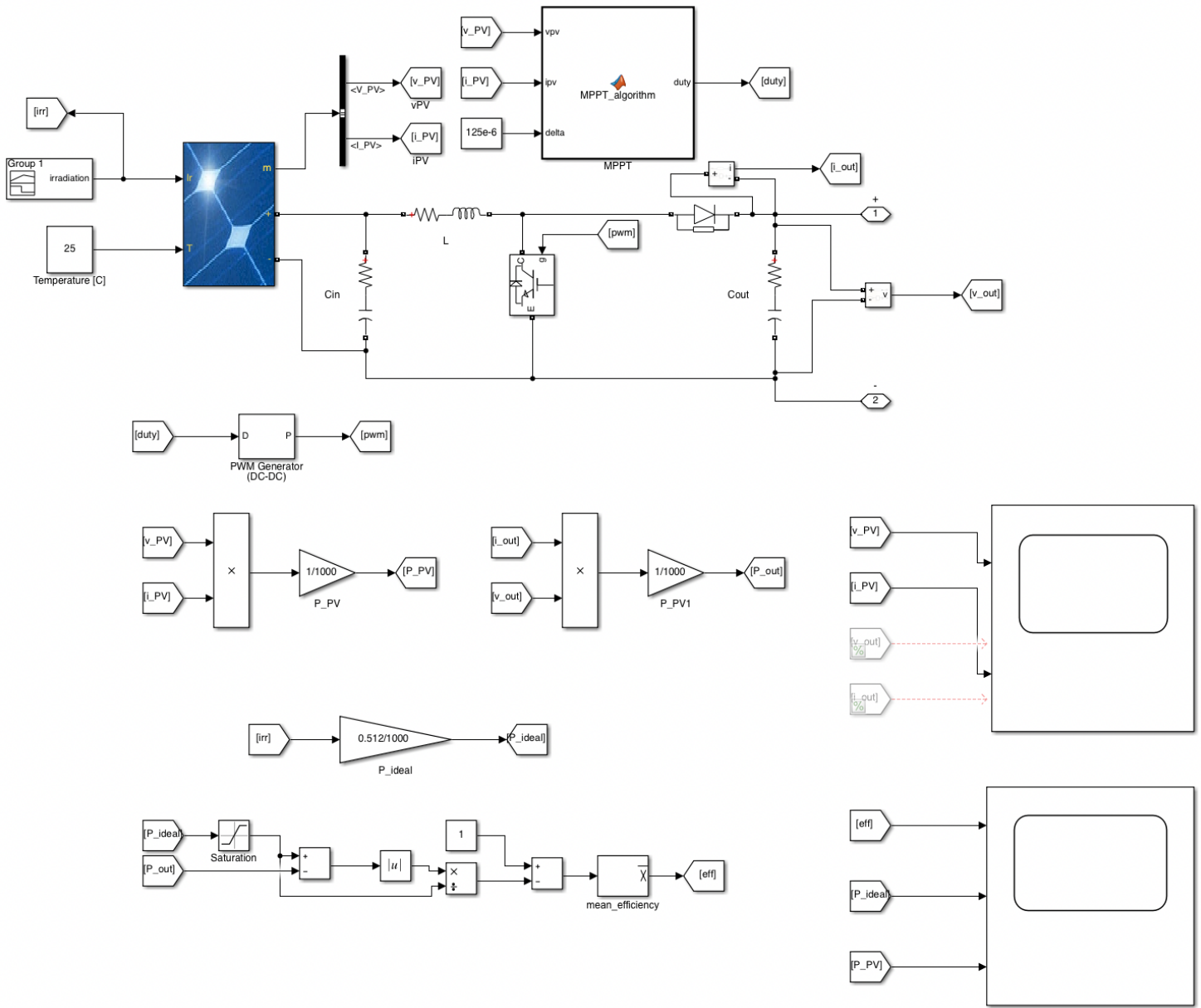
SlugCharge PV Solar Array with MPPT Charge Controller MATLAB Mathematical Modeling and Simulation
Rev. 4, Date: May 30, 2020

Jordan Tam

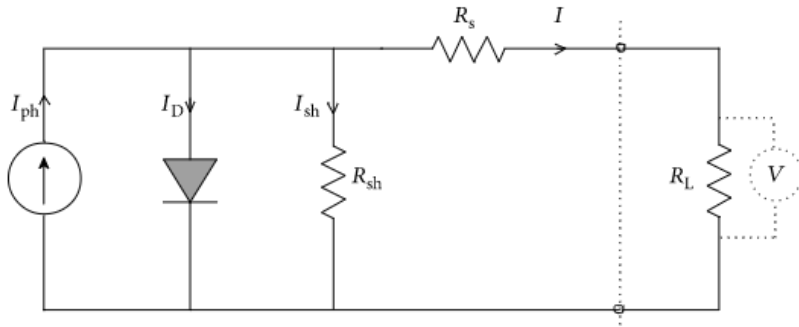


Within the Solar Panel Array are multiple blocks that dictate the structure of the system. The solar panels themselves and the MPPT charge controller and algorithm are located within this subsystem. Scopes are used to check the efficiency and the output current, voltage, and power of the array after using the MPPT for conversion. The figure below shows the diagram for the entire PV array with MPPT controller.

Figure 9: The Solar Panel Array subsystem is modeled to examine output specifications and efficiency of the solar panels after MPPT charge controller conversion



The solar panel array is constructed using the single diode model of a solar PV system. When the p-n junction of a solar cell is illuminated, the junction becomes forward biased producing photogenerated current. The circuit ultimately looks like the following diagram which shows the creation of the photogenerated current, I_{PH} .

Figure 10: Photogenerated current is created from the p-n junction of a solar cell being illuminated

The following table of values are important to the simulation of the solar PV system. Each value has a definition of what the variable term means as well as an assigned value if the term is a constant. The table is shown below.

Figure 11: Values and constants used for proper simulation of the solar panel model

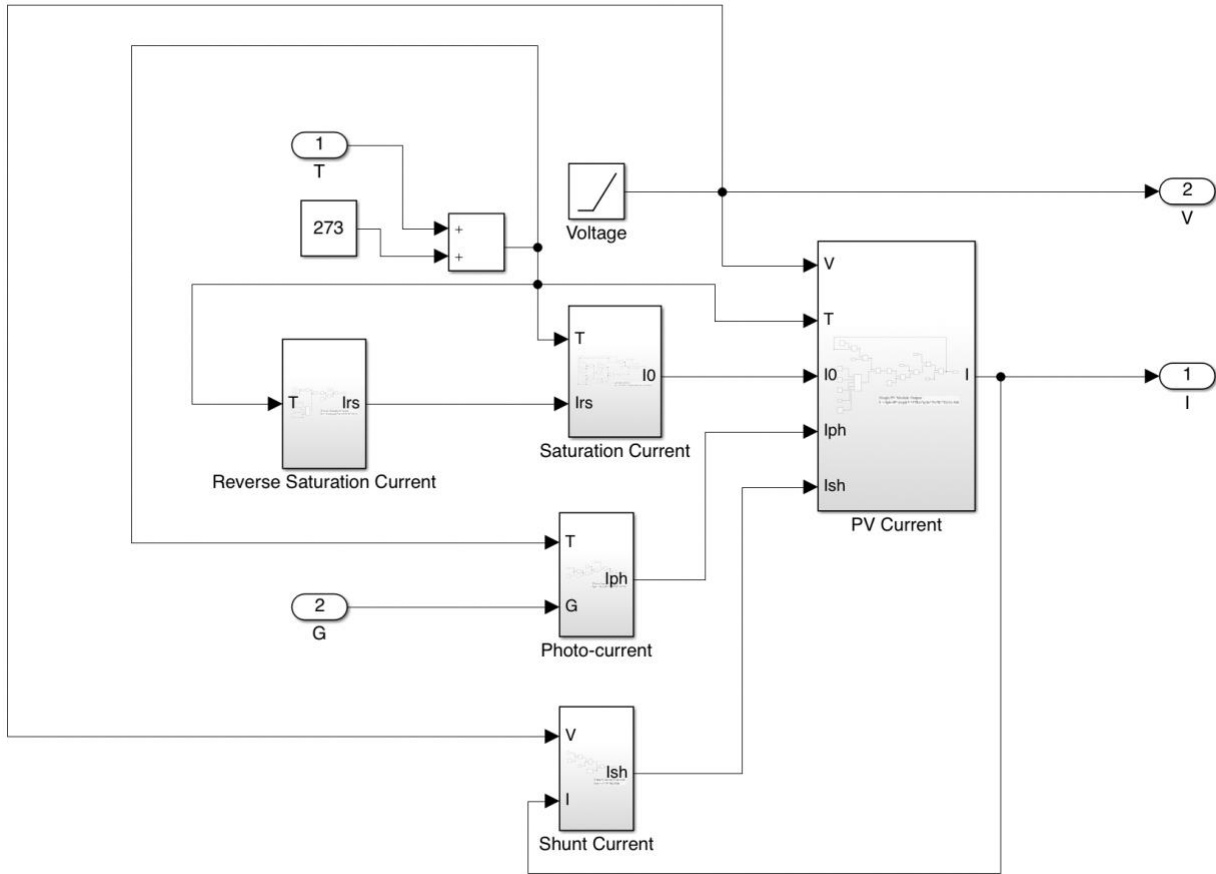
I_{ph}	photo-current (A)	I_{ph}
I_{sc}	short circuit current (A)	I_{sc}
k_i	short-circuit current of cell at 25°C and 1000 W/m ²	.0032
T	operating temperature (K)	T
T_n	nominal temperature (K)	298
G	solar irradiation (W/m ²)	G
q	electron charge (C)	1.6×10^{-19}
V_{oc}	open circuit voltage (V)	V_{oc}
n	the ideality factor of the diode	1.3
K	Boltzmann's constant (J/K)	1.38×10^{-23}
E_{g0}	band gap energy of the semiconductor (eV)	1.1
N_s	number of cells connected in series	N_s
N_p	number of PV modules connected in parallel	N_p
R_s	series resistance (Ω);	.221
R_{sh}	shunt resistance (Ω);	415.405
V_t	diode thermal voltage (V).	----

Furthermore, the battery that is used in this design has a nominal voltage of 12.8V, a capacity of 50Ah, a composition of LiFePO₄, a cutoff discharge voltage of 9.6V, a cutoff charge voltage of 14.9V, a nominal discharge current of 21.7A which is ideal for the current draw requirement of the system, an internal resistance of 0.002 Ohms, and a nominal capacity of 45.2Ah which still fulfills the energy reserve requirement that was calculated to be 40Ah at 12V.

The solar panel array has one parallel string with three solar panel modules connected in series. The specifications for each solar panel are found in the column for the BP165W solar panel in *Table 2* of this report.

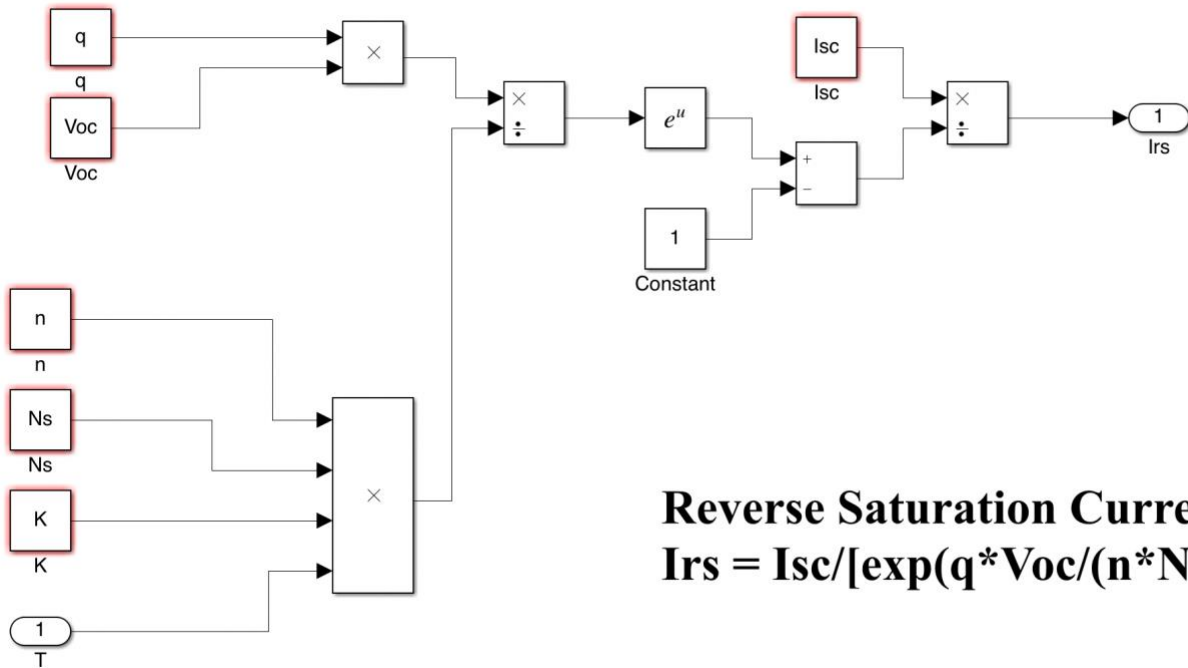
The PV model of the actual solar panel itself is shown in the following figure.

Figure 12: Connections between current created from a single solar panel



The reverse saturation current, is the part of the reverse current in a semiconductor diode caused by diffusion of minority carriers from the neutral regions to the depletion region. The reverse saturation current was modelled using MATLAB with the equation shown in the following figure.

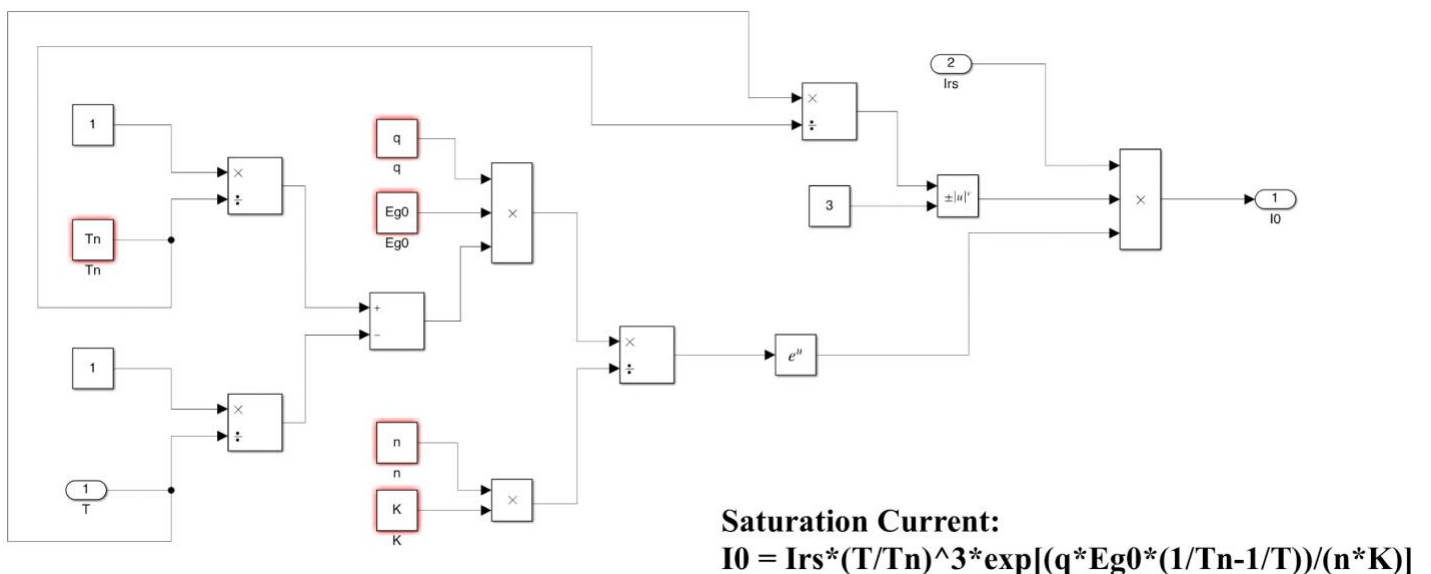
Figure 13: Reverse saturation current is created by diffusion of minority carriers from neutral regions to the depletion region



Reverse Saturation Current
 $I_{rs} = I_{sc} / [\exp(q * V_{oc} / (n * N_s * K * T)) - 1]$

The reverse saturation current is an input to the saturation current, which is simply the maximum current that can be obtained in the circuit. The model for this current is seen in the following figure.

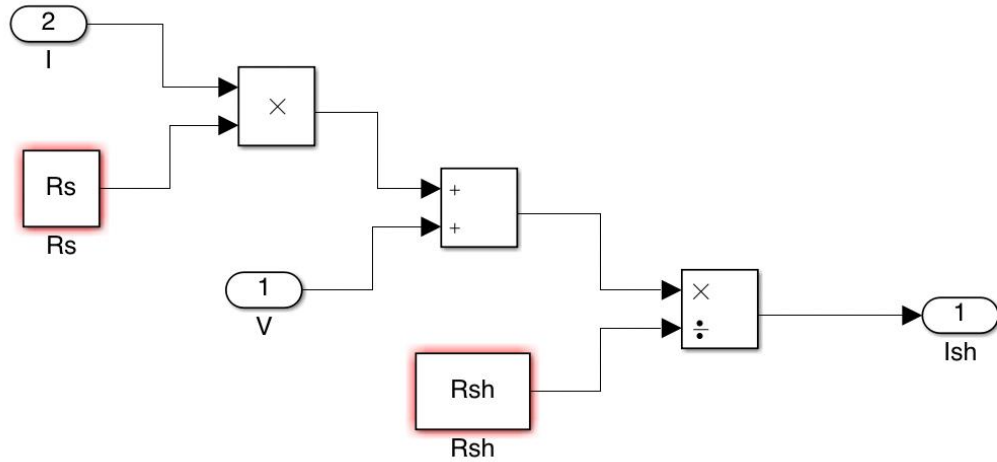
Figure 14: Saturation current model receives input from the reverse saturation and temperature to define the peak current



Saturation Current:
 $I_0 = I_{rs} * (T/T_n)^3 * \exp[(q * E_{g0} * (1/T_n - 1/T)) / (n * K)]$

Shunt current is also important to note as it is the current flowing through the shunt resistor. This shunt current subtracts from the total photogenerated current to create the output current. The shunt resistance is part of the solar panel itself but is usually very large so that little current flows through the shunt resistor and instead it flows to the load. In this case, the shunt resistance is ~415 Ohms while the series resistance is ~0.2 Ohms. This simply means that almost all the current flows to the load. The model for the shunt current is shown in the figure below.

Figure 15: The shunt current is modelled to flow through a high resistance so that the current flows through the series resistance and, subsequently, the load



Shunt Current Current: $I_{sh} = (V + I * R_s) / R_{sh}$

The last input current into the PV model is the photogenerated current created from illuminating the p-n junction of the solar cell which is modelled using a single diode. The mathematical model for the photogenerated current is shown in the figure below.

Figure 16: Photogenerated current is created by the p-n junction of a solar cell being illuminated by solar light energy

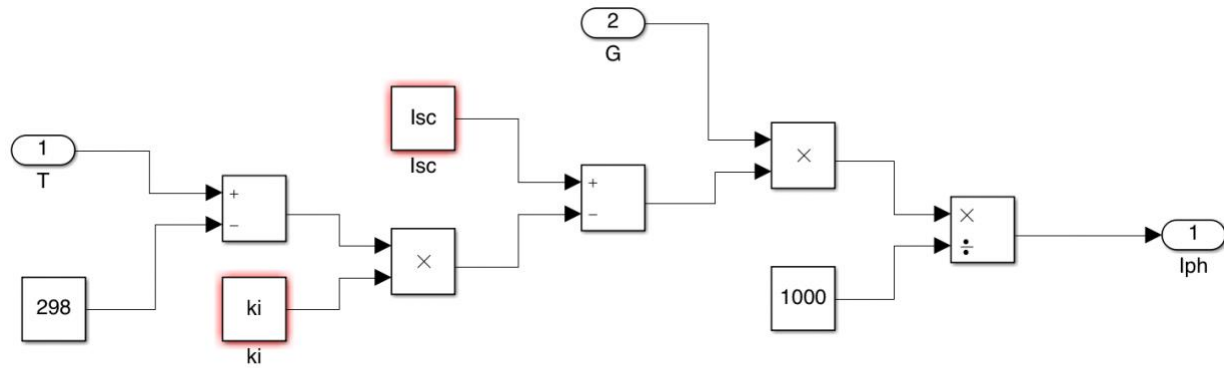
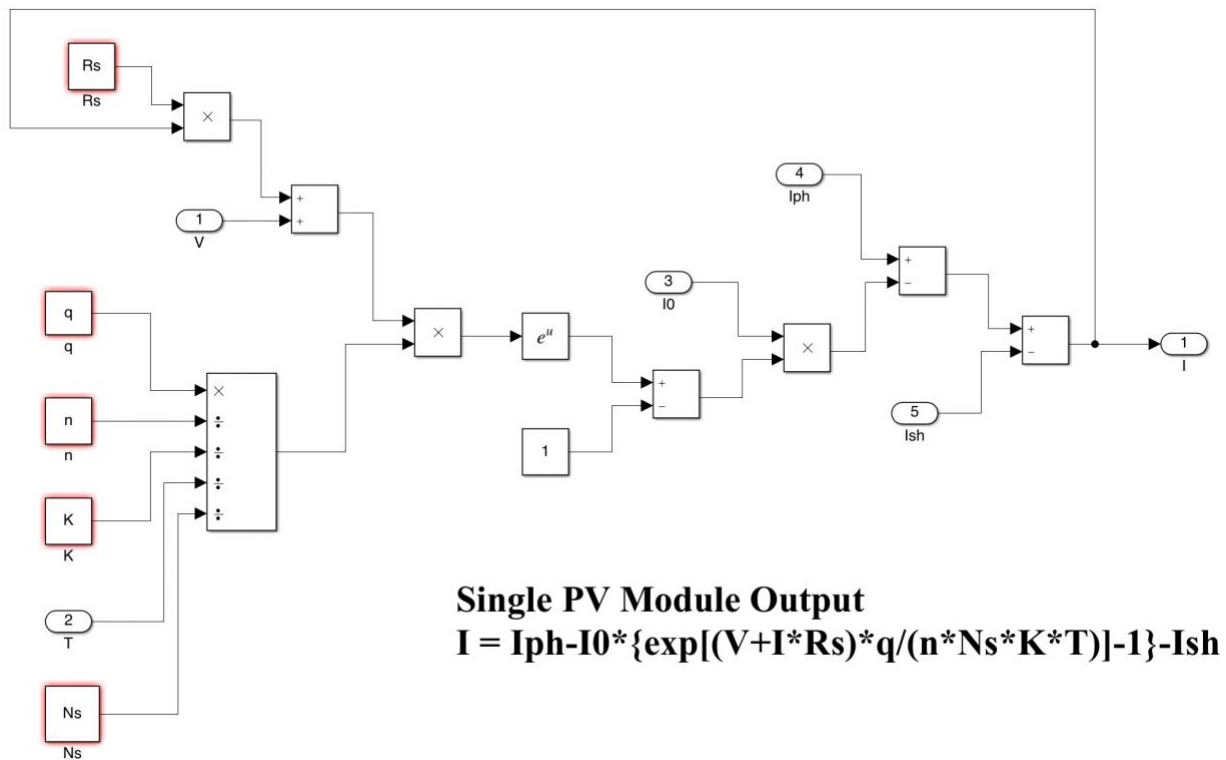


Photo-Current Current:
 $I_{ph} = \{I_{sc} + [k_i * (T - 298)]\} * G / 100$

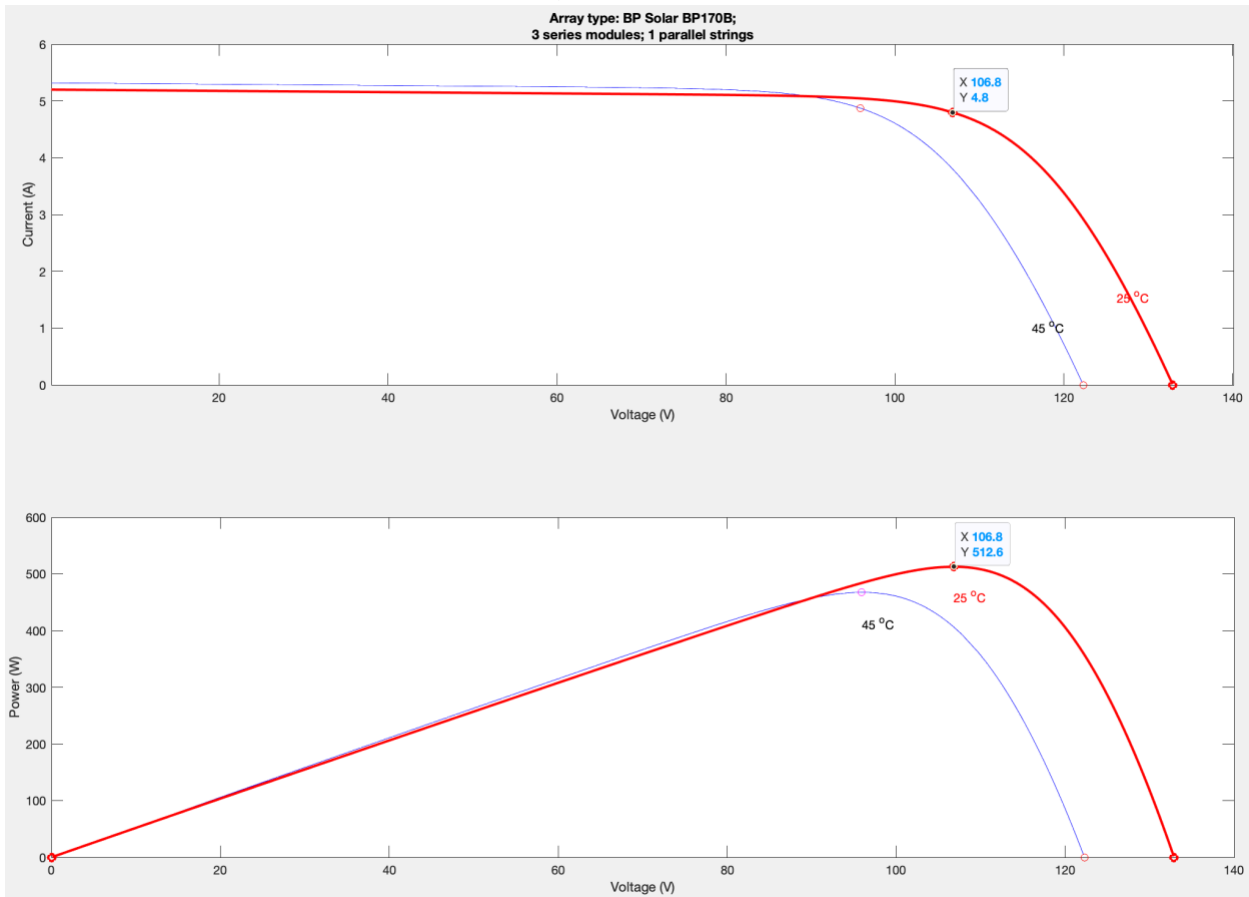
Finally, the PV module takes the currents as inputs and uses the equation listed in the figure below to calculate the output current from the PV module. This output current is modelled in the figure shown below.

Figure 17: Output current is created by using the photogenerated current and subtracting from it using the other modelled currents



The station output specifications that are important to the verification of the power systems design include the following: power output from the solar panel array, efficiency of the solar panel array, output current and voltage from the solar panel array, and the output current and voltage of the entire power system after the MPPT charge controller and voltage buck conversion and current boost conversion. The verification results from the simulation of the power system was compared to the ideal I-V and P-V curves tested at STC (20 centigrades and 1000 W/m²) for the selected solar panel. The curves can be seen in the figure below.

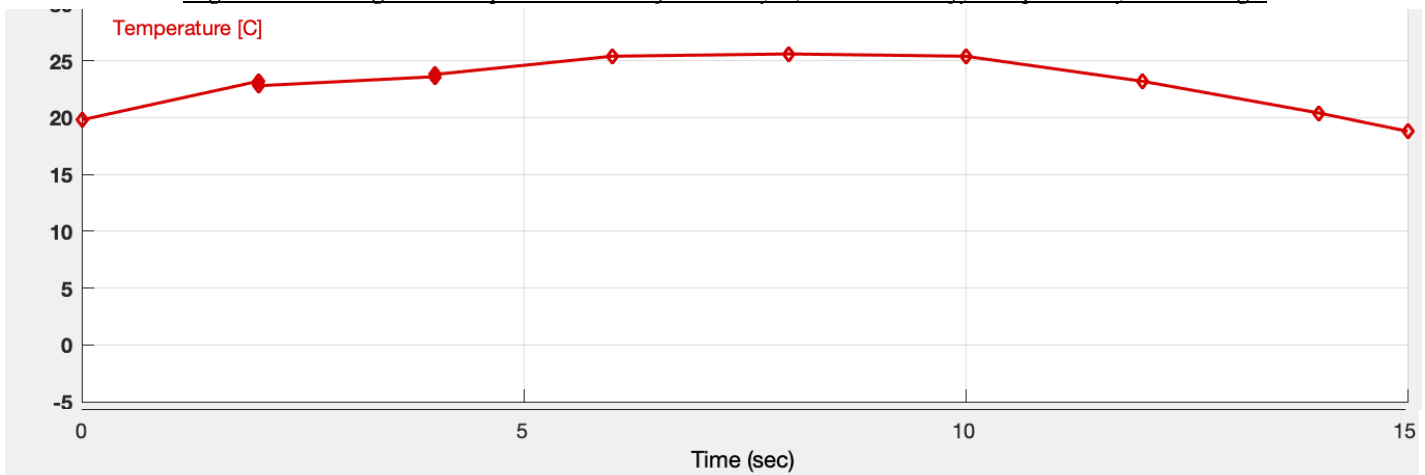
Figure 18: Using the ideal I-V and P-V curves to verify the results of the simulation of the power systems using real conditions



Note from these graphs that the short circuit current is just above 5A and the open circuit voltage is just above 130V. The maximum power was found at a voltage of 106.8V and the current at 4.8A. The maximum power is shown in the second graph at 512.6W. These values are important as they are used in comparison to the tested output voltage, current, and power. The output results should be similar to these ideal specifications for the power system to be verified.

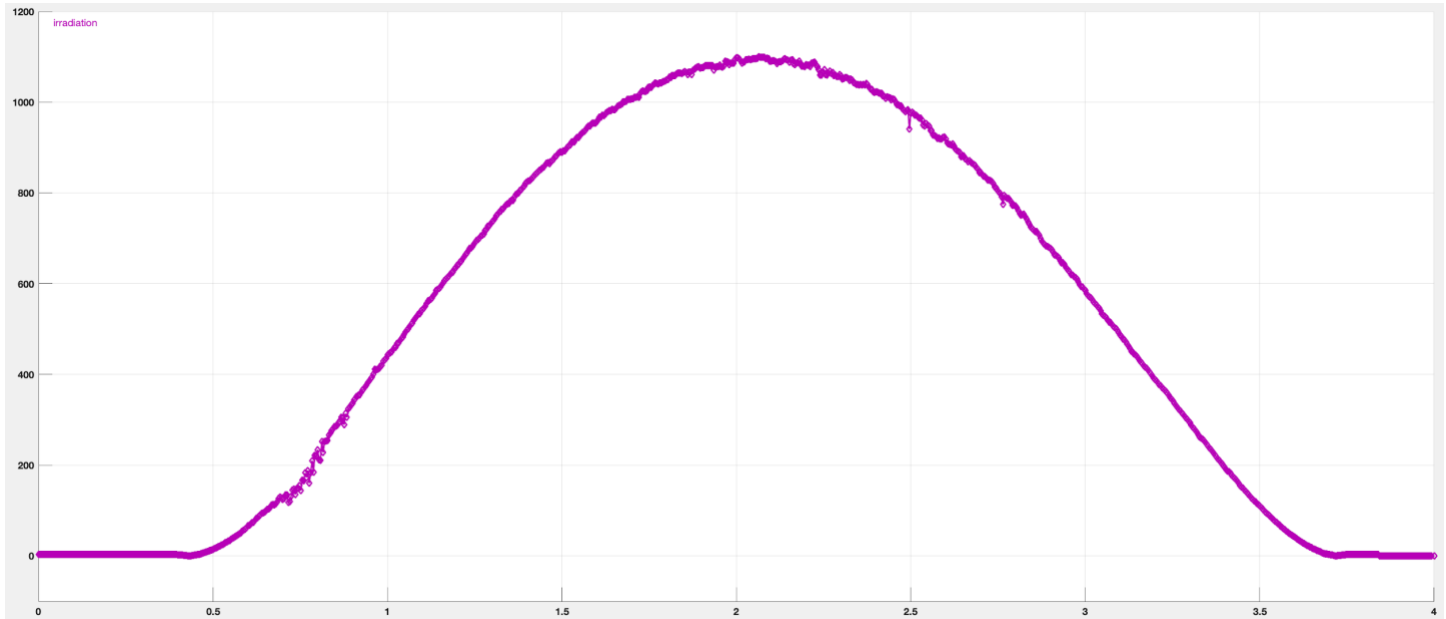
For the simulation, real weather conditions of temperature and irradiance from Santa Cruz on May 7, 2020²⁵ are used. The following graphs are signals created for the temperature and irradiance. The temperature signal sets time from 5AM-8PM. Thus, the zero point is 5AM, the five point is 10AM, the ten point is 3PM, and the fifteen point is 8PM.

²⁵ National Renewable Energy Laboratory, NREL Solar Radiation Research Laboratory (BMS). May 7, 2020. <https://midcdmz.nrel.gov/apps/plot.pl?site=BMS;start=20200101;edy=31;emo=12;eyr=9999;year=2020;month=05;day=7;time=1;zenloc=222;inst=3;inst=60;inst=74;type=plot>, accessed: June 6, 2020

Figure 19: Using real temperature data from May 7, 2020 to verify the power system design

Note that temperature stays between approximately 20 centigrades and 25 centigrades which means that efficiency was still affected by temperature. This is reflected in the output results.

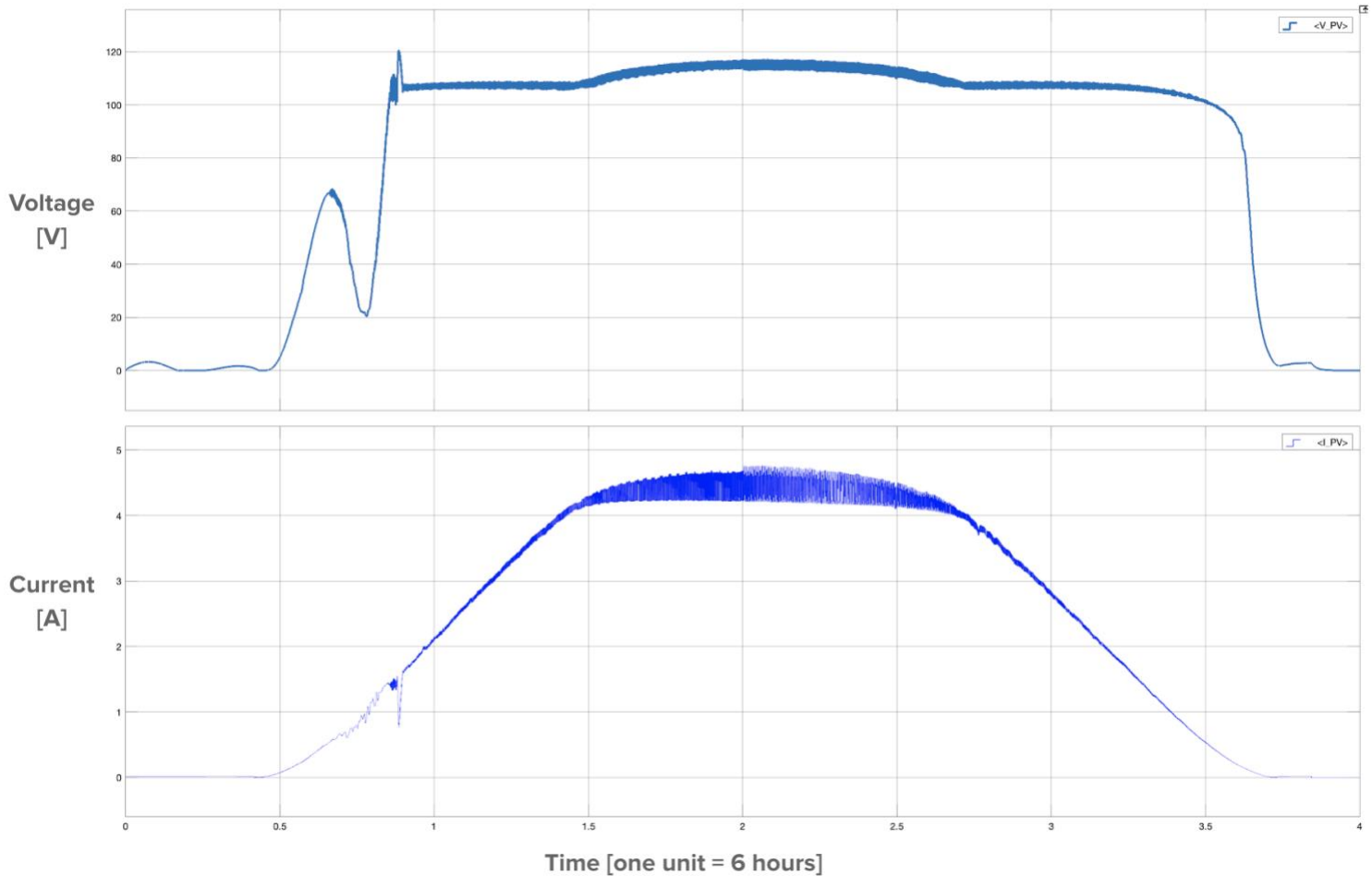
The simulation used a different signal for solar irradiance due to the volatile variation in the signal. The signal for irradiation can be seen in the following figure below. The zero point represents 12AM and each marker along the x-axis represents 6-hour increments until the four point which represents 12AM the next day.

Figure 20: Using real solar irradiance data from May 7, 2020 to verify the power system design

Note that irradiance is highest at noon. This makes sense because solar energy on days without clouds is highest during the middle of the day. This will be reflected in the output results as the output power is highest during the middle of the day.

After simulating the power system, the output voltage and output current of the solar panel array was recorded. The graphs for both current and voltage are shown in the figure below.

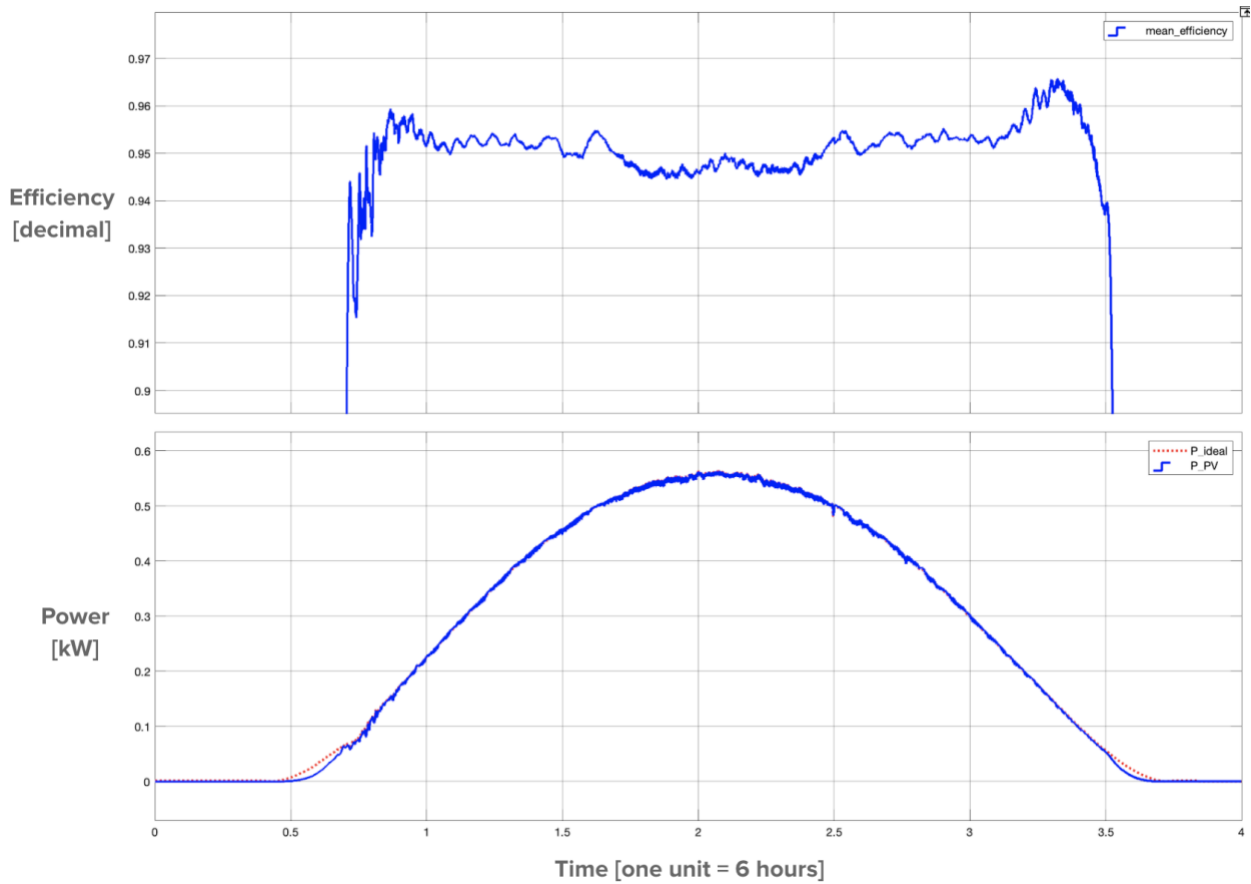
Figure 21: The output voltage and current simulation results verify the power systems design by nearly matching the ideal current and voltage for Maximum Power Point Tracking



Note that the output voltage rises to approximately 110V. This output voltage is compared to the voltage of 106.8V which represents the ideal output voltage from the previous P-V graph. The output current rises to approximately 4.5A during the peak of the day which is similar to the high output current from the ideal maximum power current of 4.8A. This means that the output voltage and current from the simulation results verify the power systems design because they are nearly identical to the ideal voltage and current for MPPT.

The output power was also recorded to be nearly the same as the ideal output power of 512.6W which was found from the ideal P-V curve of the solar panel array. The figure below shows the output power and the efficiency of the solar panel array.

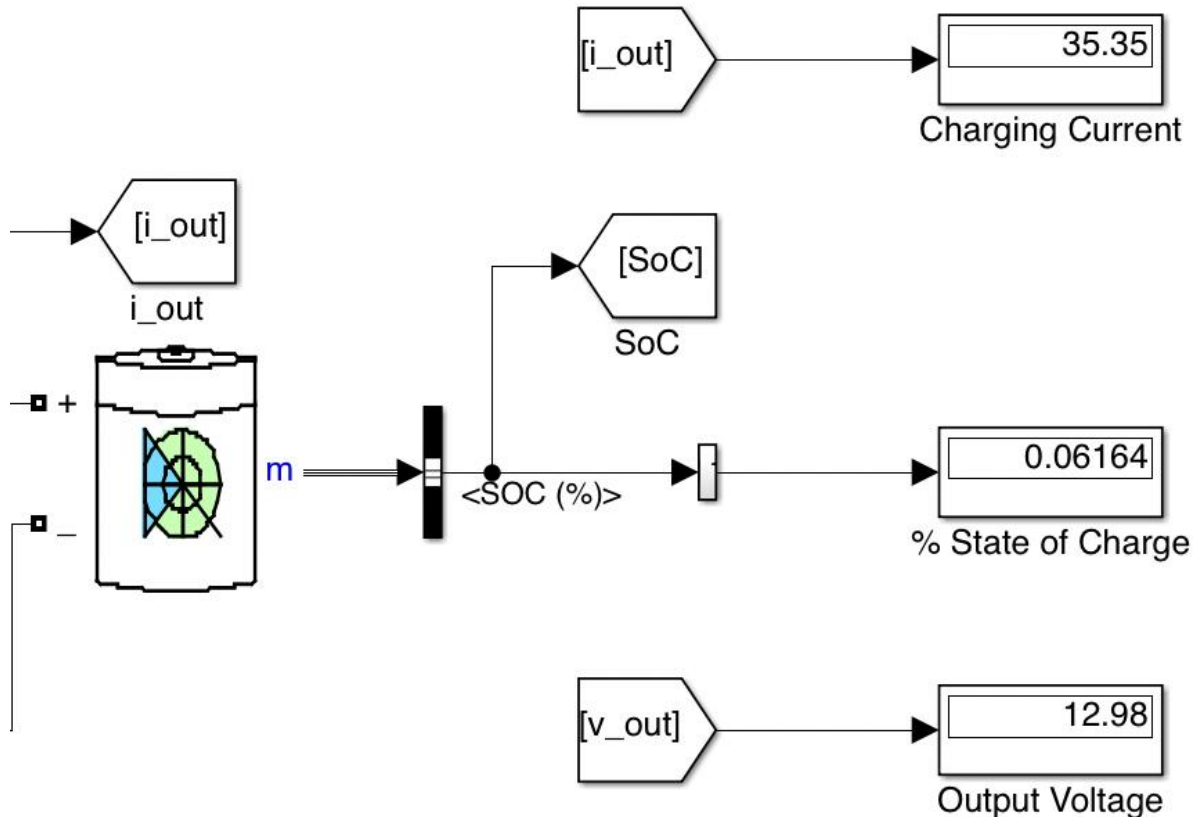
Figure 22: The resulting efficiency and output power from the simulation confirm MPPT and the verification of the power systems design



Note that the output voltage rises to a peak of approximately 550W which is higher than the ideal power because the solar irradiance was higher than the STC value of 1000 W/m^2 . Also, note that the efficiency remained at approximately 95% during the timespan of available light energy. This is further confirmation that the power system meets the ideal results of the designed requirements.

The output voltage is then regulated using a buck converter so that the voltage is appropriate for the nominal voltage of the battery, which is 12.8V. This converter also boosts the current to approximately 35A to meet the output current requirement. The figure below shows the simulated results for output voltage and current to show that the system meets the requirements for the battery to charge at the nominal voltage and at a high rate.

Figure 23: The output voltage and current from the simulation verify the requirements for the battery to charge at a nominal voltage and at a high rate



Note that the charging current remains around 35.35A during the highest point of solar irradiance and the charging voltage is regulated to 12.98V. These values compare well to the required output current of 40A and output voltage of 12.8V. This means that the power systems overall goal is fulfilled and verified through this simulation. A link to a video of the simulation is also included in the footnotes²⁶ below and in Appendix F for further verification of the power systems design.

In conclusion, seeing that the output voltage and the output current meet the requirements for a high charge rate at the nominal voltage (reasoning for these chosen required values for verification was explained at the beginning of this chapter) for the battery and the system is able to output power at an efficiency of 95%, the power systems design is verified with the simulation completed in MATLAB Simulink.

²⁶ <https://drive.google.com/file/d/1c22Wj16Ne8wlY98kC63tyyMHnNdHDmhQ/view?usp=sharing>

Power Rails Voltage Regulator Selection and Design

The power rails are a very important part of the charging station since they are required to provide 5V and 12V to the system. The 5V rail is required to power the motherboard which includes the microcontroller, SD-Card reader, LCD, locker status LEDs and other various devices as well as used to charge devices connected to the station. The 12V rail is required to power the solenoids to unlock individual lockers. Due to the rather large loads, the regulators should be able to supply a large current. The largest power consuming device in the station would be a phone charging. A phone may be supplied up to 2A at 5V for 10W charging. This requirement dictated that the regulator chosen supplies at least 2A of current. Along with this requirement, the system also required a regulator with high efficiency since the system is solely dependent on solar power and a backup battery, which means power consumption is a critical factor. These requirements led to research on the following regulators:

Table 3: Specifications comparison table for voltage regulators

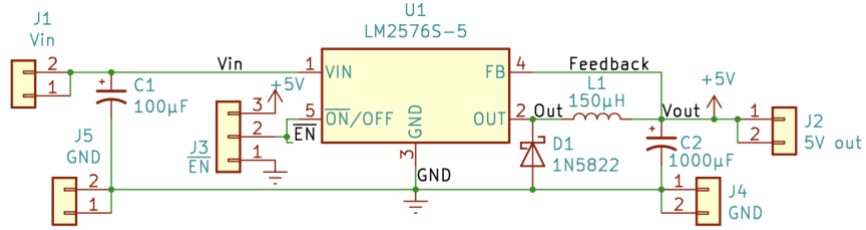
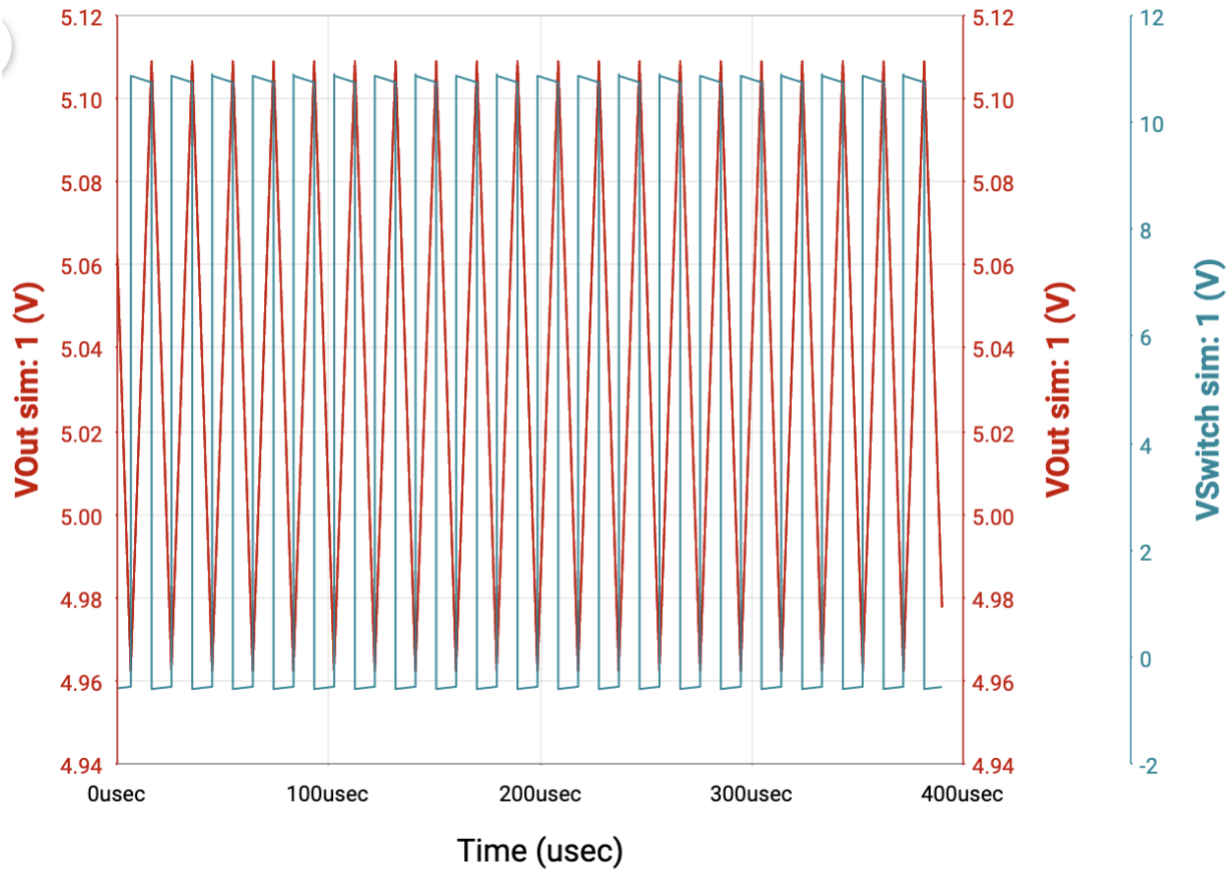
Regulator	LM2576/LM2596 ²⁷	LTC162x ²⁸	LM78xx ²⁹
Type	Switching	Switching	Linear
Efficiency	77-88%	80-95%	50-60%
Voltage Drop	2.0V	2.51V	1.5V
Max Output Current	3.0A	2.0A	1.5A
Output Ripple	$\approx 75\text{mV}$	$\approx 50\text{mV}$	--
Price(per unit)	\$1.26	\$5.50	\$0.75

The above information has been sourced from datasheets of each regulator's manufacturer as a preliminary test. By comparing the above data, the LM2576 was determined to be the most viable regulator given its relatively high efficiency, current carrying capabilities, and low cost. The 78xx family of regulators were instantly deemed not a viable solution given their low efficiency for a system where power consumption is critical. The LTC162x family of regulators were a good option given the extremely high efficiency, however a maximum output current of 2.0A would limit the usage and possibly cause thermal issues. The cost per unit is also rather high which automatically illustrated that the LM2576 was the most appropriate regulator for this design. Premade LM2576 regulator circuit modules were characterized using TI's Webench resource visualized in the following figures.

²⁷ "LM2576 - Texas Instruments" <http://www.ti.com/lit/gpn/lm2576>. Accessed 20 Jan. 2020.

²⁸ "LTC1625 - Analog Devices" <https://www.analog.com/media/en/technical-documentation/data-sheets/1625f.pdf>. Accessed 20 Jan. 2020.

²⁹ "LM340, LM340A and LM7805 - Texas Instruments" <http://www.ti.com/lit/ds/symlink/lm340.pdf>. Accessed 20 Jan. 2020.

Figure 25a: LM2576 voltage regulator schematic for 5V supply railFigure 25b: Graph displaying voltage changes over time using the LM2576 voltage regulator

Note from the above figure that the switching voltage changes between 0-12V, as expected, which is passed through the LC circuit and resolves to an average 5V DC rail. This has a 128mV output ripple. This ripple is rather high, however, it was a compromise that was made in order to preserve the efficiency. Further testing was planned for the regulator, however, due to the COVID-19 outbreak, it has been halted and is subject to availability of equipment. This testing involved measuring output ripple, analyzing thermal characteristics under max load (2.0A) and calculating actual efficiency. This regulator is planned to be substituted by a more appropriate regulator with lower ripple and a smaller footprint. Given the high ripple of 128mV, a larger list of 5V switching regulators was analyzed for the charging

circuit. These have the same requirements as before, a high efficiency ($\geq 80\%$), $\geq 2A$ I_{max} , ripple $\leq 100mV$. Given these restrictions the following switching regulators were short listed:

Table 4: Specifications comparison table for voltage regulators

Part number	Listed efficiency (%)	Price/unit (\$)	Switching frequency (KHz)	I_{max} (A)	Package
TPS62133 ³⁰	93.9	0.7	1350	3	QFN-16
LMR23625CFP ³¹	88.5	1.19	2100	2.5	SOIC-8
TLV62130 ³²	93.9	0.57	1350	3	QFN-16
TPS54260 ³³	86.3	1.36	850.96	2.5	MSOP-10
TPS54427 ³⁴	85.5	1.78	749.93	4	SOIC-8
LM25116 ³⁵	95.5	1.5	525.97	5	HTSSOP-20
TPS56637 ³⁶	91.9	1.32	559.9	6	VQFN-HR-10

Above data has been sourced for preliminary comparisons from the data sheets of each regulator respectively, as cited below. The listed regulators were further simulated using Texas Instruments provided ‘WeBench’ which offers SPICE simulations for PMICs. Following the simulations as discussed in *Appendix F (Voltage regulator selection comparison)* we came to the following ripples for each regulator:

Table 5: Ripple comparison table for selected regulators

Part number	Ripple (V) (normalized to 0V)
TPS62133	0.0143
LMR23625CFP	0.0009
TLV62130	0.0145
TPS54260	0.0014
TPS54427	0.0156

³⁰ "TPS6213x - Texas Instruments" <http://www.ti.com/slvsag7-aaj>. Accessed 2 May. 2020.

³¹ "LMR23625 - Texas Instruments" <http://www.ti.com/lit/gpn/lmr23625>. Accessed 2 May. 2020.

³² "TLV62130x - Texas Instruments." <http://www.ti.com/lit/gpn/tlv62130a>. Accessed 2 May. 2020.

³³ "TPS54260 - Texas Instruments" <http://www.ti.com/lit/pdf/slvsag86>. Accessed 2 May. 2020.

³⁴ "TPS54427 - Texas Instruments" <http://www.ti.com/lit/gpn/tps54427>. Accessed 2 May. 2020.

³⁵ "LM25116 - Texas Instruments" <http://www.ti.com/lit/gpn/lm25116>. Accessed 2 May. 2020.

³⁶ "TPS56637 - Texas Instruments" <http://www.ti.com/lit/gpn/tps56637>. Accessed 2 May. 2020.

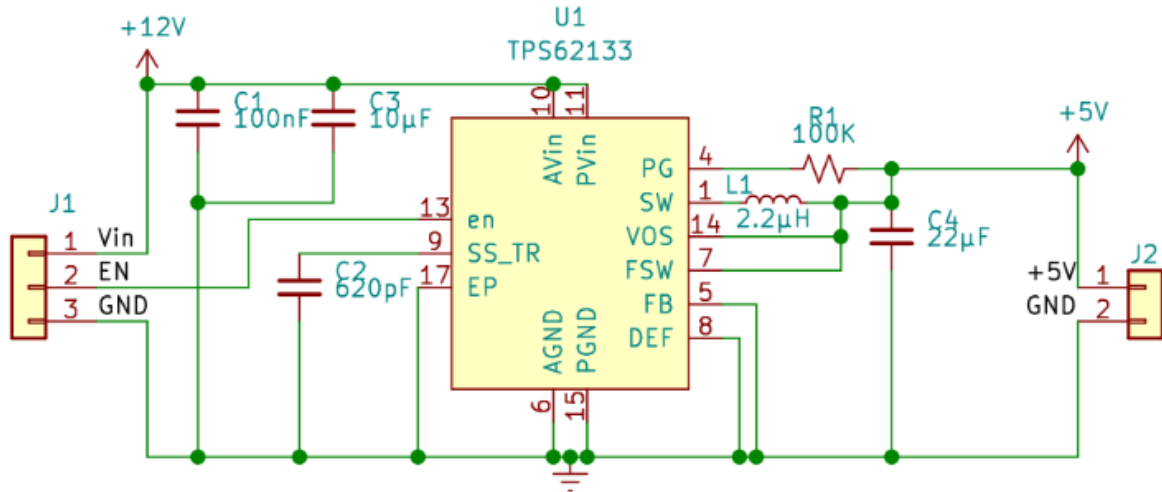
LM25116	0.0047
TPS56637	0.0133

Given the collected data, Pugh chart was created to determine the most appropriate regulator. This Pugh chart was developed by rating and giving a weight to each category as discussed above.

Table 6: Pugh chart for selected regulators

Criteria	Weight(Max 4)	TPS62133	LMR23625CFP	TLV62130	TPS54260	TPS54427	LM25116	TPS56637
Average efficiency	4	3	1	3	1	1	3	2
Cost/unit	2	3	2	3	2	1	1	2
Max V shift	3	1	3	1	3	1	2	1
External Components	1	3	3	3	2	2	1	2
Current Capability	2	3	2	3	2	3	3	3
Total	36	31	25	31	24	18	28	24

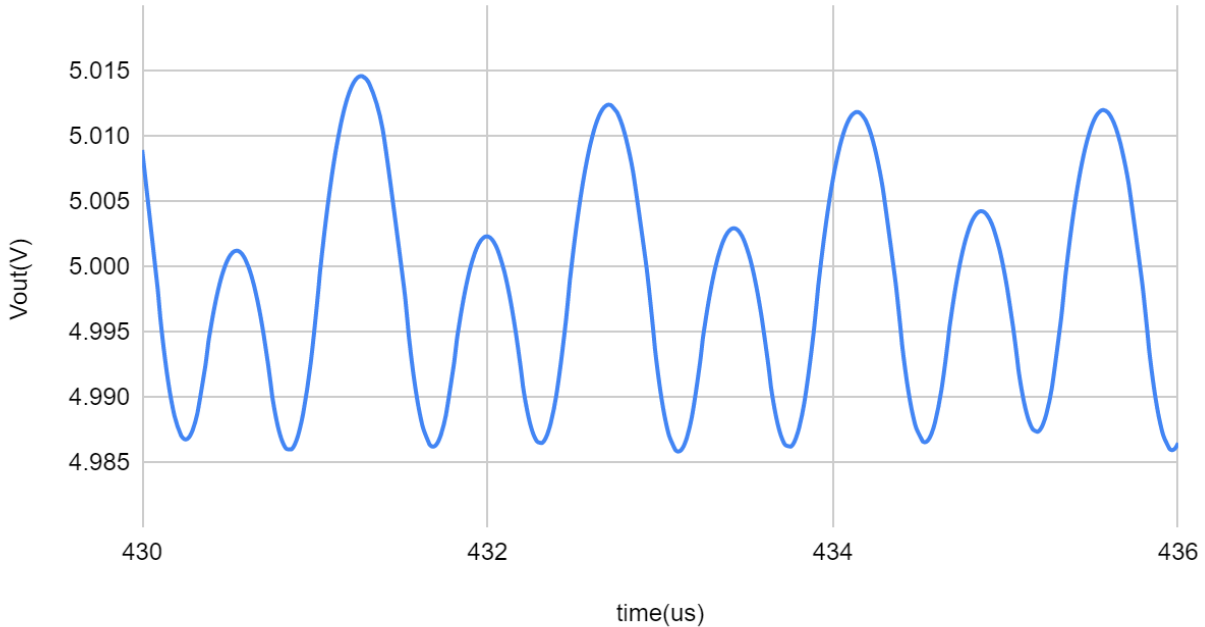
From the above chart we can see that of the seven selected regulators, TPS62133 and TLV62130 appear to be the most appropriate of the selection given their total score even though their ripple is higher than that of the LMR23625CFP, however given the lower efficiency and I_{max} along with a higher price led the team to select the TPS62133/TLV62130 over the LMR23625CFP. The LM25116 was also a close contender with a score of 28 as opposed to 31. The LM25116 was not selected however primarily given the high price, and a requirement of needing a comparatively higher number of external components since it is a switching controller instead of a regulator. This extra number of components further increases the BOM which can be avoided with the use of a switching regulator. Finally the decision was between the TLV62130 and TPS62133. Referring back to the comparison carried out, the two regulators are characterized as interchangeable given the extremely identical properties as well as an identical pinout. This meant the team could have used either of the regulators with one minor difference, the TPS62133 has a quiescent current of 15uA as opposed to 17uA of the TLV62130. This is a minute difference, however any power saved should be saved, therefore the team decided to use the TPS62133. As discussed earlier, this regulator would be used to charge devices connected to the station. This calls for the use of a USB charge control IC, given the team was unable to find a control IC given the time and testing restriction, this was left incomplete. However, the schematic for the regulator is as shown below:

Figure 26a: TPS62133 switching regulator schematic V1.0

Given the above circuit, the SPICE simulation for the regulator under a 2A load is the following:

Figure 26b: TPS62133 output ripple SPICE simulation

Vout vs time (Steady State)-Ripple



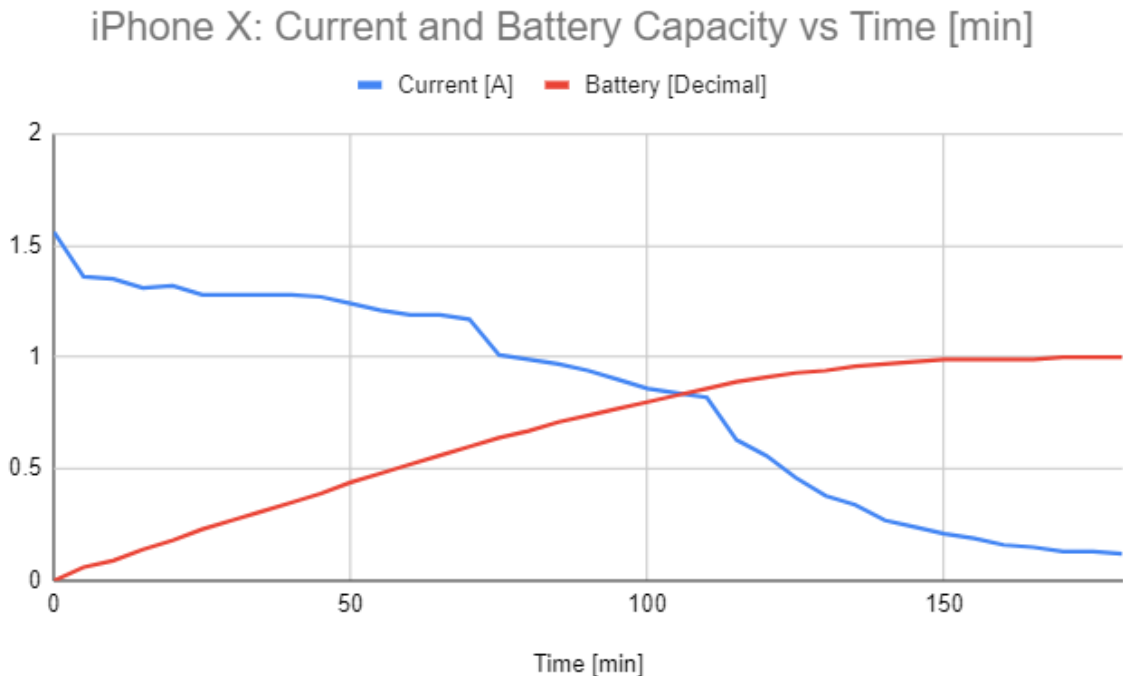
The above graph portrays the ripple of the regulator under a constant 2A load. It can be seen that the voltage averages to approximately 5.0V with a maximum value of 5.015V and a minimum of 4.985 which agrees with our previously calculated ripple of 15mV and a considerable improvement against the LM2576.

Phone Charging Circuit Design and Implementation

The phone charging circuit is connected to the 5V rail described in the previous section. This charging circuit is crucial to the success of the 5V, 2A fast max charging rate established in the team-client goals. This max charge rate tapers off as seen in the following examples below to nearly complete charge any phone over a duration of two hours. This duration was chosen because it is the standard for most fast chargers developed in industry. Fast charging protocols such as Qualcomm QuickCharge 2.0/3.0 follow the same guidelines for fast charge ratings and duration for close to complete charge.

To understand the charging requirements of smartphones, tests were conducted on two iPhones and one Android device. The charging curve characteristics were recorded as these three phones were charged using an Anker Power Core II Slim 10000 w/ Qualcomm 3.0 fast charger. This smart, fast charger has the ability to charge phones at their maximum charge rate. Tests were conducted by connecting a USB digital multimeter to the USB 3.0 port on the smart charger and recording voltage measurements on each USB pin, fluctuations in the battery percentage, and current draw every five minutes for a minimum of three hours. Three hours proved to be the common time period for a phone battery to reach a complete charge. Although, as the charging curves will exhibit, the phones were close to 100% charged by the end of two hours. The following charts were developed by using the data that can be found in the reference link listed in *Appendix F* and in the footnotes below.

Figure 28a: Graph displaying ~1.5A peak charge rate for the iPhone X with a smart charger³⁷



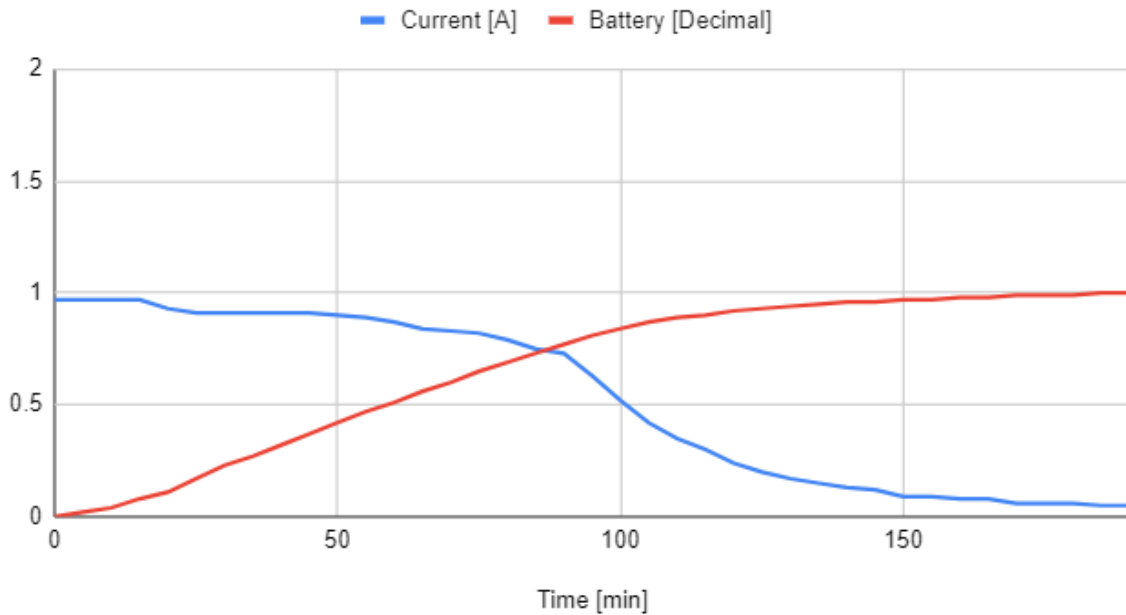
This figure illustrates the charging characteristics of an iPhone X. The iPhone received approximately 1.5A of current at its maximum charge rate. This peak occurred at the beginning of the

³⁷ <https://docs.google.com/spreadsheets/d/1XHV8rmuaQ63XyKdT4hDJGMEJASUMBLBm9jZNN08ZMPw/edit?usp=sharing>

charge cycle and tapered off as the battery increased. The charge rate dropped to approximately 0.1A when the battery was close to 100%. At close to the three-hour mark, the battery reached 100% and continued to charge at a rate of approximately 0.1A. These results will be used as the standard of successful fast charging when testing with the station's designed charging circuit.

Figure 28b: Graph displaying 1A peak charge rate at the beginning of the charge cycle for the iPhone 6 with smart charger³⁸

iPhone 6: Current and Battery Capacity vs Time [min]



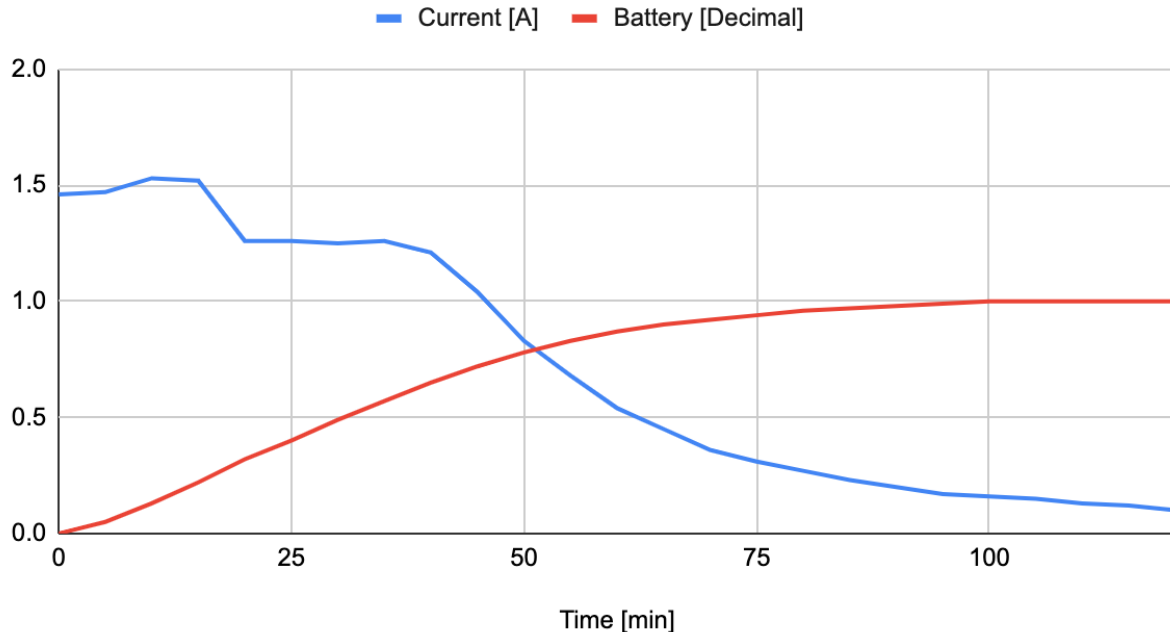
This figure illustrates the charging characteristics of an iPhone 6. The iPhone received approximately 1.0A of current at its maximum charge rate. This peak occurred at the beginning of the charge cycle and tapered off as the battery increased. The charge rate dropped to approximately 0.1A when the battery was close to 100%. At close to the three hour mark, the battery reached 100% and continued to charge at a rate of approximately 0.1A. These results will be used as the standard of successful fast charging when testing with the station's designed charging circuit.

Lastly, it is crucial to also record charging curve data using the smart charger for an Android phone with fast charging capabilities to compare with results of the designed fast charging circuit. This was accomplished by testing a Samsung S6 Edge which has the ability to receive a maximum of 5V, 2A charging. The results are displayed in the figure below.

³⁸ <https://docs.google.com/spreadsheets/d/1XHV8rmuaQ63XyKdT4hDJGMEJASUMBLBm9jZNN08ZMPw/edit?usp=sharing>

Figure 28c: Graph displaying ~1.5A peak charge rate at the beginning of the charge cycle for the Samsung S6 Edge with smart charger³⁹

Samsung S6 Edge: Current and Battery Capacity vs Time



This graph shows that an Android phone with fast charging capability charges in a similar manner to an iPhone with fast charging capability. Note that the phone was able to draw a maximum of approximately 1.5A when the phone's battery was completely depleted. These results will be used as the standard of successful fast charging when testing with the station's designed charging circuit.

The current charging curve is significant to this project as this determines the required current draw of a single phone over a charging cycle. More importantly, this illustrates that, for phones that can charge at a 2.0A rate, the maximum current draw possibility is 12.0A at one time. This would only occur if six phones with depleted batteries are being charged simultaneously. Since the battery chosen for this project has a discharge rate of 50A, the 12.0A requirement due to the phones and the minimal current draw from other internal components is satisfied by the selected battery.

The multimeter also displayed the voltage that was applied to each data pin so that a circuit could be designed to replicate these fast charging results.

The charging station uses a charging circuit called the *DROK 4pcs DC-DC Step Down Module 6-32V 12V 24V to 5V QC 3.0 Charging Module*⁴⁰. This charging circuit is capable of accomplishing fast charging by conforming to the following fast charging protocols: BC 1.2; Apple; Samsung AFC; QC 2.0/3.0; MTK PE 1.1/PE 2.0; Huawei FCP; SFCP. The charging protocols outline the different

³⁹ <https://docs.google.com/spreadsheets/d/1XHV8rmuaQ63XyKdT4hDJGMEJASUMBLBm9jZNN08ZMPw/edit?usp=sharing>

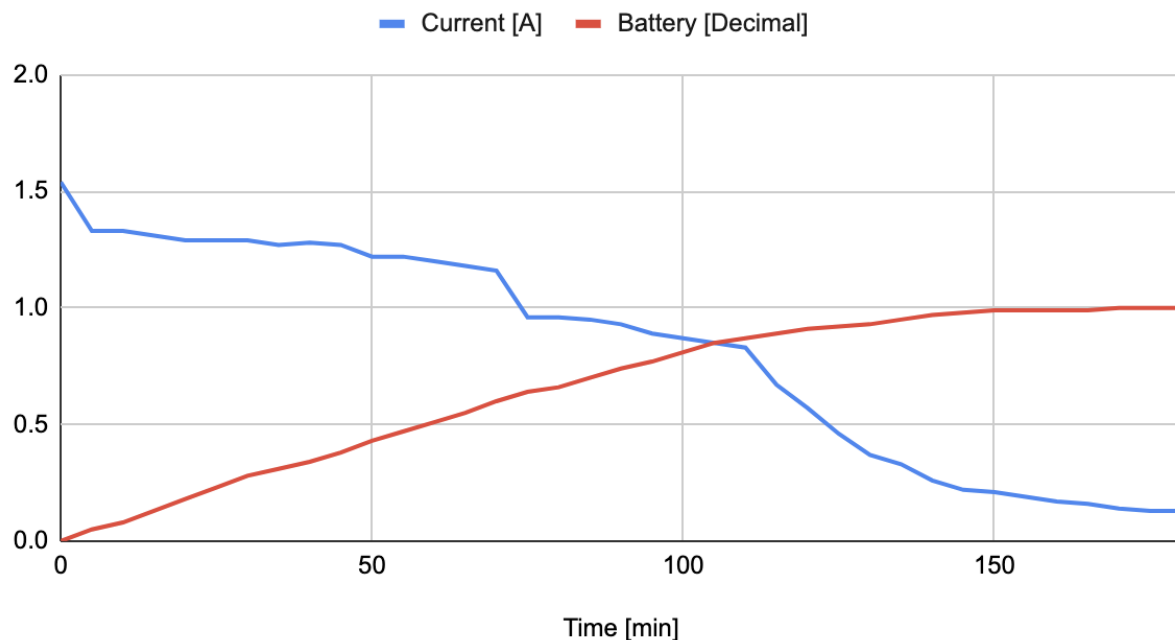
⁴⁰ DROK, Charging Module. https://www.amazon.com/gp/product/B07SQ4FV61/ref=ppx_yo_dt_b_asin_title_o06_s00?ie=UTF8&psc=1

requirements for all smartphones to accomplish fast charging. Furthermore, for phones that are incapable of reaching a max 2A at 5V. The charging circuit is still able to output the required voltage application and following the protocol to allow for the phone to draw the maximum current.

Tests were conducted in a similar fashion to the previous charging tests to see if the charging circuit could support the same charge rate established by the smart charger. The figures below display the charging curve results of the station's phone charging circuit. A reference link is available in *Appendix F* to observe the data points that create the following figures.

Figure 28d: Graph displaying ~1.5A peak charge rate for an iPhone X with the station's phone charging circuit⁴¹

iPhone X: Current [A] and Battery [Decimal] vs Time [min]

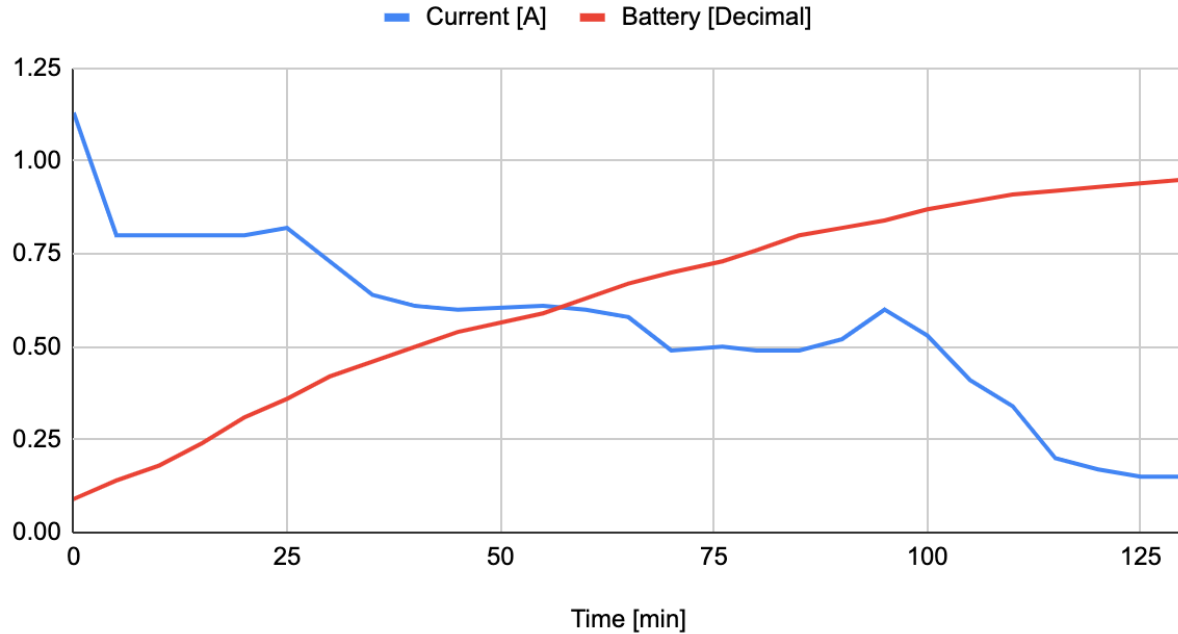


The iPhone X displayed similar results to the previous test using the smart charger. The iPhone was able to draw a maximum of approximately 1.5A when the battery was completely depleted. This charge rate declined as the battery percentage increased. The charging curve seen above follows the charging curve that was displayed when testing the iPhone X's charging capability when using the smart charger. Those test results confirm that this designed charging circuit can fast charge iPhones that have fast charging capability. This showed that the charging circuit can support the maximum charge rate for the iPhone X and verifies the charging circuit design.

⁴¹ <https://drive.google.com/file/d/19kz-XuSgh-SOxfwZELGNeKMsm1NFjgMV/view?usp=sharing>

Figure 28e: Graph displaying ~1A peak charge rate for an iPhone SE with the designed station's

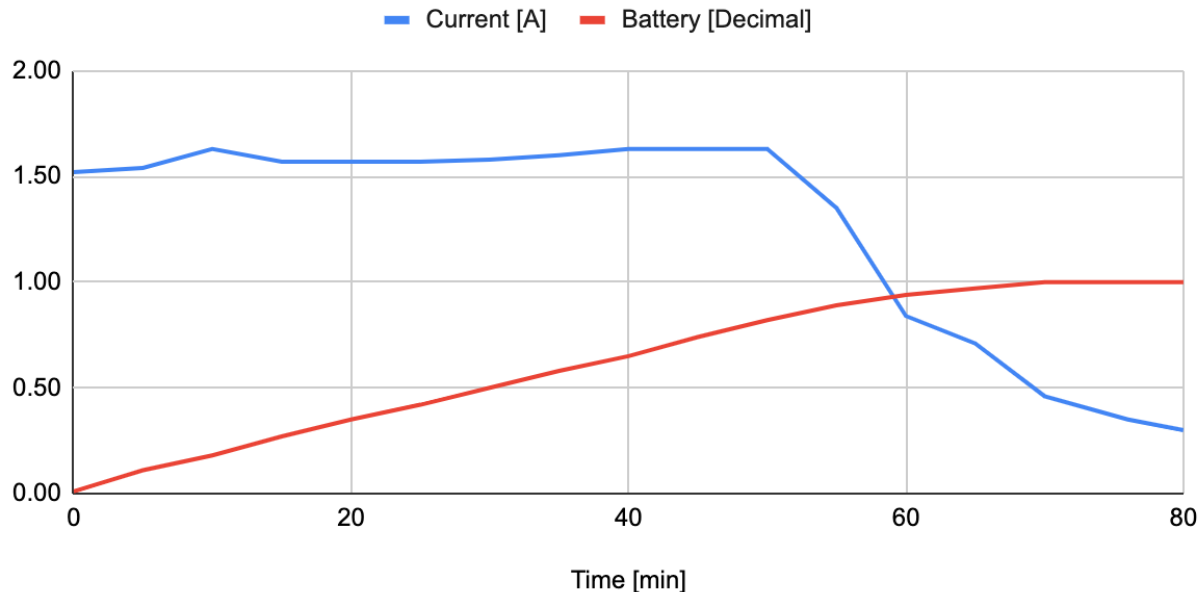
iPhone SE: Current and Battery Capacity vs Time



The iPhone SE displayed similar results to the previous test using the smart charger. The iPhone was able to draw a maximum of approximately 1.0A when the battery was close to depleted. This charge rate declined as the battery percentage increased. This showed that the charging circuit could support the maximum charge rate for the iPhone SE. Note that the iPhone SE is not capable of fast charging and can only draw a maximum current of approximately 1A. Even though the iPhone SE is not the same device as the iPhone 6 that was previously tested using the smart charger, both phones are not capable of 5V, 2A fast charging. Since the charging curves for both phones are similar, it is notable that the station's designed charging circuit can output the same current draw as the smart charger for iPhones without fast charging capability. This result shows that the station's designed charging circuit is able to support the highest charge rate for phones that are not capable of fast charging and further verifies the charging circuit design.

Figure 28f: Graph displaying 1.5A charge rate for a Samsung Galaxy S7 Edge with the station's phone charging circuit⁴²

Samsung Galaxy S7 Edge: Current and Battery Capacity vs Time



The phone charging circuit that has been implemented into the charging station is also able to support fast charging for Android devices. As seen in the figure above, the Samsung S7 Edge was able to draw a maximum current of approximately 1.5A when the battery was completely depleted. Even though the Samsung S7 Edge is not the same as the Samsung S6 Edge, which was used for testing with the smart charger, note that both phones use Samsung fast charging protocol. This protocol is met with any charger that has Qualcomm QuickCharge 2.0/3.0 capability. The data and charging curve above is verified by the charging curve that was seen when using a smart charger for the Samsung S6 Edge. Therefore, this test result verifies the ability of the charging circuit to fast charge Android phones.

Microcontroller Usage and Choice

The project requires the station to allow the user to input a 4-digit passcode of their choice to access their locker in a secure manner, provide a master unlock code of at least 6 digits to be given to the HGP staff to override and access any locker at any time, and allow the user to charge their device for up to 2 hours at a time (see Introduction, Functional Constraints: Features). The use of a microcontroller is suitable to interface the electrical components and program the behavior of the overall station as well as develop the accessibility of the user interface of the station. A microcontroller is able to process the inputs and outputs of the station to program a behavior for the locker to secure the phones.

⁴² <https://drive.google.com/file/d/19kz-XuSgh-SOXfwZELGNeKMsm1NFjgMV/view?usp=sharing>

The microcontroller must be able to support a sufficiently large number of GPIO (General Purpose Input/Output) pins for control over a wide amount of lockers as well as the user interface. The microcontroller must also be able to support a low voltage supply value and a low oscillator frequency to reduce power consumption as the station must conserve power operating on battery and solar power. The microcontroller lastly must also be able to support the program operation and must boast a sufficiently large flash memory and SRAM, tentative to the program size. Other characteristics such as cost are considered in the choice of microcontroller for prototyping, fabrication purposes, and budget constraints. The microcontroller must support a low-level language such as C with direct port access. The microcontroller must be readily available for purchase as an SMD component as the final product will not be using the Arduino Mega development board but a team-designed motherboard centered around the aforementioned microcontroller and as the main processor.

See Appendix B for the Pugh Chart of comparable microcontrollers that meets the specification of this design.

The requirement of a large number of GPIO pins is due to the need to control multiple signals for each locker that are repeated for every locker. For example a 6 locker prototype, with 5 control signals each, would require at least 30 individual I/O pins available. The microcontroller must also readily have support for use of user interfaces, such as a 16x2 LCD display, a 4x3 matrix keypad, a speaker, and a micro-SD card module. The Atmel ATmega2560 provides 54 digital pins (of which 11 support pulse width modulation) along with 16 hybrid pins that are both analog in and digital communication compatible, meeting the criteria of a large pin count.

Since the station should operate on solar power and a backup battery, the microcontroller must have reduced power consumption modes readily available such as ‘PWR_DOWN’ and ‘IDLE’ modes as documented by Atmel for the ATmega2560. The Atmel ATmega2560 further aids in reducing power consumptions by supporting a minimum Vdd of 1.8V with a maximum oscillator frequency of 2MHz at this voltage level, which further reduces quiescent and dynamic current draw.

With a large program due to control of at least 6 lockers, user interface, and other peripherals, the microcontroller must be able to support memory large enough for the program to operate. The Atmel ATmega2560 supports 256kB of flash memory and 8kB of RAM, with the current program taking approximately 40% of flash and 60% of RAM memory upon compilation (updated February 24, 2020).

To test the standalone microcontroller, the team captured and laid out a PCB that utilized the ATmega2560 with 16MHz and used a Vdd of 5V. The PCB was a crucial step towards prototyping as it proved as a proof of concept that the microcontroller can be utilized in a final design without the need for the developer board and the PCB assembly skills the team has are adequate for soldering 100-pin TQFP packages with a 0.5mm pin pitch. The ATmega16U2 microcontroller is programmed as serial to TTL converter for easy programming of the microcontroller using either the Arduino IDE or MpLabX.

The testboard was deemed to be successful with each GPIO capable of being individually addressed without any crosstalk. This was tested by soldering a simple perfboard with 68 LEDs that simply plugs into the header pins of the board. Each LED is turned on and off at equal intervals as a

preliminary test to make sure no two IO pins are shorted. If any shorts were to be observed, they would most likely exist due to human errors while assembling the PCB.

One major difficulty when testing the board was simply loading the bootloader on the AtMega16U2. By default, the Arduino IDE supports bootloader flashing, though not for the AtMega16U2 for UART communication. This resulted in soldering external wires directly to the pins of the 32pin TQFP package to break them out and use an external programmer to flash the bootloader. Even after attempting this, different versions of the bootloader had to be flashed multiple times to determine the correct version. This can further be resolved by using a different UART IC such as the CH340G or FT232R that do not require any bootloader or special kernels. A final difficulty with the board was with the USB-C connector. At the time of the layout, the team was not aware of the fact that the CC (channel configuration) pins on the connector require $5.1K\Omega$ pull down resistors and that the D+ and D- lines should be shorted since there are two of each. To fix these issues, bodge wires and resistors were soldered such that the USB port is now active and can be used with computers that actively look for the particular voltage drop across their source channel resistors.

See Appendix E and F for schematics and layout of the [custom microcontroller test PCB](#) for initial implementation of the microcontroller without the development board.

State Machine Integration of all Components

See Appendix C for the state machine diagram of the SlugCharge station and each states' brief description, detailing the behavior of the interactive systems and each of the station's programmed states that will provide the user with an accessible user interface and provide the user with security for their phones. Each edge case is covered with a 30s timer, resetting to the default state RESET_SLEEP; any form of input will reset the timer. The lockout function and master unlock function are detailed below.

Lockout Function: If a user fails to access a specific occupied locker 5 consecutive times, the microcontroller will proceed with a lockout function for added security, where the next time the user tries to access the same particular locker, the program will enter the OCCUPIED:LOCKOUT state detailed below where the user is unable to enter the password and instead the time remaining of the lockout is displayed. Each consecutive 5 failed tries in accessing the same occupied locker doubles the lockout timer, up to a maximum of 1 hour. The base timeout is 15 seconds. Successfully unlocking the locker resets the lockout counter, either through inputting the correct passcode, or through the master unlock function. A locker in lockout does not affect the other lockers. For example if locker 2 is in lockout, any other locker is available to be accessed.

Master Unlock: The HGP will act as the admins of the locker and will be notified about the Master Unlock function, where they will be able to access any locker at any particular time (see Introduction, Functional Constraints: Features). In one of the states, ACTIVATED, the user will have to press the “0” key 7 time consecutively to enter a MASTER_UNLOCK state; any key press in between will reset this counter, timing out in the ACTIVATED state also resets this counter. In the MASTER_UNLOCK state, the user will be able to enter a passcode unrestricted up to 16 digits before pressing the “0” key to indicate entering the passcode. The master passcode to enter any locker is “1293242X”, followed by a “0” key press, where the X is the locker to be opened. X must be a number

between 1 to 6 in a 6 locker system; any number greater than 6 will result in transitioning to a state displaying that the passcode entered was invalid. If the passcode does not start with “1293242” or the passcode is an empty string, the program will transition to a state displaying that the passcode is invalid. If the passcode only displays “1293242”, the program will also transition to a state displaying that the passcode is invalid. The use of the “0” key is that a Locker 0 does not exist, and continuously pressing the “0” key more than 7 times results in displaying that the passcode is invalid, as the passcode entered will register as an empty string.

Selection of Hardware Components for the User Interface

The SlugCharge station must provide an accessible interface to the user and provide security for occupied lockers. To achieve these goals, the method of accessing a locker, the locking mechanism, and the interface to display instructions are prioritized components of the station. The resulting components selected are the 3x4 matrix keypad, the lock-style pull solenoid, and the 16x2 LCD. See Appendix D for the component selection pugh chart for unlocking methods, locking mechanisms, and displays.

The HGP client requests the use of a numpad as the primary interaction with the station. The 3x4 matrix keypad requires the use of 7 pins and a library to interface the keypad with the microcontroller. The keypad buttons are connected to an internal 20k pullup resistor (value taken from the Atmel ATmega2560 datasheet) and 5V, resulting in a power dissipation of 1.25mW for each pressed row key, calculated by the equation for power $P = V^2/R = 5V^2/20k\Omega = 1.25mW$. The lock style solenoid requires 350mA of activation (experimentally determined using an ammeter) supplied by a 12V rail, resulting in a power dissipation of 4.2W, and a flyback diode for voltage spike snubbing. The maximum activation time allowed for the solenoid is 10 seconds, as suggested by the Adafruit website for the lock-style solenoid, implemented using a timer through the software program. The 1602a LCD display’s backlight sinks approximately 150mA with a 5V source (value taken from the 1602a 16x2 LCD datasheet for electrical characteristics), resulting in a power dissipation of 0.75W when activated (calculated using the equation for power $P = VI = 5V * 150mA = 0.75W$), however a pin from the microcontroller is used to control the power to the backlight, turning it off whenever needed to reduce power consumption. See Appendix E for the engineering schematics for the connection of the microcontroller to the LCD including a pin connected to the anode of the backlight.

To determine if a door is closed, defined by when the door’s locking mechanism is in a position to lock the locker, a 125V 1A snap-action switch is implemented for each locker to accurately detect if the position of the door is closed. However the snap-action switches are mechanically exposed to the user to which they may manually trigger the switch, issuing a false “door-closed” event. Therefore a DC1561 reed switch was tested however the proximity of triggering is approximately 3 inches, losing the needed precision of detecting if a door is closed. Therefore both switches are used in tandem (see *Microcontroller Input and Output Circuits, Door Detection Input (Open/Closed)*) to accurately detect a closed door. An external magnet with a shorter field may be used as an alternative. The switch is implemented with an internal 20k pullup resistor and 5V, resulting in a power dissipation of 0.25mW if both switches are closed.

Each locker comes with a 5mm green LED and a 5mm red LED depicting if the locker is vacant (green) or occupied (red); the circuit for these status (vacant/occupied) LEDs is developed such that only

one of the LEDs may be on at a time (see *Microcontroller Input and Output Circuits, Status LEDs Output (Red - Occupied, Green - Vacant)*). The primary reasons for the choice of LEDs are the high power efficiency, low power consumption, and its simplicity. The equation to determine the power dissipated given a 5V rail is calculated as below.

$$P = I_{LED} * V_{dd} = \frac{5V - V_{forward}}{R} * 5V$$

With a red LED with a forward voltage of 1.8V and a current limiting resistance of 1kΩ, the power dissipation is 16mW.

With a green LED with a forward voltage of 3.2V and a current limiting resistance of 1kΩ, the power dissipation is 9mW.

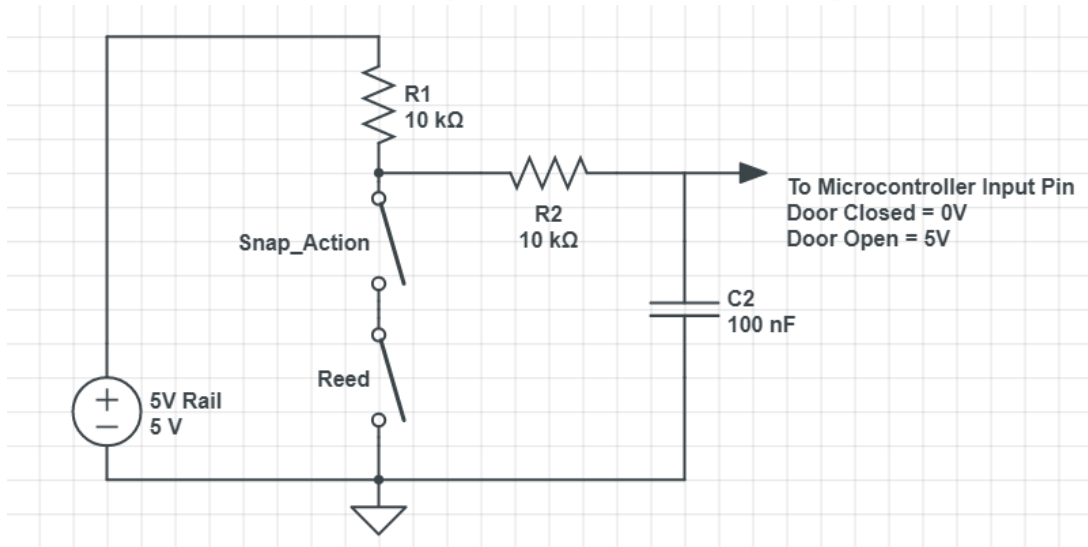
The station supports audio for the use of providing instructions to the user, to thank the user, or to play audio when initializing to signal that the station has finished initializing. An 8ohm, 30W, 1.5 inch voice coil, and 91.5db (1w/1m) sensitivity speaker is selected to facilitate audio for the station. The audio to be played are WAV files stored in the directory of a 16GB micro-SD card inserted into an SD card reader (see *Microcontroller Input and Output Circuits, LCD Display, Keypad, Speaker, and Micro-SD Card*).

Microcontroller Input and Output Circuits

See Appendix C for the state machine diagram of the station. The state machine transitions and user interactions with the station are dependent on input and output signals connected directly to the GPIO pins of the Atmel ATmega2560. The corresponding inputs and outputs are described below.

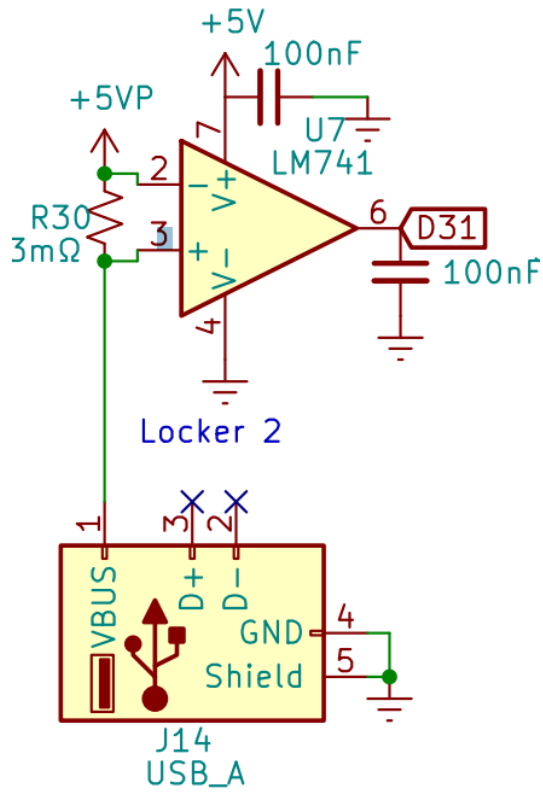
- Door Detection Input (Open/Closed). 1 Per Locker.

The door detection circuit outputs a digital signal and requires the use of a snap-action switch and a reed switch to both be closed to issue a door-closed event, active low. See [Door Design and Mechanism](#) for a description of the use of these devices. Figure 31 below illustrates the circuit detecting the input, implemented with a pullup resistor R1 and 2 series switches. A low pass filter is before the input pin as protection against noise and provides debouncing. Using the testbench described in Appendix E, the circuit outputs an active-high signal when at least 1 switch is open, and an active low signal when both switches are closed, successfully discerning if the locker doors are closed or open.

Figure 29: Door Open/Closed Detection Circuit (Input)

- Phone Connection Detection Input (Plugged/Unplugged)

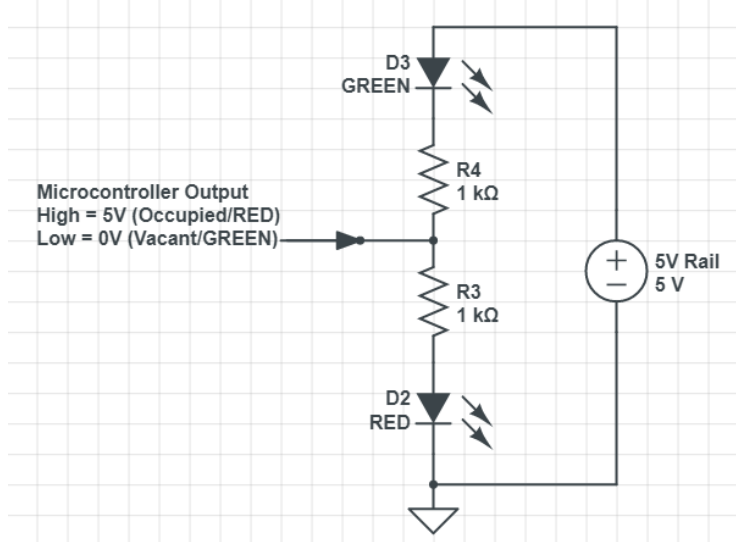
The phone-usb connection detection outputs a digital signal representing if the phone is plugged in the charging station to verify if a locker is currently charging a phone or not, verifying if a locker is accurately occupied or not. The basis is using a small shunt resistor to develop a voltage difference so a comparator outputs an active-low when current flows through the USB and active-high if not. The use of a small resistor is to minimize hindrance to current flow to charge the phones. This was developed on a perfboard for verification which produced inconsistent results. Choices for improvement include using a dedicated comparator circuit with small hysteresis or use a voltage divider with the USB and connect it to an analog pin to poll for analog values.

Figure 30: Phone Charging Current Sensing Circuit

- Status LEDs Output (Red - Occupied, Green - Vacant). 1 Per Locker.

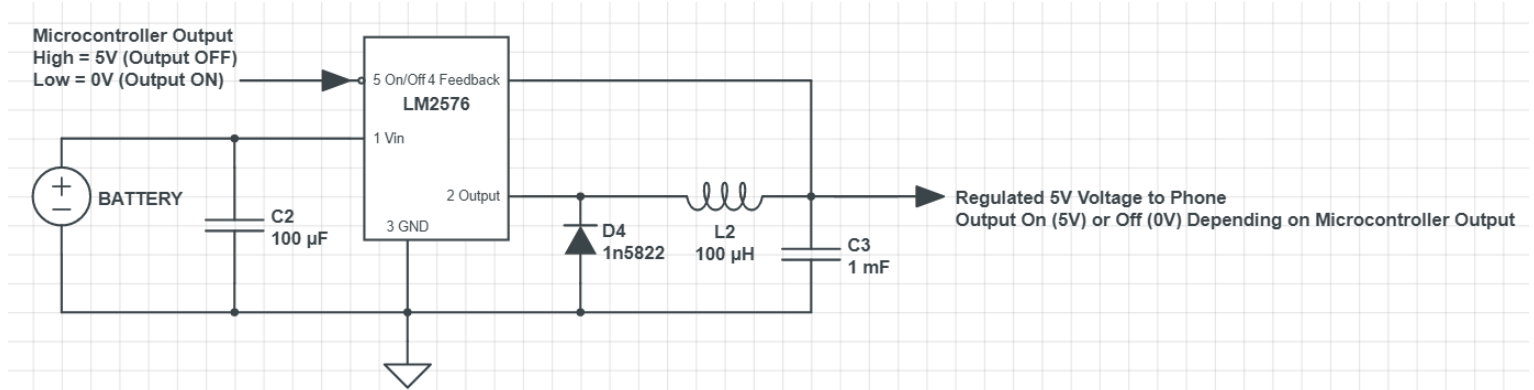
Status LEDs are presented on the lockers as indication to the user if the locker trying to be accessed is vacant or occupied.

The microcontroller pin will output a logic HIGH for the red LED to activate, signifying the locker is occupied. As the voltage difference across the green LED is 0V, the green LED will not turn on. The microcontroller pin will output a low 0V for the green LED to activate, signifying the locker is vacant; as the voltage difference across the red LED is 0V, the red LED will not turn on. See Appendix E for the schematic of the testbench; the operation of the status LEDs verifies where exclusively only 1 LED is on, depending on the digital output signal from the microcontroller controlling the status LED circuit. R3 and R4 are $1k\Omega$ current limiting resistors for the LEDs. Figure 33 below illustrates the circuit controlling the status LEDs on the lockers.

Figure 31: Status LEDs Circuit (Output)

- Charging Switch Output (On/Off). 1 Per Locker.

The voltage regulator LM2576 connected to the USB ports of the charging circuit can be switched on or off depending on the voltage applied to pin 5 on the buck regulator. After 2 hours, the power to the device is disabled, and the user must come back to pick up their phone. If the user wishes to extend the charging time, they may repeat the process starting from selecting an available locker. The 2 hour charge time is deployed to provide an incentive for the user to return to collect their phones. Figure 34 below illustrates the microcontroller connection to the buck regulator to switch the output on or off. Using a breakout board of the LM2576, connecting the enable pin to 5V or 0V, and probing the voltage output using a voltmeter, the LM2576 output pin sources a 5V output if the enable pin is connected to ground, and sources 0V output if the enable pin is connected to 5V.

Figure 32: LM2576 Buck Regulator Output Control to the Phones

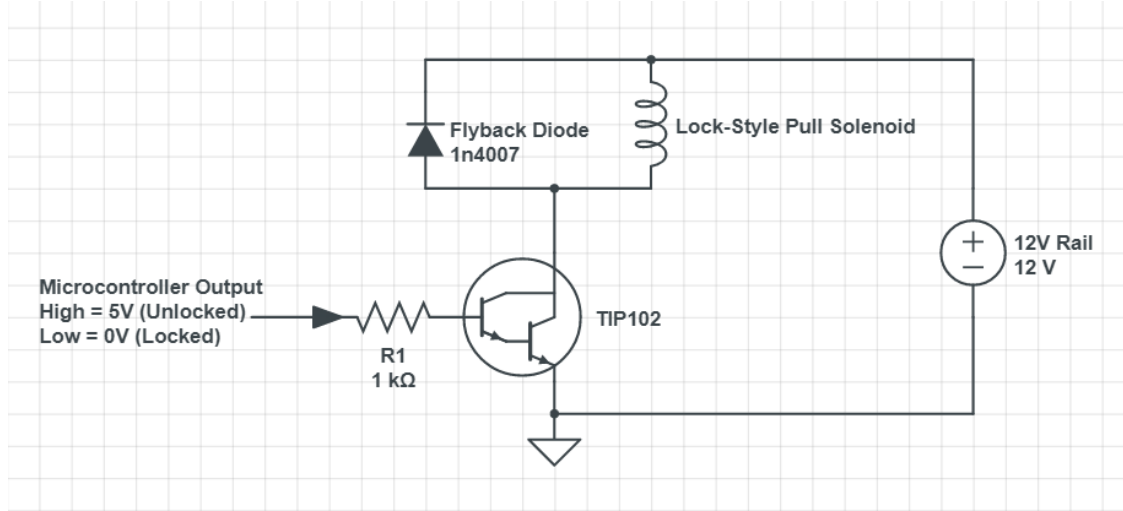
- Solenoid Control Output (Locked/Unlocked). 1 Per Locker.

If the user successfully selects a locker, the locking mechanism will trigger the solenoid to unlock. The maximum solenoid latch time is 10 seconds to prevent overheating and damaging the solenoid; the locking mechanism will then release the solenoid. As the locking mechanism is a lock-style

pull solenoid, delivering power to the solenoid will unlock the door while releasing power to the solenoid will release the solenoid and the door can be pushed back to lock.

As the solenoid requires 350mA to activate (unlock) and the microcontroller output pin can only supply 40mA, a TIP102 Darlington Pair is used as a switch for the 12V rail to supply the solenoid. A $1\text{k}\Omega$ resistor is connected to the base to limit the base-emitter current. A flyback diode 1n4007 is used to snub voltage spikes from the inductive load of the solenoid. Figure 35 below illustrates the circuit controlling the solenoid. Using the testbench in Appendix E, whenever the control pin is a high 5V, the solenoid retracts its plunger and whenever the control pin is a low 0V, the solenoid releases its plunger.

Figure 33: Solenoid Control Circuit (Output)



- LCD Display, Keypad, Speaker, and Micro-SD Card

The user interface devices include the use of a 1602a LCD display, a 3x4 matrix keypad, and a 8ohm speaker. The 3x4 matrix keypad column pins are connected to an AND-gate IC (74HC08) for an active-low external pin interrupt. Figure 36a illustrates the 1602a LCD display connections to the microcontroller. Figure 36b illustrates the keypad connections to the microcontroller and the 74HC08 which feeds into an interrupt pin; the use of a 1k resistor and 100nF lowpass before the interrupt pin is for input protection and hardware-debouncing. The use of 100nF capacitors also provides decoupling high-frequency noise on the input. Figure 36c illustrates the audio amplifier and the 8ohm speaker with a 1n4007 flyback diode for voltage spike snubbing. Using the testbench described in Appendix E and programming the microcontroller to communicate to the LCD using the Arduino LCD.h/cpp library, the LCD prints the intended characters to the display. In addition with the anode pin connected to a microcontroller pin, the LCD backlight turns on when the anode pin is connected to 5V, or off when the anode pin is connected to 0V.

Figure 34a: 1602a LCD Display Circuit
LCD Display

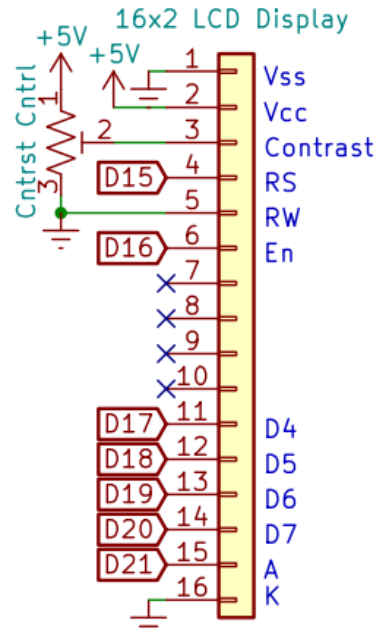


Figure 34b: 3x4 Matrix Keypad Circuit

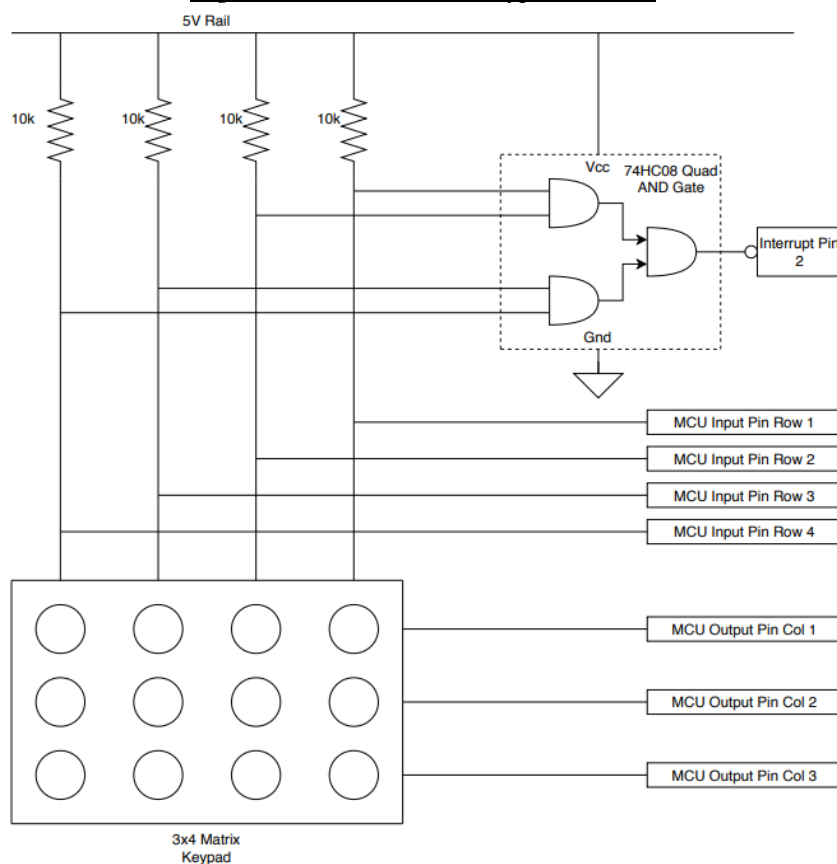
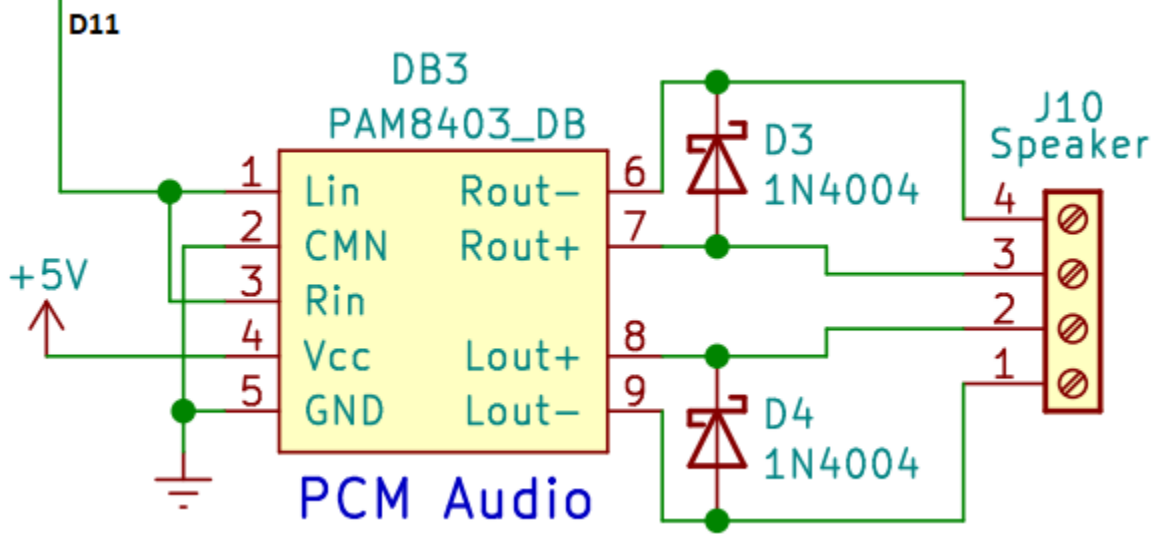


Figure 34c: Speaker Circuit

A micro-SD card module is connected and communicated with the aid of an SPI (Serial Peripheral Interface) bus for station initialization and to contain the WAV audio files to be played through PCM (Pulse Code Modulation).

The PCM audio must be stored onto the directory of the SD card and the open source library, tmrPCM.h, must be included in the program. See Appendix F for the link to the library. The audio files to be played must be converted to 8bit, mono, PCM, WAV files before being played. The audio files illustrated in Figure 36b, the SD card directory, contains audio instructions: PCTD.wav (“Please Close The Door”), PIYP.wav (“Please Insert Your Phone”), PRYP.wav (“Please Remove Your Phone”), SLCH.wav (“Slug Charge Startup Audio”), and TYPCA.wav (“Thank You, Please Come Again”). These files can be found on the Github repository linked in Appendix F.

The SD card directory also contains an “init.txt” file containing the station information of the locker for the purpose of initializing the station to a previous state if the system loses power as a failsafe. The information parsed from this file includes the number of lockers charging, which lockers are vacant, and which lockers are occupied along with its stored passwords. The “init.txt” file is formatted as below.

```

<Number of Lockers Charging>
<Locker Number 1><1:Occupied or 2:Vacant><The 4 digit password, if Occupied>
<Locker Number 2><1:Occupied or 2:Vacant><The 4 digit password, if Occupied>
<Locker Number 3><1:Occupied or 2:Vacant><The 4 digit password, if Occupied>
<Locker Number 4><1:Occupied or 2:Vacant><The 4 digit password, if Occupied>
<Locker Number 5><1:Occupied or 2:Vacant><The 4 digit password, if Occupied>
<Locker Number 6><1:Occupied or 2:Vacant><The 4 digit password, if Occupied>
"
```

The software will additionally read from EEPROM to confirm the contents of the SD card in

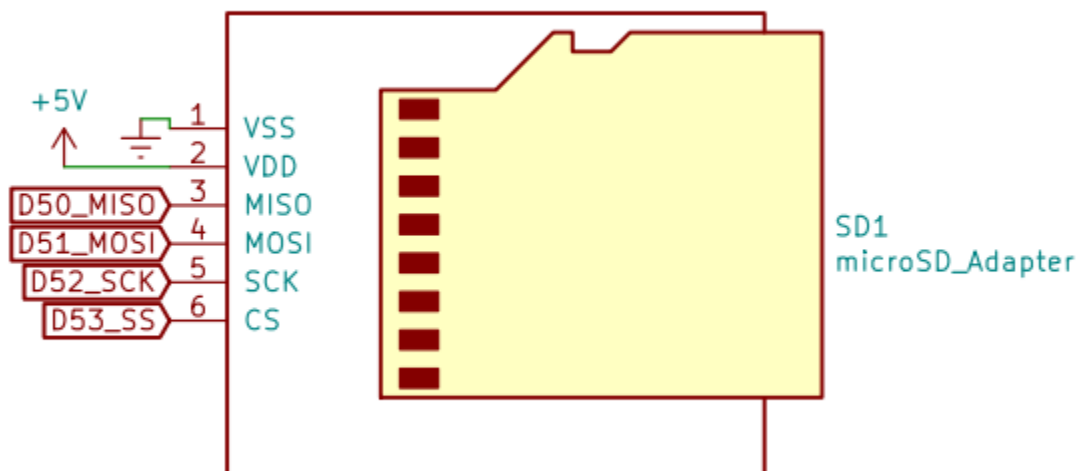
response to potential single point failure. The EEPROM address begins at address 0 up to address 32, intended to contain the same information as the SD card. Starting from the address of 0, the data of the lockers stored in EEPROM are configured such that address 0 contains the byte representing the number of lockers charging, address $4*(\text{lockerNumber}-1)+\text{lockerNumber}$ contains the byte representing if the locker is occupied (1) or vacant (2), and each 4 bytes after this address are the characters of the 4 digit password of each respective locker number. For example if accessing the information of Locker 3 in EEPROM, address 11 contains the byte representing if the locker is vacant or occupied, followed by address [12, 13, 14, 15] containing the bytes representing the respective ASCII characters of the 4 digit passcode of Locker 3.

If the contents of “init.txt”, located on the SD card directory, and the EEPROM are not consistent, the program will halt and the LCD will display to the user that there is an initialization error.

Figure 37a illustrates the connection of the SD card reader to the microcontroller. Figure 37b illustrates the content of the SD card directory.

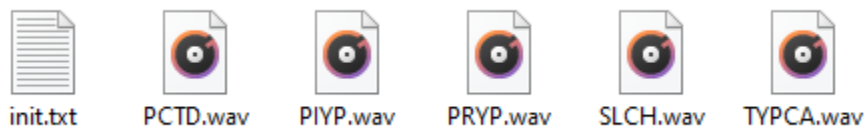
Figure 35a: SD Card Reader - Microcontroller Circuit

Micro-SD Adaptor



This is a placeholder for a premade adapter

Figure 35b: SD Card Directory Contents. See Appendix F For Link to the Repository Containing The WAV Files



- Low-Battery Detection

See Figure 38a and 38b for the low battery circuit block diagram and schematic. The design of the low-battery detection circuit is to read off the battery voltage since its voltage level is proportional to its state of charge and produce an active-high output to indicate to the connected microcontroller that the battery is in low-power. With a lithium iron phosphate battery of nominal voltage of 12.8V with cutoff voltages at 14.6V and 10V, the low-power issues at 12V but the microcontroller will respond to a low-battery until the battery charges back to 12.6V, 200mV under nominal voltage. The circuit is designed to raise an active-high interrupt to an input pin for the microcontroller to respond through the low-battery interrupt ISR. See Appendix C for the state machine and state descriptions for the response to low-battery, marked in yellow. Therefore to produce an active-high interrupt when the battery voltage reaches 12V and remain active-high until the battery charges back up to 12.6V, a comparator with hysteresis is the primary design behind this circuit.

The choice of the comparator requires low-power and rail-to-rail output. The TLV3201 features a push-pull output and features low-power with a quiescent current of $40\mu A$, taken from the TLV3201 datasheet. The TLV3201 is powered by 5V so the circuit utilizes a 5V LDO regulator, the LM7805 to power the circuit. The input to the comparator cannot go beyond the rails therefore the voltage of the battery is dropped to a fourth to match the input range. Using a $\frac{1}{4}$ voltage divider before the input, the range of the input is the cutoff voltages divided by 4, or $10V/4 = 2.5V$ to $14.6V/4 = 3.65V$, which fits the input range. The voltage divider resistors, R1 and R2, are chosen considerably large at 300k and 100k respectively, to limit power consumption. Since the input is dropped to a fourth, the thresholds, 12V and 12.6V, must also be a fourth to match the input to the comparator. This leads to the trigger point thresholds to be at voltages of $12V/4 = 3V = V_{low}$ and $12.6V/4 = 3.15V = V_{high}$.

The hysteresis feedback resistor ratios are dependent on the output voltage of the comparator. Since the comparator features rail-to-rail output, the equations of the threshold are $V_{low} = 5V * R3/(R3 + R4||R5)$ and $V_{high} = 5V * (R3||R5)/(R3||R5 + R4)$. With a V_{low} of 3V and a V_{high} of 3.15V, the relation is $R5 = 20R3$ and $R5 = (37/3)R4$. See Figure 38b for the schematic of the circuit, the chosen resistor values are $R5 = 400k$, $R3 = 20k$, and $R4$ rounded to $32.4k$. These components are chosen considerably high to limit current and power consumption.

For input pin current surge protection and noise reduction, the output of the comparator is connected to a 10k resistor and a decoupler 100nF capacitor, creating a RC low pass filter with a cutoff frequency of approximately 159Hz, calculated with $f_{cutoff} = [2\pi RC]^{-1}$. The output of the circuit is connected to an LED to indicate to the user that the station entered low-power mode, intended to replace the use of the LCD to indicate to the user that the station entered low-power mode, saving the power consumption of the LCD (5V, 130mA, 650mW), to using a 5mm red LED with a 10k resistor. Using the equation of the LED which is $P = I_{LED} * V_{dd} = \frac{5V - V_{forward}}{R} * 5V$ and given that the forward voltage drop of a red 5mm LED is 1.8V with a 10k resistor, the power consumption instead is calculated to be 1.6mW, reducing the overall power consumption while in low-power mode. See Figure 38b for the schematic of the circuit, to prevent R6 and R7 from creating a voltage divider which reduces the output voltage below logic level, the output node is connected to the gate of a NMOS device, the IRF520, and the LED and its current limiting resistor are connected to its source in series to isolate the components. The LED and its current limiting resistor is connected to 5V and the source of the FET is connected to

ground to produce a V_{gs} of 5V with the threshold voltage of 3V, taken from the IRF520 datasheet.

Figure 36a: Low-Battery Circuit Block Diagram

SlugCharge: LOW-BATTERY DETECTION CIRCUIT (ACTIVE HIGH INTERRUPT)

VERSION 3, MAY 8 2020

+ adjusted hysteresis bounds
+ added LED output displaying to the user if the station is in low-battery mode

Design Intent: To output active-high signal to an active high interrupt pin when the battery is below 12V.

After, if the voltage rises back up to 12.6V, the output would be an active-low signal for signalling the microcontroller to exit a low-battery state.

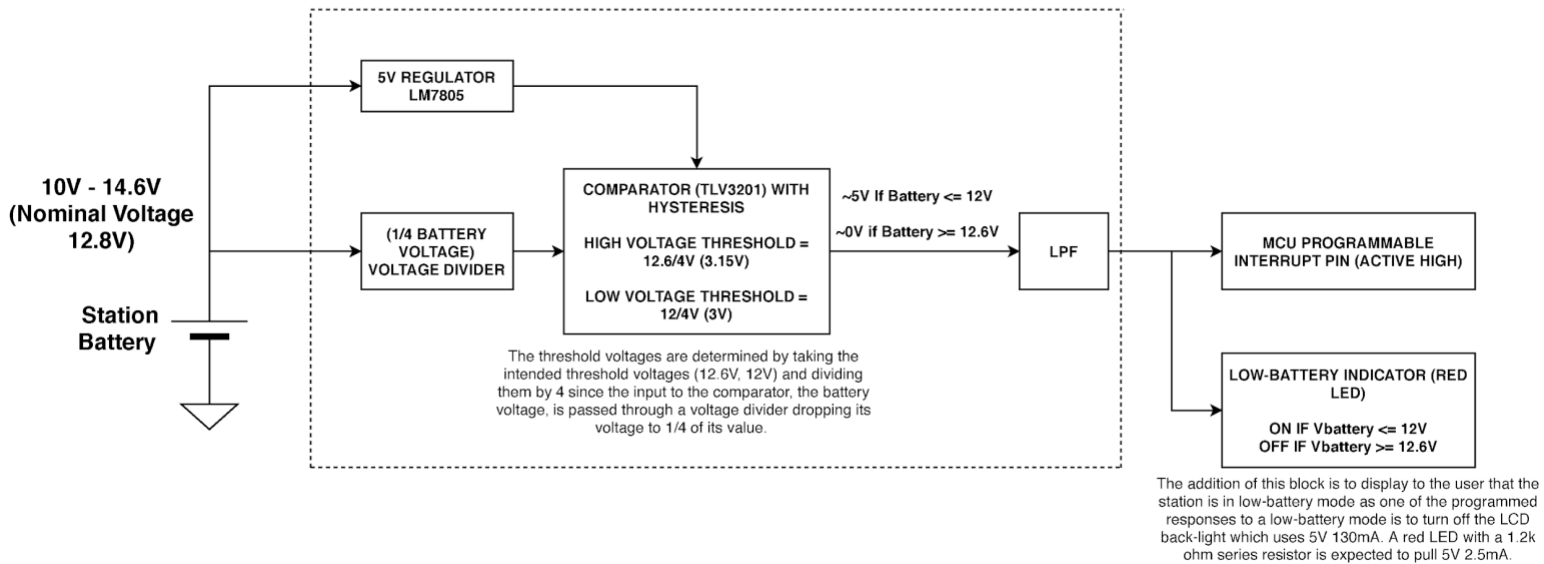
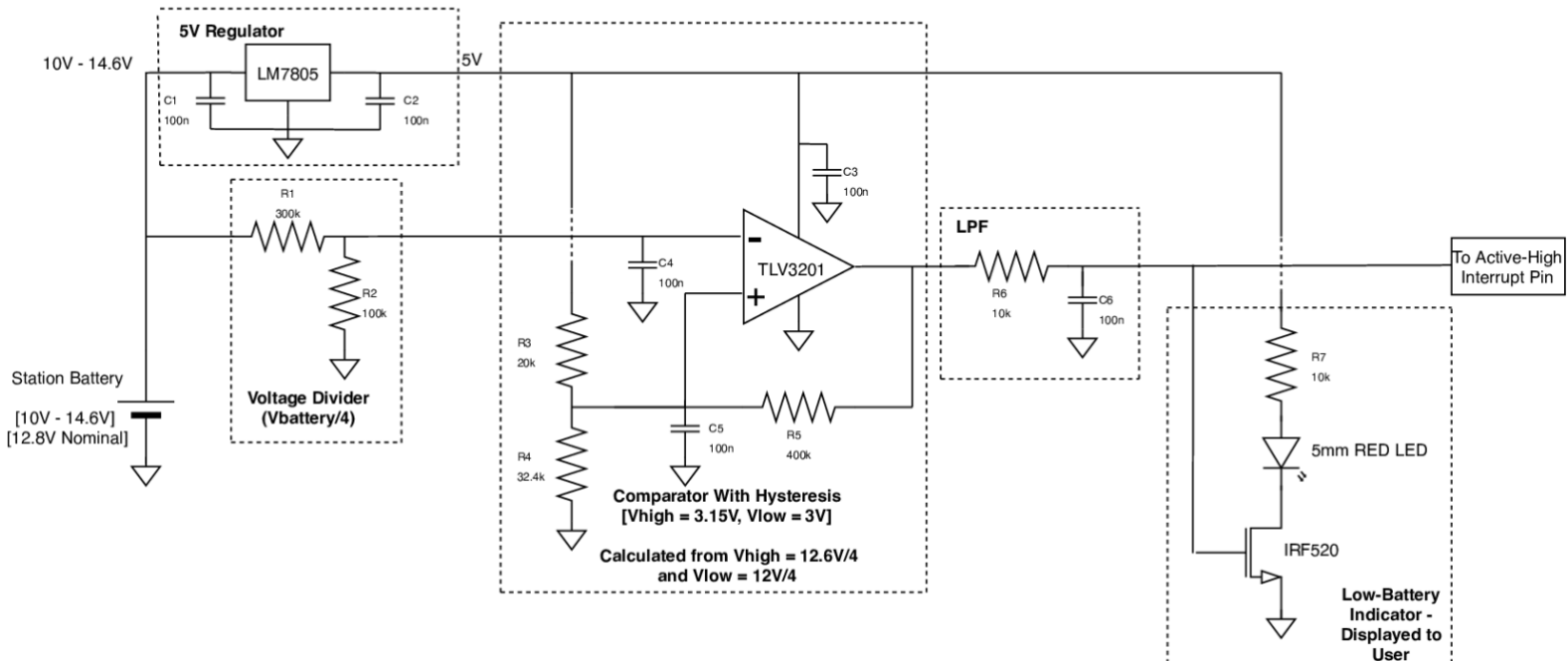


Figure 36b: Low-Battery Circuit Schematic

SlugCharge: LOW-BATTERY DETECTION CIRCUIT (ACTIVE HIGH INTERRUPT)

VERSION 6
May 27, 2020

- + Adjusted Hysteresis Resistor Values (R3, R4, R5)
- + Added Power FET - Buffer Output Voltage to Red LED



The circuit is simulated in LTspice to verify its behavior. See Figure 39a, 39b, and 39c for the simulation circuit with SPICE models taken from Texas Instruments site, the hysteresis voltage DC sweep plots, and the output voltage DC sweep plots respectively. Each simulation is DC swept with the battery voltage representing the battery depleting cutoff voltage to cutoff voltage (14.6V to 10V) and the battery gaining cutoff voltage to cutoff voltage (10V to 14.6V). The plot in Figure 39b verifies that once the battery depletes to 12V, the hysteresis voltage adjusts from 3V to 3.15V, as designed, and the output voltage goes from active-low 0V to active-high 5V, as designed. In addition the plot in Figure 39c verifies that once the battery charges to 12.6V, the hysteresis voltage adjusts from 3.15V to 3V, as designed, and the output voltage goes from active-high 5V to active-low 0V.

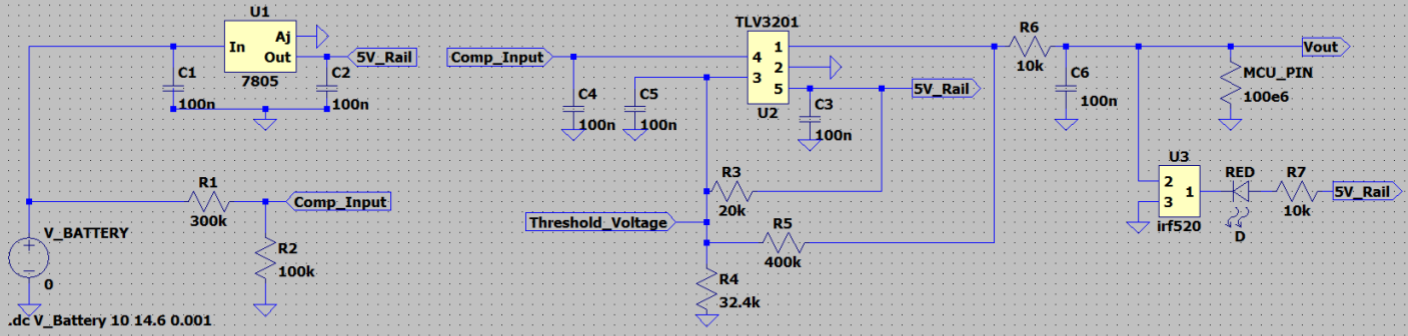
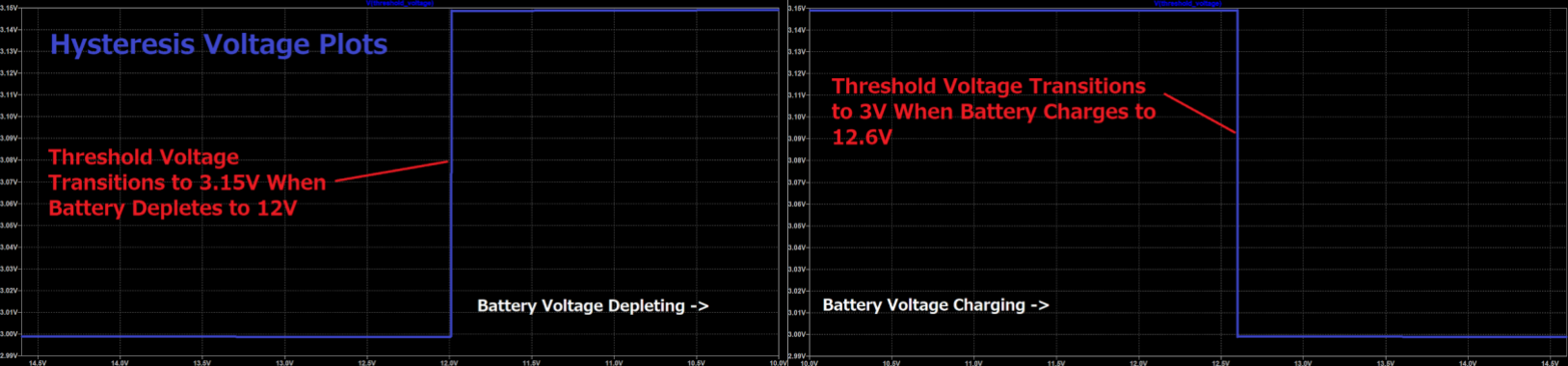
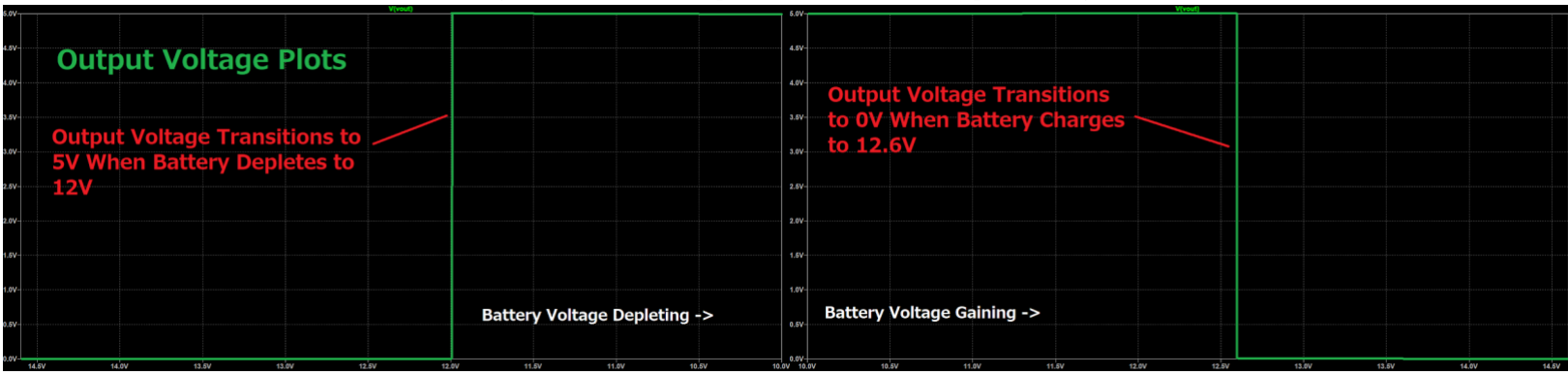
Figure 37a: Low-Battery Simulation Schematic*Figure 37b: DC Sweep Simulation Plot: Hysteresis Voltage (150mV Hysteresis)*

Figure 37c: DC Sweep Simulation Plot: Output Voltage

This circuit requires prototyping and testing before being considered completely verified.

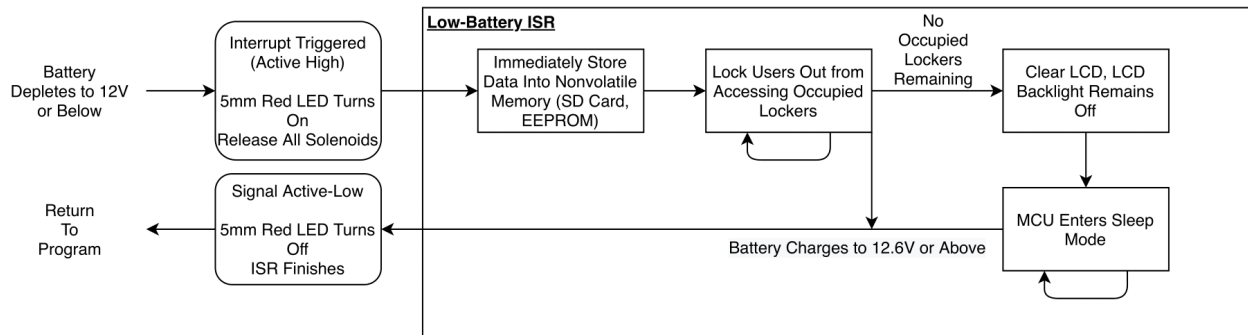
Software Architecture

See Figure 41 for the software architecture of the station, detailing its software behavior, and see Appendix F for a link to the SlugCharge program repository. The software architecture is event-driven, featuring an EventQueue (EventQueue.h/cpp) which is a queue linked list data structure featuring an Event struct. This event struct contains data of an EVENT_TYPE (enum type), EVENT_PARAMETER (the key of a keypad press or null), and LOCKER_NUMBER (the relevant locker associated with the event or null), which the main driver function will poll when demanding input. The system features 2 interrupt routines triggered by an external interrupt on an universal programmable interrupt pin, one for the keypad interrupt (active low) and a low-battery interrupt (active high) which will produce an event struct with the respective contained information and append it to the event queue. See Figure 40 for the flow chart of the low-battery ISR. For inputs such as a door sensor and load sensor, the main driver file will poll these inputs whenever the driver file loops.

Figure 38: Low Battery ISR

Low-Battery ISR Flow Chart v2

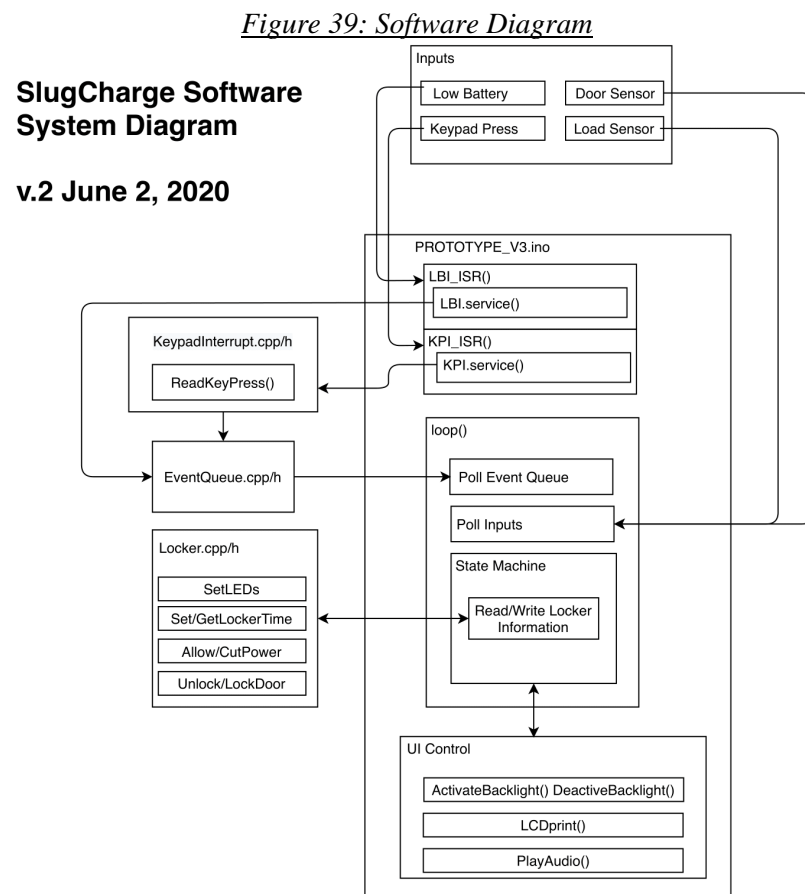
May 27, 2020



The software also features C++ object oriented programming using “Locker” objects

(Locker.h/cpp). The Locker objects represent each 6 lockers and on instantiation contains information of the relevant pins, data representing if the locker is occupied or vacant, the passcodes associated with the locker which are the users' input passcodes, the time since the locker entered an occupied state for purposes of implementing the grace period function, input pin reading functions that reads off their respective pin which the driver function will poll for inputs (door open/closed), and output pin writing functions that controls the power to the locker charging circuit and status LEDs. The Locker objects also have respective getters/setter functions that alter and return the locker data which are 1) the locker being vacant or occupied, 2) the time elapsed since the locker entered occupied, and 3) the stored passcode of the locker. These functions are referenced in the driving file's state machine which is the state-machine implementation in code, which primarily determines how the user will interact with the station and how the station will process input/outputs as well as storing locker information.

The state machine function implementation will actively control the user interface which includes controlling the backlight of the LCD, the characters printed on the LCD, and the audio to be played to the user through a speaker. Every loop in the state machine will actively control these devices depending on the state. See Appendix C for the state machine diagram of the station.



Engineering Schematics

See Appendix E and F for the engineering schematic of the microcontroller system testbench. Above mentioned code was further implemented on a custom test bench designed by the team which was an extension to the first microcontroller test board. This testbench was a necessary step towards prototyping stages since it determined what components may need to be updated, eradicated or added depending on the purpose. To develop this testbench, the team started with developing a schematic ported from the initial microcontroller breakout board and adding necessary components. The testbench uses LEDs and buttons to simulate inputs and outputs while also sending the same signals in parallel to standard header pins for testing with actual selected parts. The team then proceeded to layout the PCB for testing purposes. This PCB was necessary in order to further the team into a prototyping stage where the PCB could be directly installed into the physical model the mechanical team was implementing without having the need of multiple breadboards and floating wires.

The PCB was a success as it served as an exceptional proof of concept since it was able to do everything the code required it to do. The PCB was able to accept a 12v input that was regulated down to a 5V rail for the digital processes as well as supply the unregulated 12V to the solenoids. The PCB also housed all necessary components on board mitigating the requirement of breadboards and floating wires. The PCB was deployed for testing until further major changes to the code and required devices were made.

An obstacle we faced with the PCB was layout errors and selecting incorrect footprints for the 5V and 3.3V regulators (AMS1117-x.x) as well as the pin headers for the 16x02 LCD and 3x4 keypad. For the two latter devices, the pins were placed mirrored which was soon fixed by implementing simple daughterboards that revered the pinout. After implementation of these daughterboards, the testbench functioned as expected.

See Appendix E and F for schematics and PCB layout of the first [system level testbench](#).

Final implementation of the code was done on a two part system with a motherboard hosting the microcontroller and the essential devices required for appropriate functioning. To complete the system, this motherboard used an array of IDC connectors to communicate with each locker that received a daughterboard to itself. The motherboard included components such as the 5V and 12V regulators (LM2576), audio amplifier (PAM 8403), interrupt detection (74HC08) and SD-card. The motherboard is designed to be central to the unit and irreplaceable. The daughter board that each locker received is identical and helps the system function as per the requirements. These boards control the phones being charged, regulating voltage down to 5V and detect phones being plugged in. These PCBs were scheduled to be fabricated and assembled for the last two weeks of March 2020, however due to the given circumstances, they have been delayed until circumstances allow and are subject to availability of components and test equipment.

The schematics were deemed a success by the team as they depicted the communication between the microcontroller, user and the devices in between along with a reasonable flow of signal.

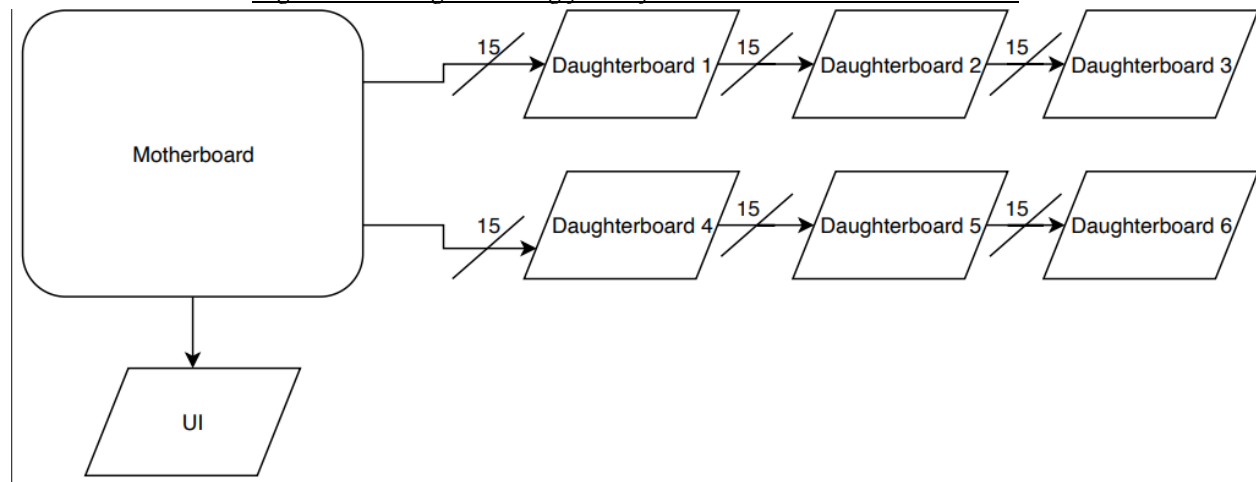
One difficulty these schematics, especially the motherboard, pose are problems for an unfamiliar reader who may not be as adept at reading schematics. Reading these schematics may be tough for unfamiliar people due to the multi page capture and rather discrete net names along with small text sizes. Another inefficiency in the daughter board schematic is the use of a TL081 in comparator topology to detect when a device is plugged in. This is not the most effective way to detect when a device is connected to the station, rather a design that detects a device using the data pins would be more effective. One last inefficiency on this schematic is use of standard 2.54mm header pins to breakout the status LEDs and door sensor; these connectors should have been MOLEX or JST type connectors, however due to time constraints we chose to implement the header pins instead.

See Appendix E and F for schematics and PCB layouts for the [motherboard](#) and [daughterboard](#).

PCB Integration

Given the physically large stature of the station, the system would require a central PCB (motherboard) that further communicates with each individual locker. These lockers should be controlled with a PCB of its own (daughterboard). This partitioning of PCBs aids in streamlining service of the station if required as well as reduces the number of interconnects required inside the station. This is achieved by connecting the motherboard with the daughterboards using 16-position IDC cables that would carry the control signals. As shown in the image below, the motherboard is connected to only two daughterboards beyond which the other daughterboards are connected in series with the neighboring daughterboards:

Figure 40: Image showing flow of communication between PCBs



On a given IDC connector, say for the top line controlling daughterboards 1 through 3, each daughterboard receives signals for all the other daughterboards on that line, however the correct signals are selected for processing using T5SA3357 SP3T switches. The correct signal set will be selected by providing the appropriate binary select input. Follow appendix F for the schematics and GERBER files of the motherboard and daughterboard.

Chapter 6: Lessons Learned

This chapter outlines the important lessons that were learned throughout this project. Key lessons on documentation, technical errors, and team organization have been learned during this project.

At the beginning of this project, documentation was a primary example of an area that needed development amongst the team members. The first quarter of this project was spent on brainstorming ideas for the operation and design of the charging station, strategizing testing methods, and creating goals required for the charging station to meet. The early development of this charging station required the team to focus on documenting information from team, client, and instructor meetings so that crucial information would be recorded for future designs. Furthermore, documenting communication through Slack was important as this allowed team members to keep up to date with each other's work instead of relying on weekly meetings for check-ins. Documentation of the early stages of this project has allowed the team to implement many design and test ideas in the later stages. By developing documentation habits, the team was able to verify design decisions based on previously set goals that were recorded at the beginning of this project.

The team also learned from mistakes made in the design stages of this project. For instance, the team made mistakes in the estimation of power usage, mechanical designs, layouts of PCBs, and considerations of edge cases in the state machine. The team learned through meetings with instructors on properly sizing a battery based on well-organized and appropriate specifications listed in the power budget. The team was able to size the battery down from a previously estimated 12V, 100Ah to 12V, 50Ah. This was important because it gave the team better insight on estimating power usage and also reduced costs for components. Mechanical designs were also altered to accommodate the goal of promoting user accessibility. The team learned from allowing people outside the team to test and simulate the process of charging a phone. Testers suggested modifying the internal design of the single locker compartment to allow users more space to place their phone inside and to plug in their charging cable. These suggestions were then implemented into the most recent design of the prototype and have proven successful in promoting user accessibility after further simulations from testers outside the team. Furthermore, as denoted by the revisions of the mother and daughter PCB layouts, the team learned how to properly implement testbench circuit designs onto PCBs. There were some errors made while laying out the PCBs, but modifications were made to reduce the physical space that each PCB would occupy in the charging station. Lastly, through many team, client, and instructor meetings, the team was able to create a list of edge cases that may occur during operation of the charging station. For example, the team took into account issues of users leaving their phones inside the station without closing the locker door. Alterations to the state machine were made by triggering an audible notification using a speaker to alert the user to close the door. Many other edge cases were also taken into consideration, but, ultimately, the team learned that it is important to receive feedback from the client testing prototypes or inquiring about design decisions in order to promote the most efficient and effective design that could be implemented in the final product.

Lastly, the team also learned that it is important to have meetings on self and peer evaluations and to have well-defined action items for each week to keep the team accountable. For instance, the team first began this project by dividing labor and setting up sub-team leaders. This allowed for effective use of

each member's skills. Although this also meant that each sub-team would have to constantly be in communication with the rest of the team so that the ultimate goal of accomplishing the team-client requirements would be fulfilled. As the project progressed the team learned to reorganize responsibilities and reorient team member commitments so that efforts in completing the project would not be undermined. The team learned that it is sometimes important to reorganize responsibilities so that the completion of tasks could be delivered on time.

The lessons that were learned throughout the development of this charging station have given the team a better perspective on proper documentation, technical applications, and team management. These skills have been crucial in aligning the team's efforts in completing tasks that fulfill the goals set by the team and client at the beginning of this project.

Chapter 7: Possible Future Work

This chapter outlines the future work and next steps that could be taken if the project were to be extended past the Spring quarter of 2020 or if a future senior design team decided to continue the project. These tasks have been brainstormed by the team to provide areas where the charging station could be improved.

The current prototype is developed in medium density fibreboard (MDF), which is not effective in resisting damage from weather conditions or theft. The current design considers the use of polycarbonate plastic for the outer enclosure, 316 stainless steel for the inner enclosure, and an aluminum frame. Due to budget constraints and technical constraints, purchasing these materials and fabricating the mechanical parts of the station were challenges presented due to the outbreak of COVID-19. Potential future work would be to improve on the mechanical design of the station including material selection and fabrication. Power devices could then be procured to integrate with mechanical and microcontroller hardware.

The Atmel ATmega2560 power consumption can be reduced by lowering the voltage supply and the external oscillator frequency (CPU power consumption scales at $P_{CPU} = CV_{dd}^2 f_{osc}$). The microcontroller power ratings could be reduced to a minimum of 1.8V with a maximum oscillator safe frequency of 2MHz. Reducing the power consumption this way requires reevaluating all the I/O circuits, compensating for the timing differences in software, and the addition of another voltage rail from the power systems. Although this would promote the overall power efficiency of the charging station.

The current program uses C++ for the speed of development. The Atmel ATmega2560 supports programming in embedded C and doing so would enhance the performance of the software as C programming language does not have any processing overheads such as actively checking for memory leaks or automatic garbage collection. Only the syntax of the program will be changed as the logic remains the same.

Ultimately, these potential future tasks could promote the effectiveness and efficiency of the system. These action items could be completed by future senior design teams.

Chapter 8: Conclusions

The designs established in the power systems have been verified through analysis of datasheets and compilation of specifications in the power budget. The tests that have been conducted on the voltage regulator and phone charging circuits have shown positive results that meet performance and electrical interface constraints elucidated in the team-client goals. Although the charging circuit requires improvements to allow for fast charging to Android devices and fabrication of the charging station utilizing robust materials such as 316 stainless steel and polycarbonate plastic would bolster theft and weather damage prevention efforts. The microcontroller PCB design and programming successfully allow the mechanical components in the design to interact according to the operation flowchart and state machine diagram. The test results for all designs display validation of the design decisions.

As designed currently, the power system components align with the requirements listed in the power budget. The components displayed in the power systems block diagram illustrates the overall, summarized design of the power system. The solar panel array has been sized to meet energy requirements of the battery and the electrical components in the charging station. The MPPT charge controller allows the system to convert the extra voltage from the solar panels to allow for a maximized current output into the battery. This means that the battery would be able to charge at an extremely high rate while still remaining safely under the battery's current rating as the fuses prevent surges. The battery then connects to the PCBs with voltage regulators that provide proper powering to the internal electrical components inside the charging station and to charge the phones.

The software design of the system successfully meets the criteria of providing the ability for the user to interface the lockers, select a vacant or occupied locker, enter their own 4-digit passcode, and insert their phone while the station detects if the phone is inserted to the USB or not. The software checks for any 30 second timeout edge cases and other cases that detect if the locker is accurately vacant or occupied using the sensors connected such as current sensing the USB port and detecting the door being opened or closed. To provide a robust system, the software detects if the user has been in a state where a locker door is open and responds by transitioning to a state where the locker plays audio stored on the local SD card to warn the user or provide audible instructions. To respond to cases when the station may lose power while the lockers are occupied, data representing the number of phones charging, which lockers are occupied or vacant, and the passwords of each occupied locker is stored on the volatile memory of the SD card. This means that when the station is rebooted, the lockers are initialized to their previous states before the power has been cut off. Writing to EEPROM is the next step to improve on this method as the on-chip EEPROM provides another means to storing data on nonvolatile memory. The SD card contents may be verified with EEPROM memory which resolves single point failures of the SD reader hardware. The software actively checks for open doors with timer interrupts to notify the user if a non-intended locker door is open to resolve issues of faulty door-sensor or lockpicking. The station also actively checks the lockers for the time allotted for charging such that after 2 hours, the software sends a signal to a switch to disconnect the phone from the power source to introduce an incentive to come back and pick up their phones. The software also optimizes its power consumption by putting the microcontroller in sleep mode when the locker is not in use. These features are documented in the system level block diagram and the state machine diagram. Overall the software introduces an interface from the

power system to the mechanical and hardware systems and meeting with the HGP client to demonstrate the design of the project determines and validates the design goals of the project.

The mechanical design is currently a work in progress as the CAD files of the prototype design has been completed; however with the design specifications outlined in the *Technical Design and Implementation* chapter, the locker must be able to resist weather and theft. Due to budget and fabrication constraints to the mechanical design, an MDF model prototype has been developed for demonstration. For the complete project, the mechanical design decisions include the use of 316 stainless steel and polycarbonate plastic materials.

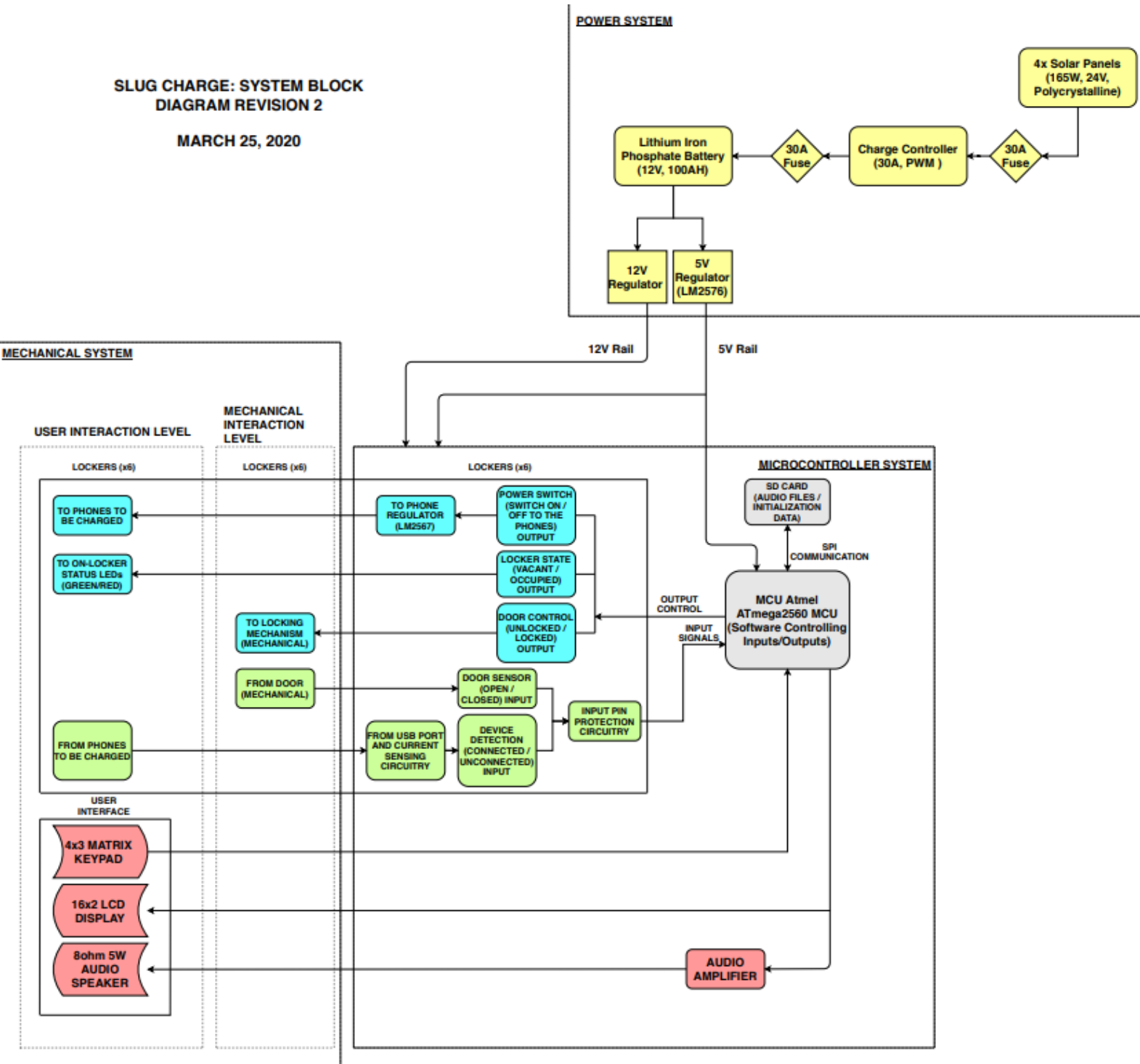
Installation of this designed charging station accomplishes all the final goals based on the design specifications outlined in the *Technical Design and Implementation* chapter.

Appendix A: System Block Diagram

Figure AP-A1: System Block Diagram Rev. 2

**SLUG CHARGE: SYSTEM BLOCK
DIAGRAM REVISION 2**

MARCH 25, 2020



Appendix B: MCU Choice Pugh Chart

Figure AP-B1: MCU Pugh Chart Rev 2

Microcontroller Pugh Chart:

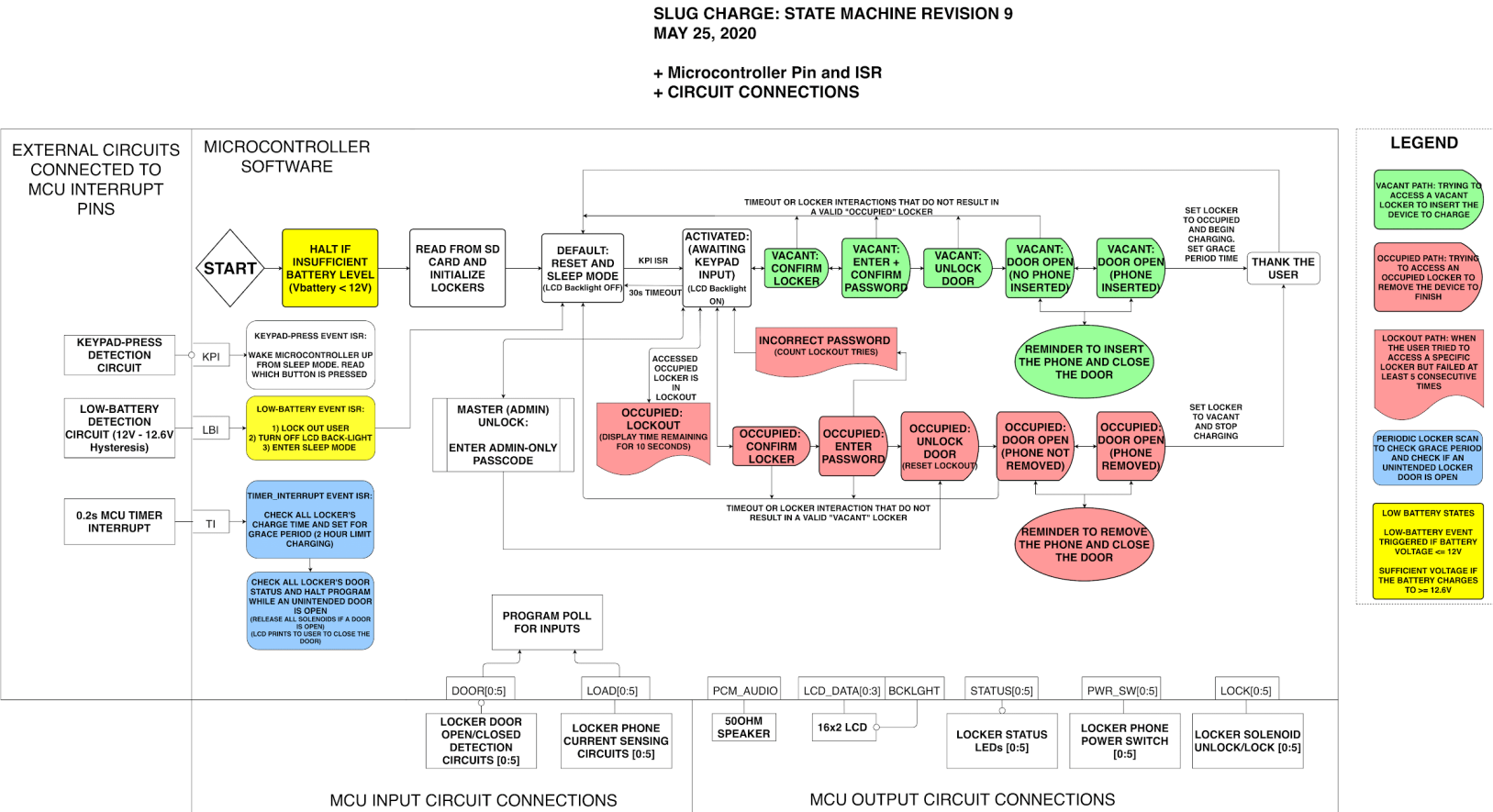
Scale: from -3 to +3 with +3 being the best and 0 being neutral

Microcontroller Choices	Vdd Requirement	Operating Frequency	Number of GPIO Pins	Programming Language ¹	Memory	Cost (Chip)	Total
Weighting	2x	1x	3x	2x	2x	3x	
STM32 NUCLEO - L053R8	2 (1.8V - 3.6V)	1 (120MHz)	2 (64 pin count)	3 (C/C++)	2 (64kB Flash, 8kB SRAM)	3 (~1.5 USD DigiKey)	30
ATmel ATmega328P (Arduino Uno)	3 (1.8V - 5.5V)	3 (0Mhz - 16Mhz)	-2 (14 digital pins, 6 analog pins)	3 (C/C++)	-3 (32kB Flash, 2kB SRAM)	3 (~2USD Microchip)	12
Atmel ATmega2560 (Arduino Mega2560)	3 (1.8V - 5.5V)	3 (0Mhz - 16Mhz)	3 (54 digital pins, 16 analog pins)	3 (C/C++)	3 (256 kB Flash, 8 kB SRAM)	2 (~6USD lcsc)	36
IMXRT1062 (Teensy 4.0)	2 (1.25V - 3.7V)	1 (24MHz Typical)	2 (40 pin count)	3 (C/C++)	1 (2MB Flash, 1MB SRAM)	0 (~11USD Mouser)	19
MK66FX1M0 (Teensy 3.6)	2 (1.7V - 3.6V)	2 (3MHz - 32MHz)	1 (33 pin count)	3 (C/C++)	1 (1MB Flash, 256kB SRAM)	-1 (~17USD DigiKey)	14
PIC32MX320F064H	2 (2.3V - 3.6V)	3 (0MHz - 80Mhz)	3 (64 pin count)	3 (C)	3 (64kB Flash, 16kB SRAM)	2 (~8USD Microchip)	35
Raspberry Pi 4 ²	2 (5V)	1 (1.5GHz)	2 (40 GPIO pins)	3 (Preloaded with Python, but C/C++ Available)	1 (32GB Flash, 1GB SDRAM)	-1 (~35USD Amazon)	14

Appendix C: State Machine Diagram

Figure AP-C1: State Machine Diagram Rev. 9

A brief description for each state is noted below:



START: Where the station will begin operating upon starting up. Automatically transitions to **INITIALIZATION** state.

INITIALIZATION: The locker will then read the SD card for any startup information (number of lockers charging, which lockers are occupied or vacant, the passwords of occupied lockers) and initialize the lockers with previous vacant/occupied status and the passwords for each locker. Automatically transitions to **DEFAULT** state.

DEFAULT: A state of no-activity. The LCD backlight is turned off to conserve power and the microcontroller is put in sleep mode. If a user presses any key on the keypad, the microcontroller will move onto the **ACTIVATED** state.

ACTIVATED: A state where the user wakes the microcontroller via a keypad press. The user can pick a locker to access from this state using the keypad. The admin may also use the **MASTER_UNLOCK** in this state as well. Depending on if the number pressed represents a locker that is occupied or vacant, the

locker will transition to confirm the locker in either vacant or occupied path. After 30 seconds of inactivity, the program will transition to DEFAULT state.

MASTER_UNLOCK: After the required interaction from the admin, the admin may enter a predetermined passcode to unlock a locker and enter OCCUPIED:UNLOCK_DOOR state. After 30 seconds of inactivity, the program will transition to DEFAULT state.

THANK_THE_USER: After a completed OCCUPIED or VACANT path, the program will enter a blocking state for 5 seconds where the station will display through LCD a “Thank You, Please Come Again” message as well as audio saying “Thank You, Please Come Again”. This further transitions to the DEFAULT state.

From here, the user may enter either color coded paths, depending on if the locker selected is either **VACANT** or **OCCUPIED**. These paths determine how the user will be able to access a locker, enter a 4 digit passcode saved onto the microcontroller and secures the phone if a user attempts a wrong password at an occupied locker; these are to meet the software functional goals (see Introduction, Functional Constraints: Features). The vacant path allows the user to access a vacant locker and enter a passcode which is saved onto the microcontroller, the occupied path allows the user to try to access an occupied locker and enter a password saved onto the microcontroller. If the passcode is wrong, the user will not be able to access the locker; if the passcode is correct, the user will have access to their phones.

VACANT:ENTER+CONFIRM_LOCKER: The user may enter their own 4-digit passcode that will save to the locker. The user may re-enter from this state and re-enter their locker password until confirmed or canceled. After 30 seconds of inactivity, the program will transition to DEFAULT state.

VACANT:UNLOCK_DOOR: The locker the user has accessed will unlock the door for 10 second maximum. The user may open the door to proceed or wait out the 10 second to return to the DEFAULT state. Opening the door will transition to the VACANT:DOOR_OPEN state. After 30 seconds of inactivity, the program will transition to DEFAULT state.

VACANT:DOOR_OPEN: The locker the user has accessed will enter a state where the door is open but the phone is not plugged in. The program waits for the user to close the door, transitioning into the DEFAULT state, or insert their phone, transitioning into the VACANT:PHONE_INSERTED state. After 10 seconds of inactivity, the program will transition to VACANT:REMINDER state.

VACANT:PHONE_INSERTED: The locker the user has accessed will enter a state where the door is open and the phone is connected to the USB. The program waits for the user to close the door, transitioning into the THANK_THE_USER state, or unplug the phone, transitioning into the VACANT:DOOR_OPEN state. After 10 seconds of inactivity, the program will transition to VACANT:REMINDER state.

VACANT:REMINDER: The locker the user has accessed will enter a state after a period of inactivity that will display to the user to plug in their phone and close the door. Audio instructions will be played to the user until this requirement is met. Removing the phone or closing the door will revert back to its previous state before entering.

OCCUPIED:CONFIRM_LOCKER: The user will see the locker number they are trying to access on the LCD and asks to confirm if the user would like to try to receive their phone. After 30 seconds of inactivity, the program will transition to DEFAULT state.

OCCUPIED:ENTER_PASSWORD: The user will try to enter their locker’s password up to 4 digits.

After 30 seconds of inactivity, the program will transition to DEFAULT state.

OCCUPIED:INCORRECT_PASSWORD: If the user incorrectly inputs their password to match the occupied locker's password, they will enter a blocking state where the LCD indicates to them they entered an incorrect password. A Lockout counter will be iterated for the Lockout function. This then transitions to the DEFAULT state.

OCCUPIED:LOCKOUT: If the user fails to enter a locked out locker 5 consecutive times, the next time the user tries to access that locker, the program will enter a temporarily blocking state displaying that the locker is in lockout and the time remaining. This will display for 5 seconds before transitioning to the DEFAULT state.

OCCUPIED:UNLOCK_DOOR: The locker the user has accessed will unlock the door for 10 second maximum. The user may open the door to proceed or wait out the 10 second to return to a previous state.

OCCUPIED:DOOR_OPEN: The locker the user has accessed will enter a state where the door is open but the phone is not removed. The program waits for the user to close the door, transitioning into the DEFAULT state, or remove their phone, transitioning into the OCCUPIED:PHONE_REMOVED state. After 10 seconds of inactivity, the program will transition to OCCUPIED:REMINDER state.

OCCUPIED:PHONE_REMOVED: The locker the user has accessed will enter a state where the door is open and the phone is removed from the USB. The program waits for the user to close the door, transitioning into the THANK_THE_USER state, or plug the phone, transitioning into the OCCUPIED:DOOR_OPEN state. After 10 seconds of inactivity, the program will transition to OCCUPIED:REMINDER state.

OCCUPIED REMINDER: The locker the user has accessed will enter a state after a period of inactivity that will display to the user to remove their phone and close the door. Audio instructions will be played to the user until this requirement is met. Inserting the phone or closing the door will revert back to its previous state before entering.

Periodically the program will check on timer interrupt to scan each locker of the station for Grace Period and open doors.

SCAN_LOCKERS: The program will scan all of the station lockers. This will then transition into GRACE_PERIOD_CHECK state.

GRACE_PERIOD_CHECK: The scanned lockers will be checked for charging over 2 hours and switch off the power to the phone if the phone is detected to be charging over 2 hours. This provides an incentive for the user to return to pick up their phone, and is one of the project goals of software (see Introduction, Functional Constraints: Features).

DOOR_STATUS_CHECK: The scanned lockers will be checked for open doors for lockers that are not being accessed. If an unintended locker door is open, the program will halt, release all solenoids, and print to the user via LCD screen to close the door until the door is closed. The program will then return to where it was before interrupted.

Appendix D: Component Selection Pugh Chart

Component: User Unlock Mechanism	Power Efficiency	Number of Pins	Cost	Simplicity	Total
Weighting	3x	1x	3x	1x	
Fingerprint Scanner	0 (5V, 120mA)	1 (4)	-3 (~30\$)	-2	-10
RF ID	1 (3.3V, 13mA)	1(4)	0 (~0\$)	0	4
Keypad	3(5V, 0.5mA)	0 (7)	3 (-5\$)	3	21

Component: Locking Mechanism	Power Efficiency	Number of Pins	Cost	Mechanical Strength	Activation Speed	Simplicity	Total
Weighting	3x	1x	3x	3x	2x	1x	
Servo	0 (5V, 10mA IDLE)	1 (3 pin)	1 (~10\$)	-3	0 (~1s)	1	-4
Solenoid	0 (5V, 350mA ACTIVATED, 0A IDLE)	3 (1 pin)	1 (~10\$)	3	3 (Effectively Immediately)	3	24
Door Strike	-2 (12V, 220mA)	3 (1pin)	-3 (~44\$)	3	3 (Effectively Immediately)	2	5

Component: Display	Power Efficiency	Number of Pins	Cost	Simplicity	Total
Weighting	3x	1x	3x	1x	
16x2 LCD	0 (5V, ~150mA w/Backlight)	0 (7 pin, 4 pin with I2C)	3 (-5\$)	3	12
128x32 OLED	0 (5V, ~150mA w/Backlight)	0 (4 pin with I2C)	2 (~22\$)	-1	6

Materials for Outer Housing	Cost	Weight	Ease of Manufacturing	Maintainability	Weather Resistance	Vandalism/Theft Resistance	Ventilation Capabilities	Carbon Footprint	Total
Weighting	3x	1x	1x	2x	3x	2x	2x	2x	
Acrylic	+2	+1	+2	-1	-1	-3	-1	-2	-8
Steel	-3	+3	-3	+3	1	+3	+1	+1	+10
Aluminum	-1	+2	0	+2	0	+1	+1	+2	+11
MDF	+3	0	+3	-3	-3	-3	-3	0	-15
ABS Plastic	-1	+1	+1	+2	+2	+1	-1	-2	+11
PET Plastic	0	-2	+2	+1	+1	+1	-1	-2	+1
Polycarbonate plastic	-2	+3	+3	+3	+3	+1	0	-2	+13

Materials for Inner Housing	Cost	Weight	Ease of Manufacturing	Maintainability	Vandalism/Theft Resistance	Ventilation Capabilities	Form Factor Considerations	Carbon Footprint	Total
Weighting	3x	1x	1x	2x	3x	2x	2x	2x	
Carbon Steel	-1	-2	+1	+1	+1	+1	+1	+1	+7
Alloy Steel	+1	-2	-1	+1	+1	+1	+1	+1	+11
Stainless Steel	-1	-2	+2	+3	+3	+2	+2	+1	+22
Tool Steel	0	-2	+2	-2	+1	0	0	+2	+3
Cast Alloy Aluminum	-2	+1	-2	+1	0	+2	+2	+2	+7
Wrought Alloy Aluminum	-3	+1	-3	+2	+1	+2	+2	+2	+8
Polycarbonate plastic	-2	+2	-2	+2	+1	-1	-1	-2	-11
ABS Plastic	-1	+2	-1	+1	0	-1	-1	-2	-8
MDF	+3	+3	+3	-3	-3	-3	-3	0	-12
PET Plastic	0	+2	0	0	0	-1	-1	-2	-6

Appendix E: Engineering Schematics and PCB Layouts

This appendix exhibits the motherboard and daughterboard engineering schematics and PCB layouts. The original versions of the microcontroller testbench schematic and systems level testbench are also included in this appendix.

Microcontroller Test PCB v1

*Higher resolution PDFs of the following schematics and layout can be found in Appendix F

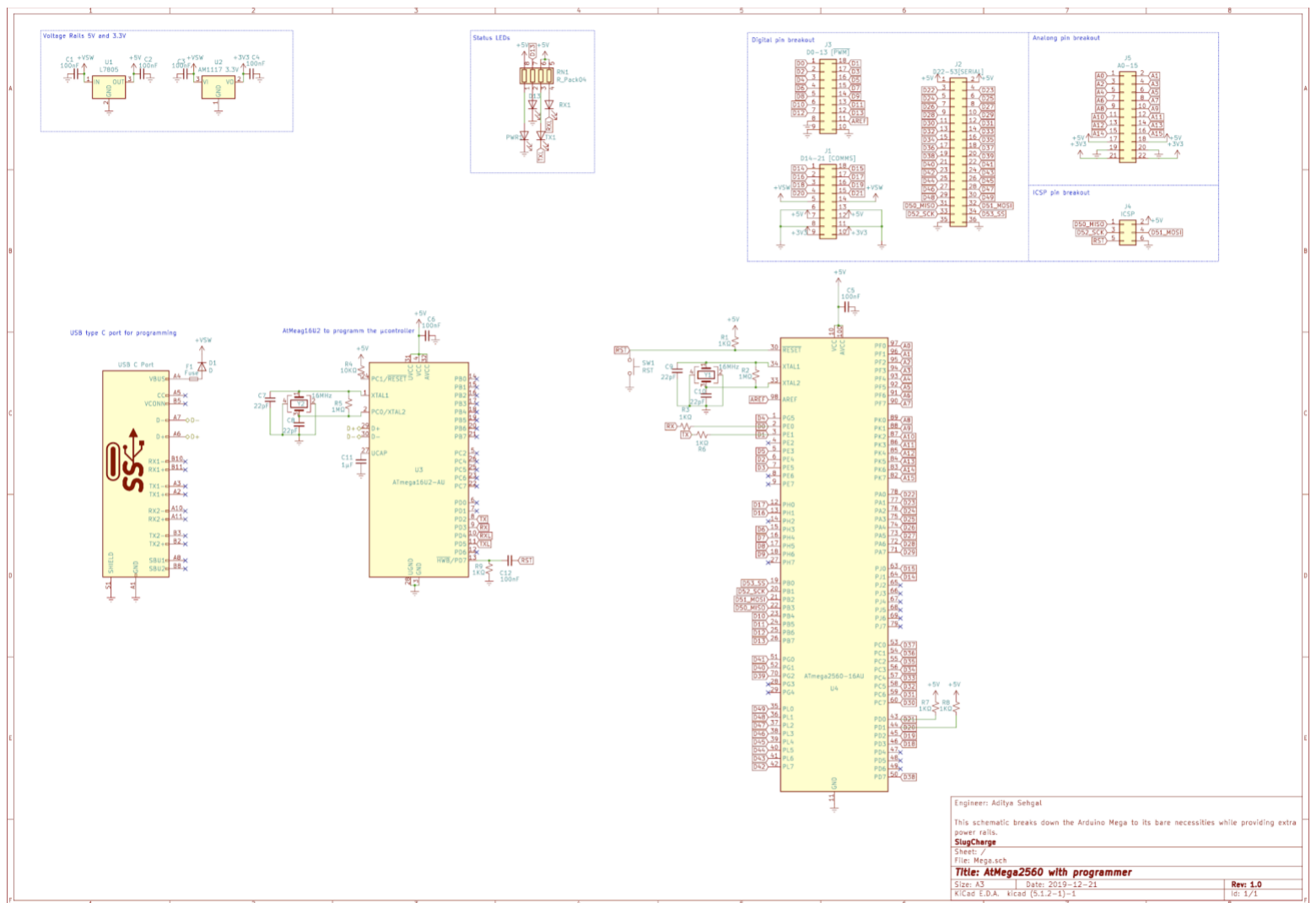
Figure AP-E1: Microcontroller Testbench Rev 1 Schematic Capture

Figure AP-E2: Microcontroller Testbench Rev 1 Top Layer

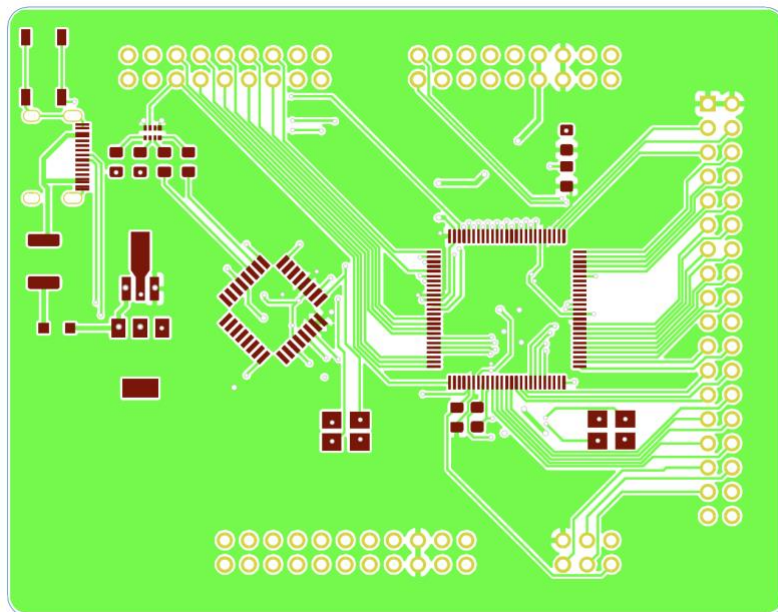
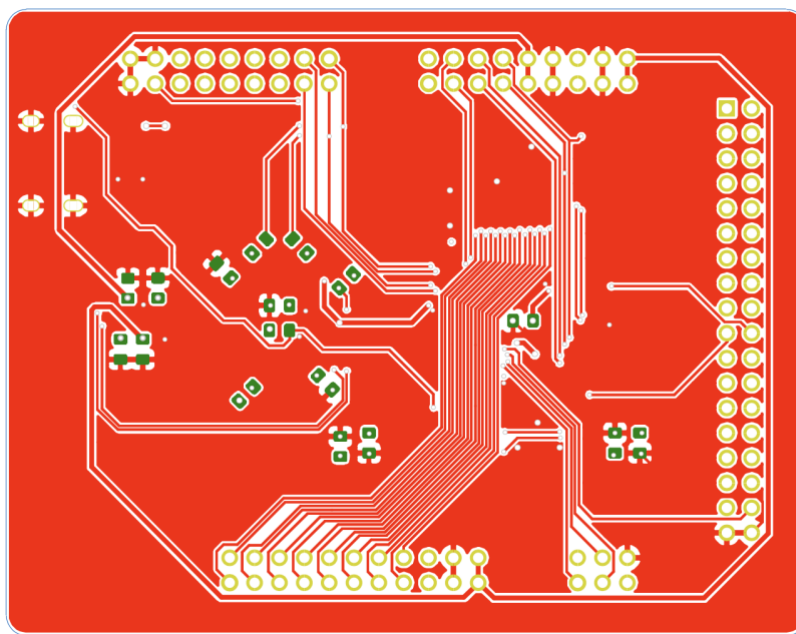


Figure AP-E3: Microcontroller Testbench Rev 1 Bottom Layer



System Level Testbench v1

*Higher resolution PDFs of the following schematics and layout can be found in Appendix F

Figure AP-E4: System Level Testbench Rev 1 Schematic Capture

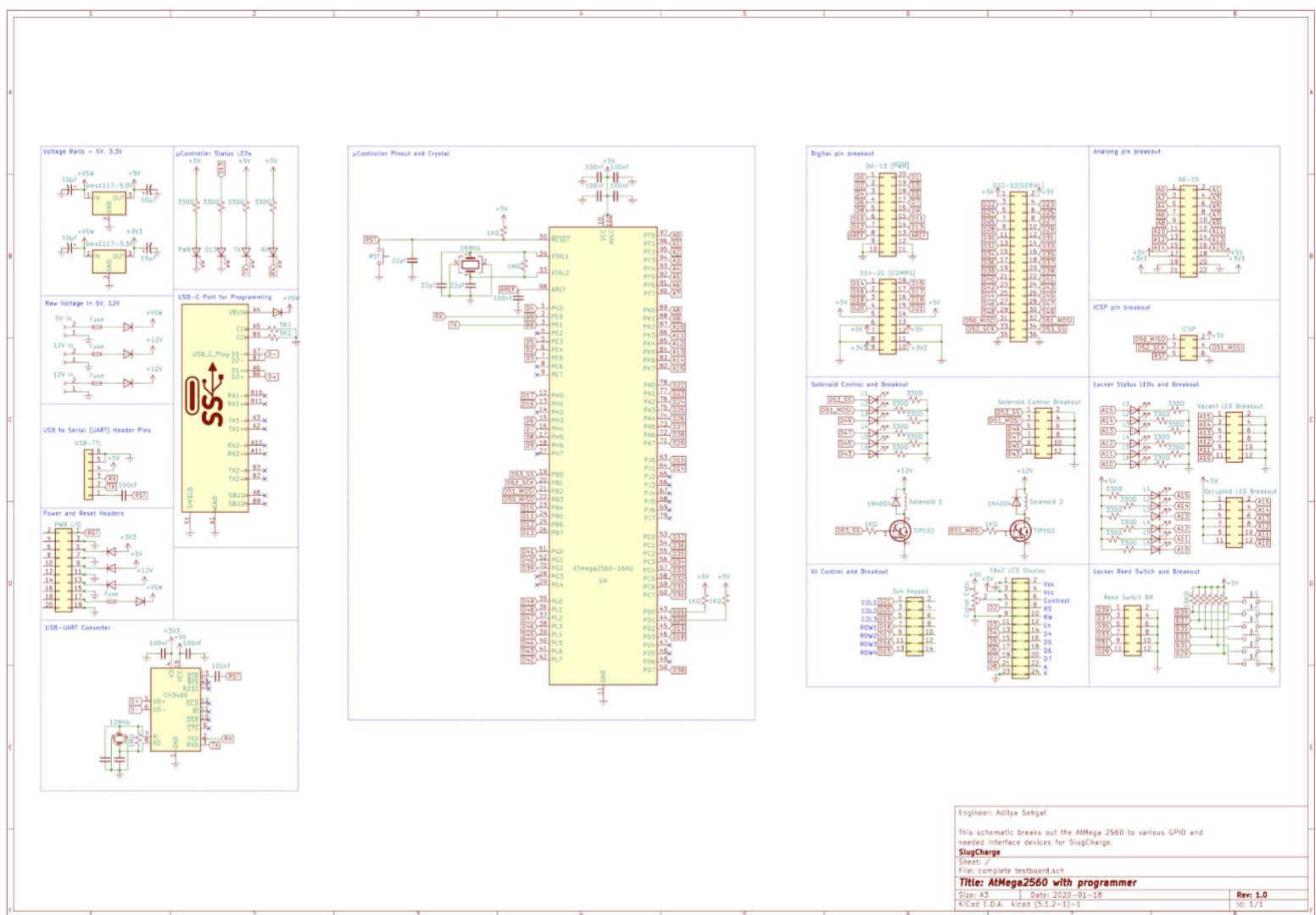


Figure AP-E5: System Level Testbench Top Layer Rev 1

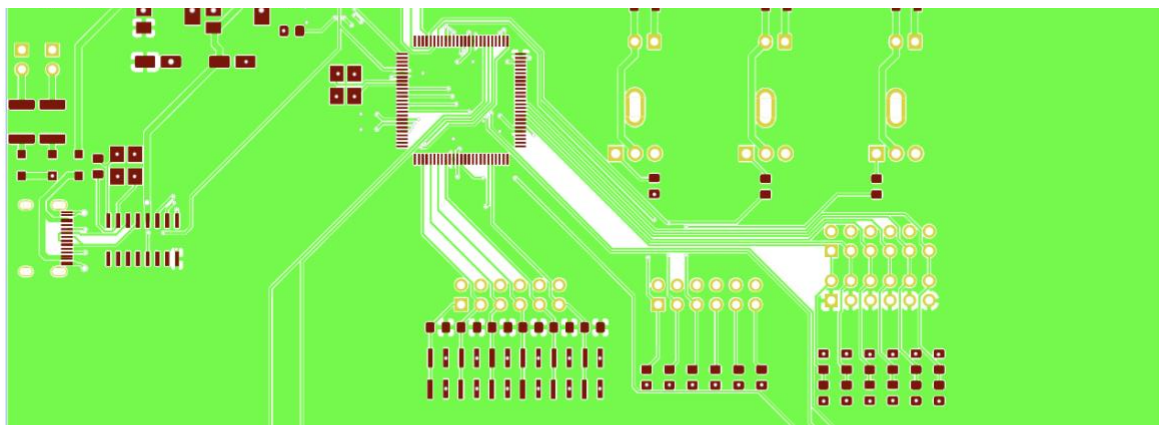
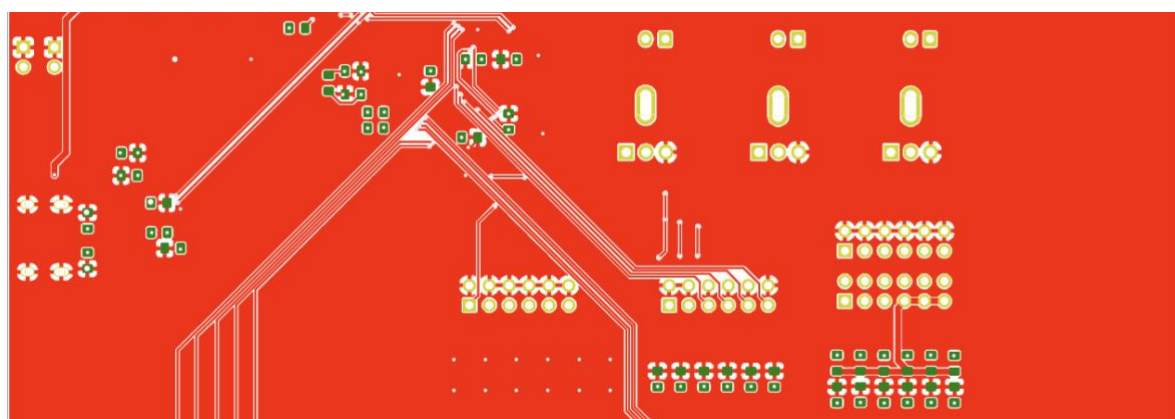


Figure AP-E6: System Level Testbench Bottom Layer Rev 1



Motherboard PCB v2

*Higher resolution PDFs of the following schematics and layout can be found in Appendix F

Figure AP-E7: Motherboard PCB Schematic V4.1 Page 1/2

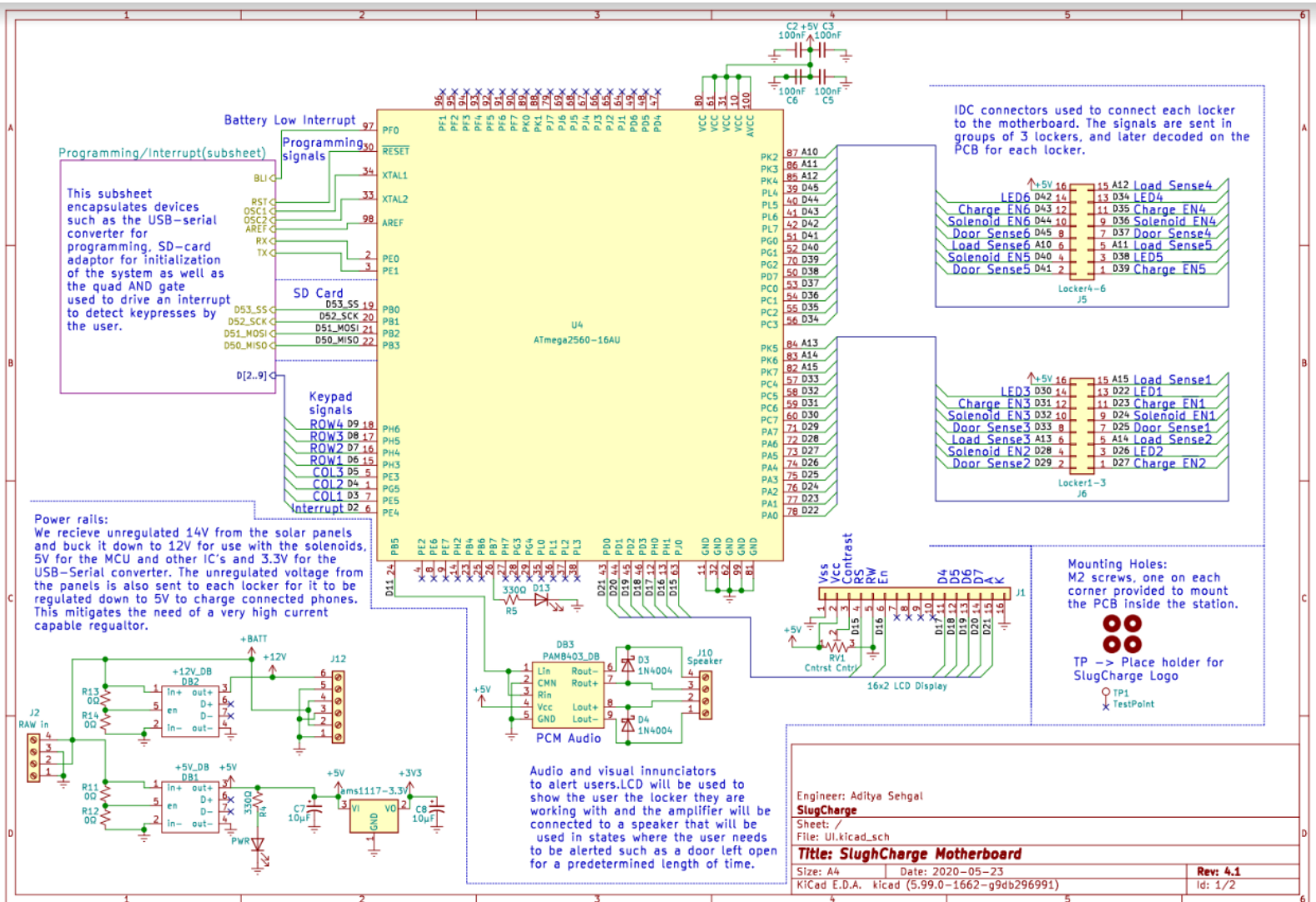


Figure AP-E7: Motherboard PCB Schematic V4.1 Page 2/2

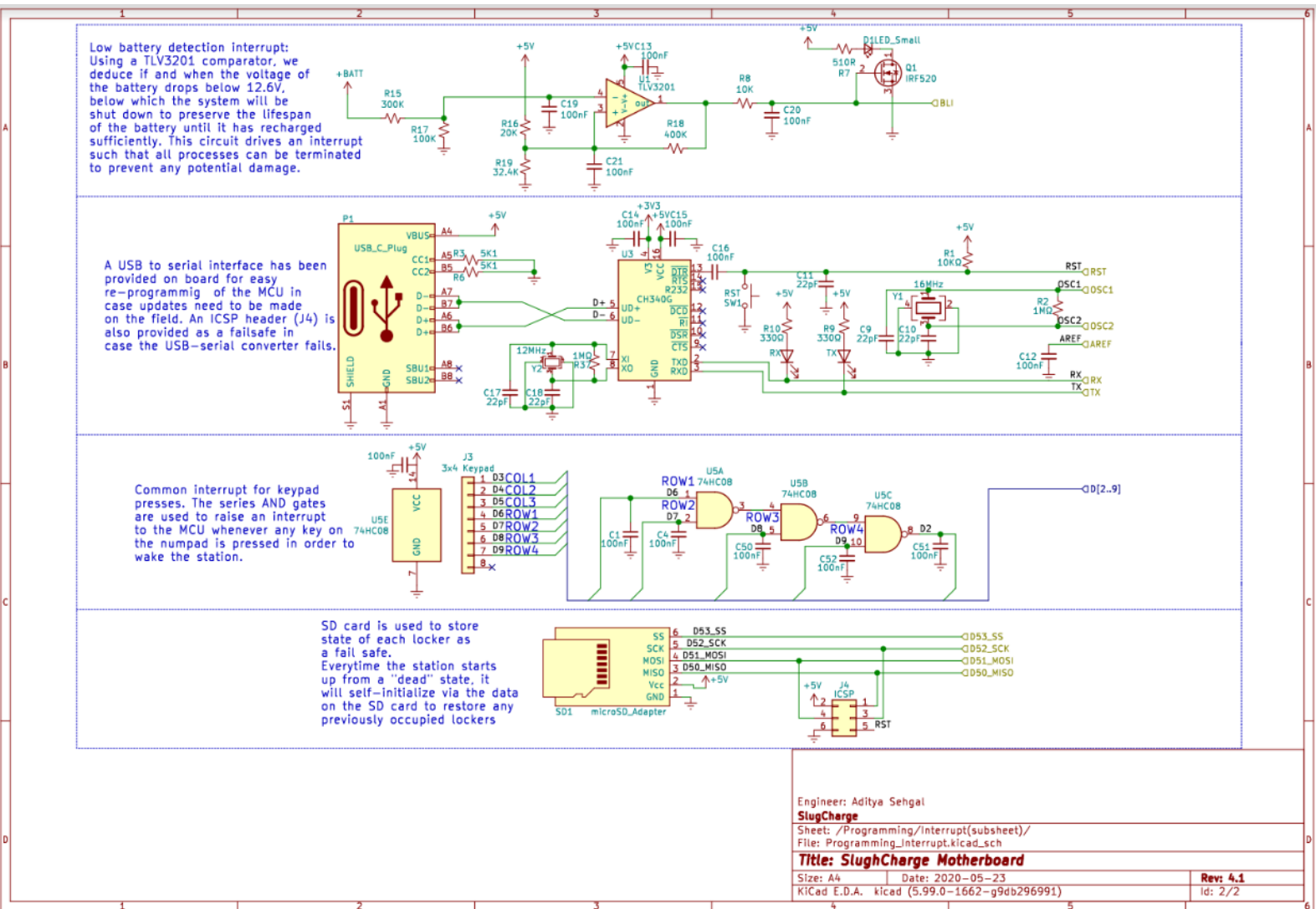


Figure AP-E9: Motherboard PCB Layout Top Layer V2.4

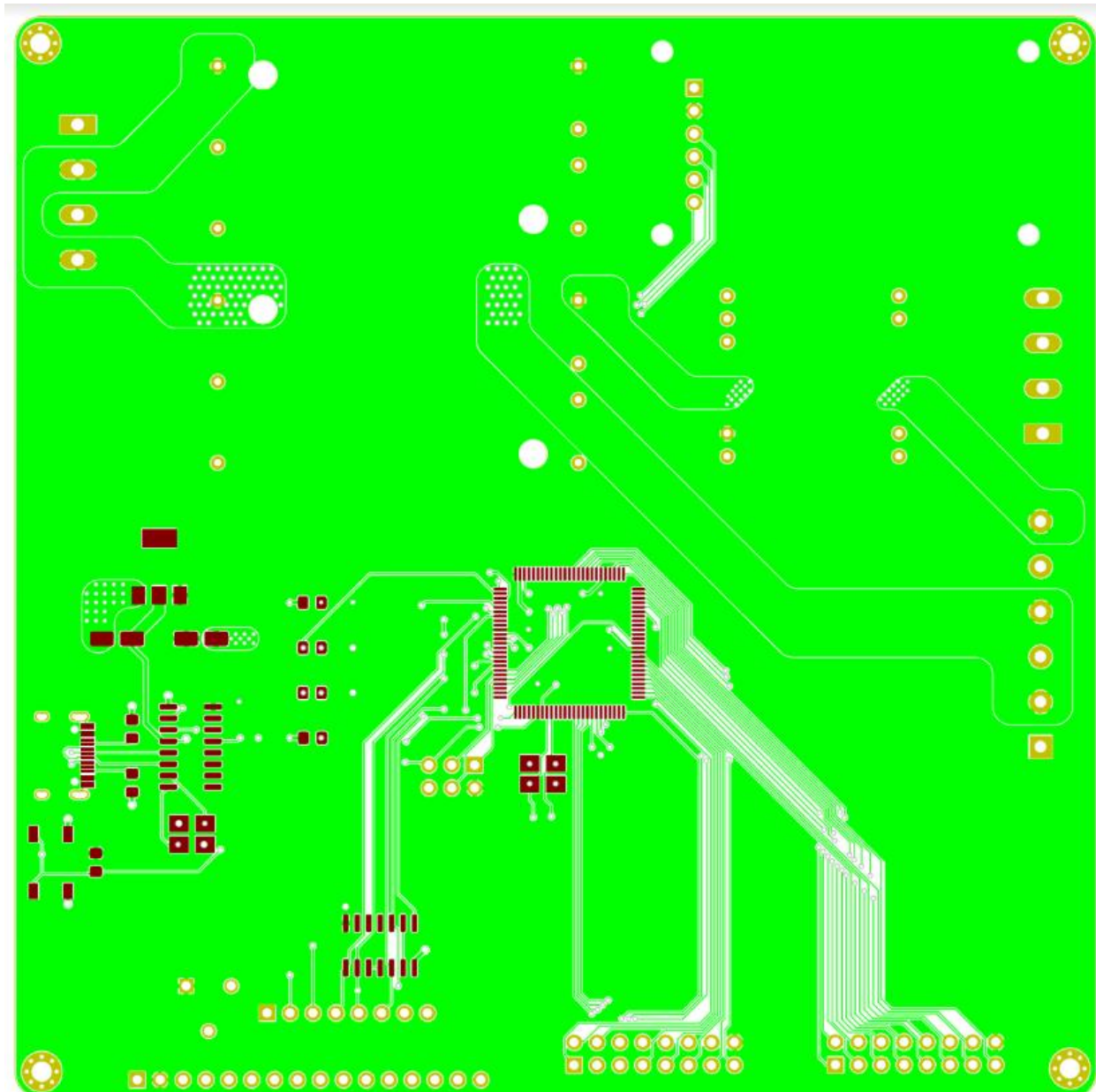
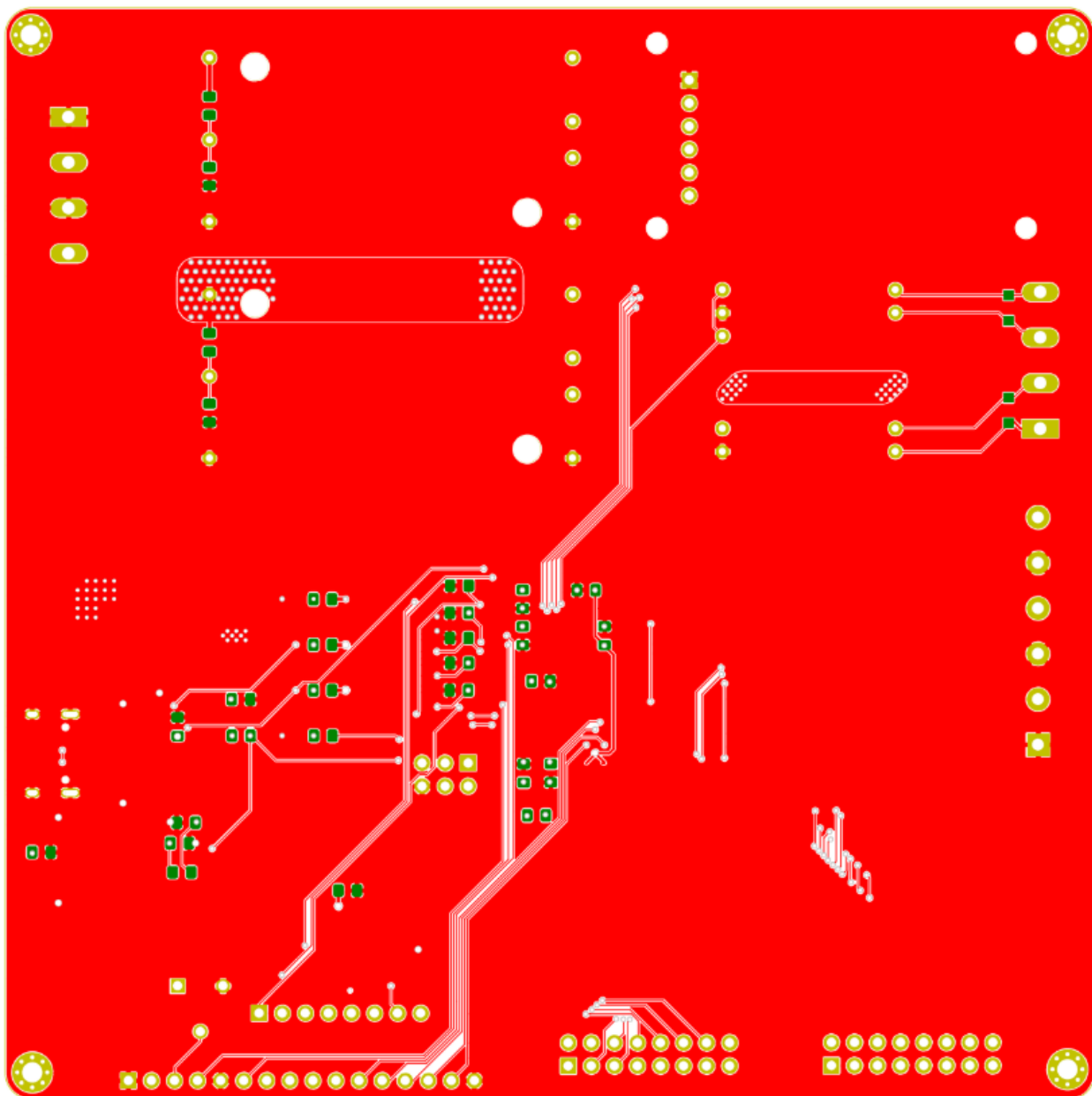


Figure AP-E10: Motherboard PCB Layout Bottom Layer V2.4



Daughterboard PCB v2

*Higher resolution PDFs of the following schematics and layout can be found in Appendix F

Figure AP-E11: Daughterboard PCB Schematic V4.0

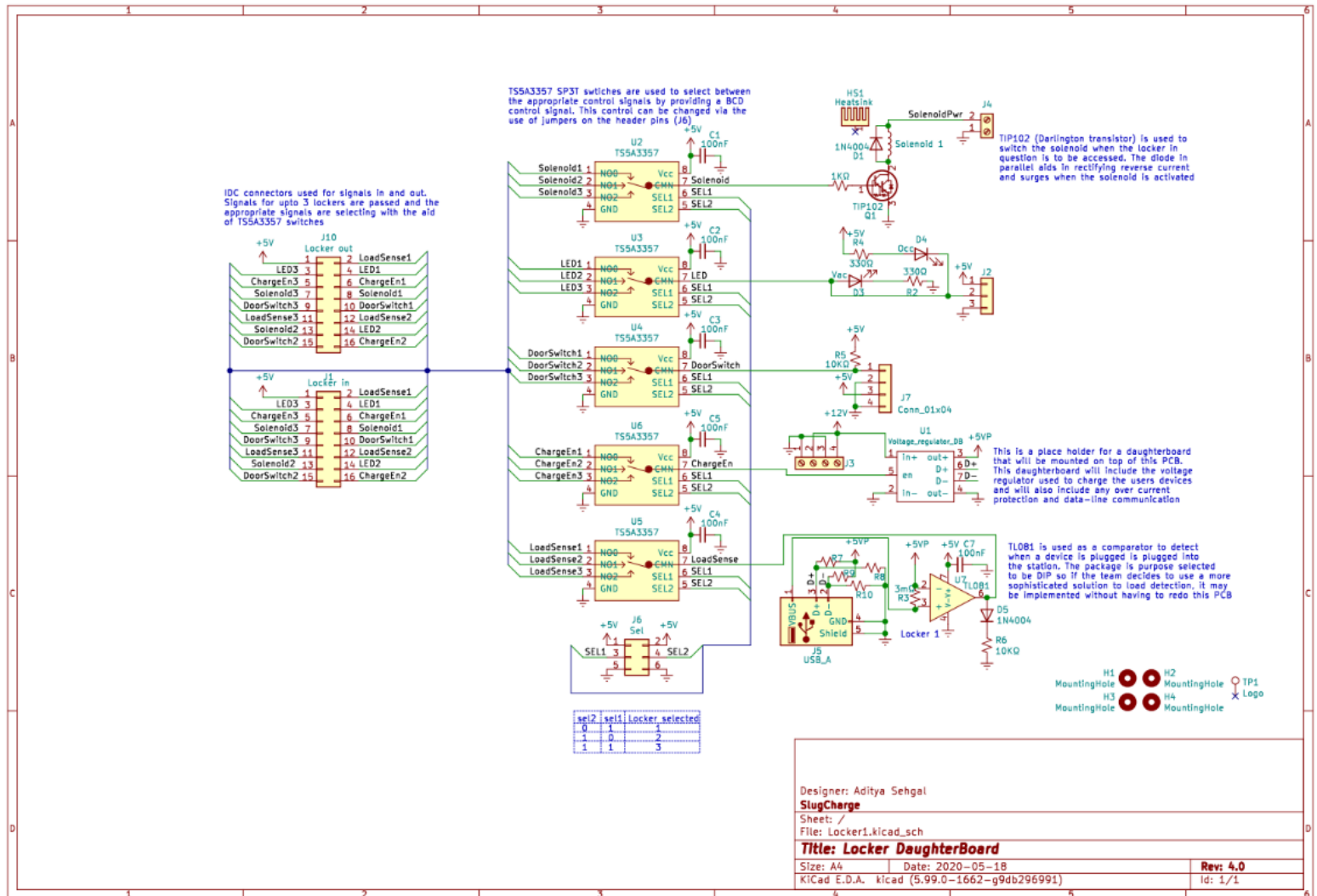


Figure AP-E12: Daughter PCB Top Layer Rev 2

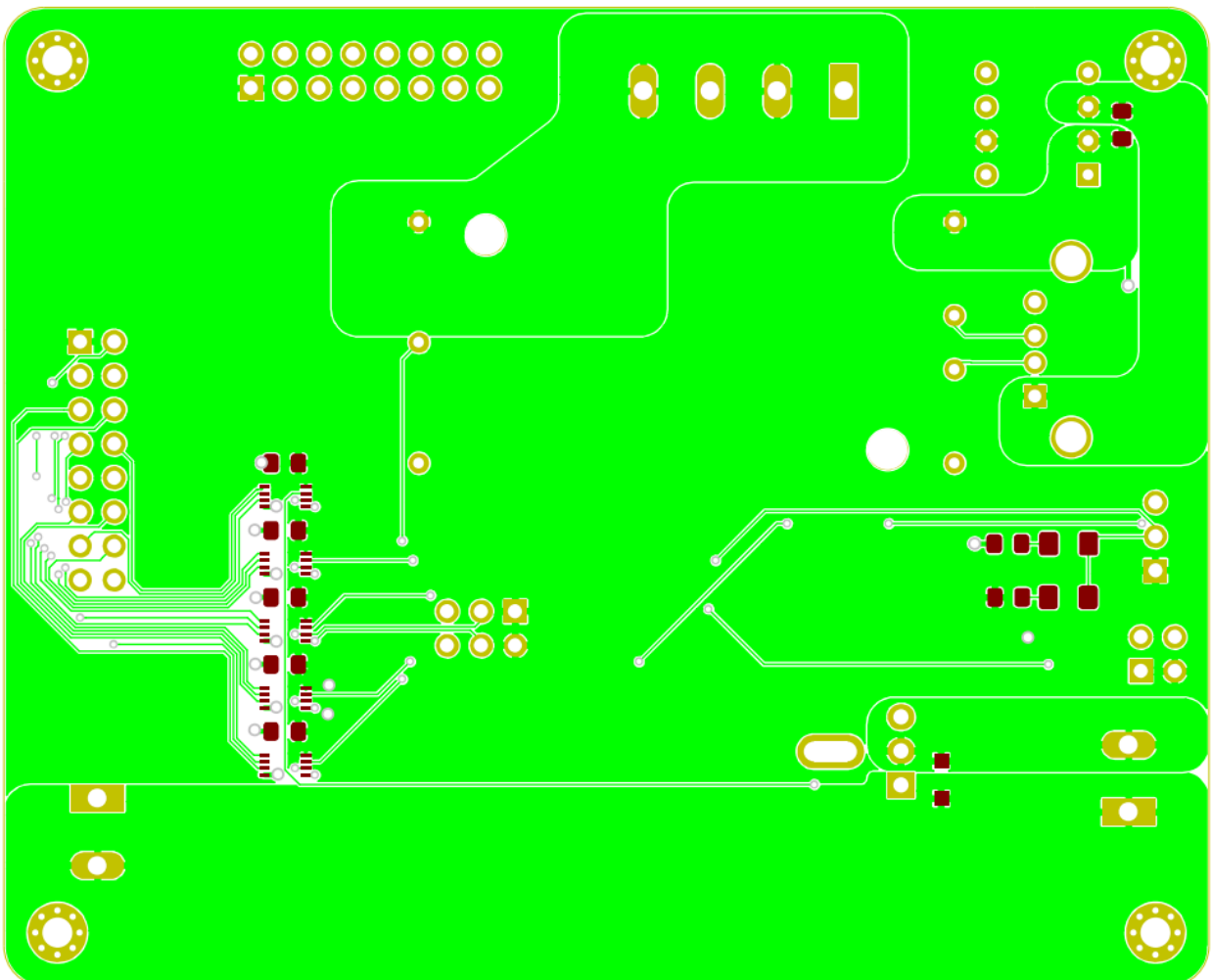
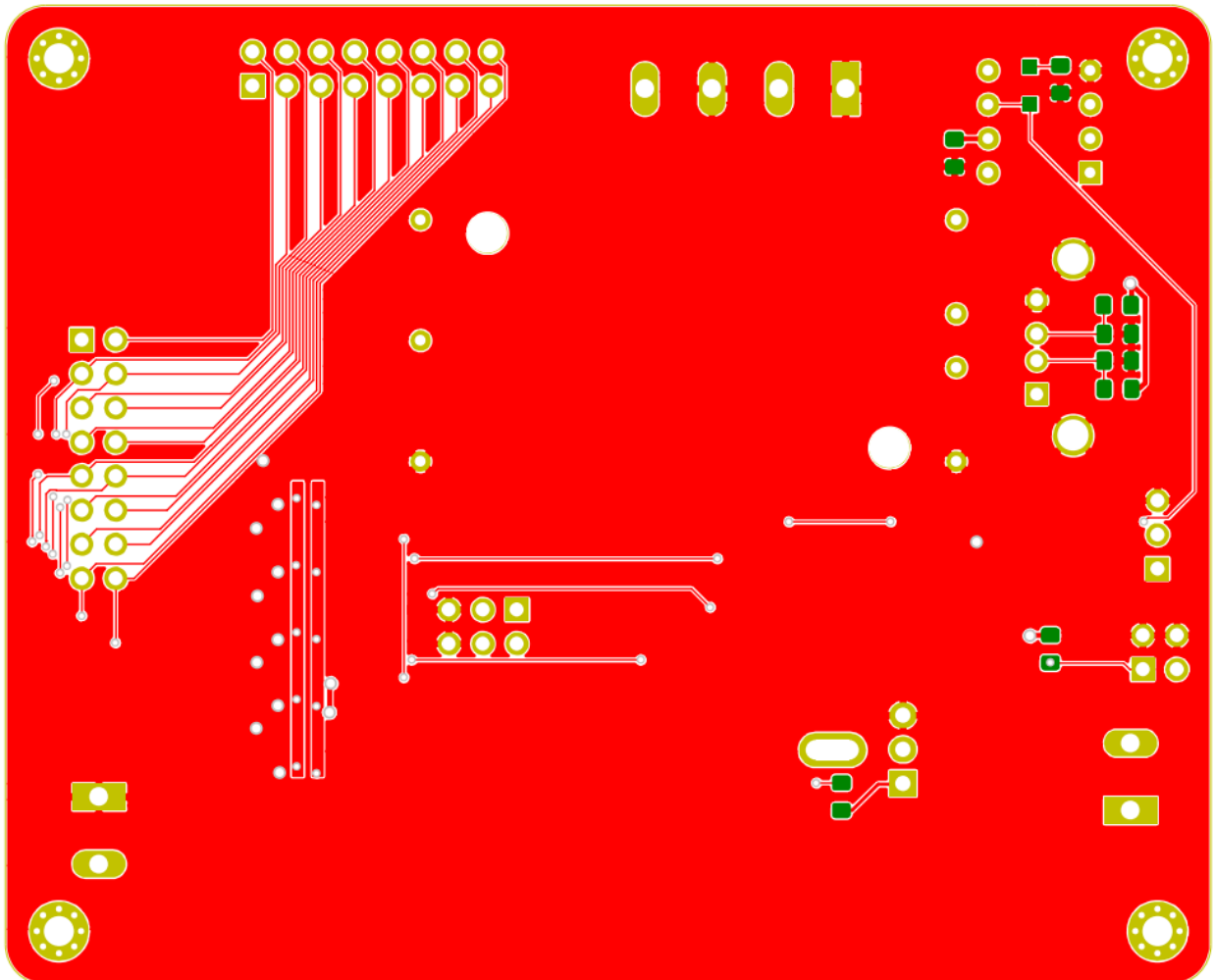


Figure AP-E13: Daughter PCB Bottom Layer Rev 2



Appendix F: Relevant Resource Links

SlugCharge Code Repository (Github):

<https://github.com/jeffreyloalt/SlugCharge>

PCM Audio Library, Open Source:

<https://github.com/TMRh20/TMRpcm>

SlugCharge Power Budget v17 (April 20, 2020):

https://drive.google.com/file/d/1jPmQjeSzCVY3QaD_JMbqSGqo6sQEcj6D/view?usp=sharing

SlugCharge Demand Factor Power Budget v2 (April 21, 2020):

https://drive.google.com/file/d/1jPmQjeSzCVY3QaD_JMbqSGqo6sQEcj6D/view?usp=sharing

Power Usage per State v1 (April 27, 2020):

<https://drive.google.com/file/d/1v6U0OVjHBuJJWFmCbxqTeMYFdSYvnLO/view?usp=sharing>

Phone Charging Test Data Using Smart Charger v3:

<https://docs.google.com/spreadsheets/d/1XHV8rmuaQ63XyKdT4hDJGMEJASUMBLBm9jZNN08ZMPw/edit?usp=sharing>

Phone Charging Test Data Using Designed Charging Circuit v1:

<https://drive.google.com/file/d/19kz-XuSgh-SQXfwZELGNeKMsm1NFjgMV/view?usp=sharing>

Custom Microcontroller Test PCB v1:

<https://drive.google.com/drive/folders/1SXOPhP2tiEkAI4nqvnlMANdWIvOpIM7F?usp=sharing>

System Level TestBench v1:

https://drive.google.com/drive/folders/1XTE4GmiXga8eIJvs7TsPCf8Rz_VeGpL?usp=sharing

Motherboard PCB v2.4:

https://drive.google.com/open?id=1BTbSBwQA4I7pv0hvCgYMTgsu5s4_Qj6G

Daughterboard PCB v3.1:

<https://drive.google.com/open?id=1lb2Z5epbJGQHbYIL1OE9zSN9zAzIOgAT>

TPS62133 module v1.0:

<https://drive.google.com/drive/folders/1JMQomFczhfSbDT1tm1r2cbcTwqR45pOc?usp=sharing>

Voltage regulator selection comparison:

<https://drive.google.com/open?id=1xHHXllioPhJUEPFiNAkxPcOrYp5hm-VgfF2J932iA0M>

Mechanical drawings:

<https://drive.google.com/open?id=1fT0Iwt18-ac8WUPDuMK1rvd9Q4lJV189>

Mechanical simulations(tutorials):

<https://drive.google.com/open?id=1fE12OG43ChwbL7WK-8ElcGb5ZIFUQDRu>

Power systems design simulation video:

<https://drive.google.com/file/d/1c22Wj16Ne8wlY98kC63tvyMHnNdHDmhQ/view?usp=sharing>